UNIVERSITY OF POTSDAM
DOCTORAL THESIS
10/2019

Electro-acoustical probing of space-charge and dipole-polarization profiles in polymer dielectrics for electret and electrical-insulation applications

QUYET D. NGUYEN


Universität
Potsdam

UNIVERSITY OF POTSDAM
Faculty of Science
Institute of Physics and Astronomy
The dissertation was accepted for the defence of the degree of Doctor of Engineering
(Dr.-Ing.) on 27th November 2019

Supervisor: University Professor Dr.rer.nat.habil. Dr.-Ing. Reimund Gerhard,
Institute of Physics and Astronomy, Faculty of Science,
University of Potsdam
Potsdam, Germany

Co-supervisor: University Professor Dr.-Ing. Ronald Plath,
Chair of High-Voltage Engineering, Faculty of Electrical Engineering and Computer Science,
Technical University of Berlin (TU Berlin)
Berlin, Germany

Mentor: Professor Dr. Dmitry Rychkov,
Institute of Physics and Astronomy, Faculty of Science,
University of Potsdam
Potsdam, Germany
now at Deggendorf Institute of Technology,
Technische Hochschule Deggendorf
Weißenburg in Bayern, Germany

Defence of the thesis: 20th December 2019, Potsdam

Quyet D. Nguyen

Signature

Published online at the
Institutional Repository of the University of Potsdam:
https://doi.org/10.25932/publishup-44562
https://nbn-resolving.org/urn:nbn:de:kobv:517-opus4-445629

UNIVERSITY OF POTSDAM
DOCTORAL THESIS
10/2019

Elektroakustische Abtastung von elektrischen Ladungs- und Polarisationsprofilen in Polymerfolien für Elektret- und Isolations-Anwendungen

QUYET D. NGUYEN


Universität
Potsdam

Statement

Quyet Doan Nguyen,
student matriculation number 779837

I, Quyet Doan Nguyen, formally submit my thesis “Electro-acoustical probing of space-charge and dipole-polarization profiles in polymer dielectrics for electret and electrical-insulation applications” in partial fulfillment of the requirements set forth by the Regulations for awarding the title “Doctor of Engineering” (Dr.-Ing.) in the Faculty of Science of the University of Potsdam.

I declare that the work presented in this thesis has not been submitted as an exercise for a degree to any other university.

The work described herein is entirely my own, except for the assistance mentioned in the Acknowledgments and collaborative work mentioned in the Author’s contributions to the publications. The present thesis work was completed within the “Applied Condensed-Matter Physics” (ACMP) group at the Intitute of Physics and Astronomy in the University of Potsdam.

September 2019.

Contents

List of Publications

Publication I: Q. D. Nguyen, J. Wang, D. Rychkov, and R. Gerhard, "Piezoelectrically-generated pressure steps (PPSs) for studying charge distributions on corona-charged polypropylene films," in *2017 IEEE 16th International Symposium on Electrets (ISE) Book of Abstracts*. IEEE, 2017, p. 145

Publication II: Q. D. Nguyen, J. Wang, D. Rychkov, and R. Gerhard, "Depth profile and transport of positive and negative charge in surface (2-d) and bulk (3-d) nanocomposite films," in *2019 IEEE 2nd International Conference on Electrical Materials and Power Equipment (ICEMPE)*. IEEE, 2019, pp. 300–302, doi:10.1109/ICEMPE.2019.8727256

Publication III: Q. D. Nguyen and R. Gerhard, "LDPE/MgO nanocomposite dielectrics for electrical-insulation and ferroelectret-transducer applications," in *2018 IEEE 2nd International Conference on Dielectrics (ICD)*. IEEE, 2018, 4 pages, doi: 10.1109/ICD.2018.8514713

Publication IV: Q. D. Nguyen, T. Raman Venkatesan, W. Wirges, and R. Gerhard, "Non-uniform polarization profiles in PVDF copolymers after cyclical poling," in *2019 IEEE International Symposium on Applications of Ferroelectrics (ISAF)*. IEEE, 2019, 4 pages (accepted)

Publication V: A. T. Hoang, Q. D. Nguyen, W. Wirges, R. Gerhard, Y. V. Serdyuk, and S. M. Gubanski, "Open-circuit thermally stimulated currents in LDPE/Al_2O_3 nanocomposite," in *2016 IEEE Conference on Electrical Insulation and Dielectric Phenomena (CEIDP)*, 2016, pp. 611–614, doi: 10.1109/CEIDP.2016.7785595

Author's Contributions to the Publications

I For Publication I, I planned the experiments, carried out the measurements, evaluated and discussed the results, and wrote the first draft of the manuscript.

II For Publication II, I planned the measurements, carried out the experiments, evaluated and discussed the results, and wrote the the first draft of the manuscript. The PP films chemically surface-treated with phosphoric acid were kindly prepared by my colleague M.Sc. Jingwen Wang. The LDPE/MgO nanocomposites films were kindly provided by Professor Gubanski and his research group.

III For Publication III, I researched the state of the art, developed the questions to be asked and planned the measurements, carried out the experiments, evaluated and discussed the results, and wrote the first draft of the manuscript. The LDPE/MgO nanocomposites films were kindly provided by Professor Gubanski and his research group.

IV For Publication IV, I initiated the work, contributed to the planning and the development of the experiments, carried out the hysteresis, the piezoelectric-coefficient and the PPS measurements. I also did the polarization-vs-electric-field hysteresis data processing, evaluated and discussed the hysteresis, the PPS data and wrote the first draft of the manuscript.

V For Publication V, I participated in the discussions about the project and in the planning of the experiments, I carried out part of the corona-charging and thermally-stimulated-discharge (TSD) experiments of the LDPE/Al_2O_3 nanocomposite films and I contributed to the evaluation of the experiments and to the description of the results and their discussion.

Abstract

Electro-acoustical probing of space-charge and dipole-polarization profiles in polymer dielectrics for electret and electrical-insulation applications

Electrets are dielectrics with quasi-permanent electric charge and/or dipoles, sometimes can be regarded as an electric analogy to a magnet. Since the discovery of the excellent charge retention capacity of poly(tetrafluoro ethylene) and the invention of the electret microphone, electrets have grown out of a scientific curiosity to an important application both in science and technology. The history of electret research goes hand in hand with the quest for new materials with better capacity at charge and/or dipole retention. To be useful, electrets normally have to be charged/poled to render them electro-active. This process involves electric-charge deposition and/or electric dipole orientation within the dielectrics ' surfaces and bulk. Knowledge of the spatial distribution of electric charge and/or dipole polarization after their deposition and subsequent decay is crucial in the task to improve their stability in the dielectrics.

Likewise, for dielectrics used in electrical insulation applications, there are also needs for accumulated space-charge and polarization spatial profiling. Traditionally, space-charge accumulation and large dipole polarization within insulating dielectrics is considered undesirable and harmful to the insulating dielectrics as they might cause dielectric loss and could lead to internal electric field distortion and local field enhancement. High local electric field could trigger several aging processes and reduce the insulating dielectrics' lifetime. However, with the advent of high-voltage DC transmission and high-voltage capacitor for energy storage, these are no longer the case. There are some overlapped between the two fields of electrets and electric insulation. While quasi-permanently trapped electric-charge and/or large remanent dipole polarization are the requisites for electret operation, stably trapped electric charge in electric insulation helps reduce electric charge transport and overall reduced electric conductivity. Controlled charge trapping can help in preventing further charge injection and accumulation as well as serving as field grading purpose in insulating dielectrics whereas large dipole polarization can be utilized in energy storage applications.

In this thesis, the Piezoelectrically-generated Pressure Steps (PPSs) were employed as a nondestructive method to probe the electric-charge and dipole polarization distribution in a range of thin film (several hundred μm) polymer-based materials, namely polypropylene (PP), low-density polyethylene/magnesium oxide (LDPE/MgO) nanocomposites and poly(vinylidene fluoride-co- trifluoro ethylene) (P(VDF-TrFE)) copolymer. PP film surface-treated with phosphoric acid to introduce surfacial isolated nanostructures serves as example of 2-dimensional nano-composites whereas LDPE/MgO serves as the case of 3-dimensional nano-composites with MgO nano-particles dispersed in LDPE polymer matrix. It is evidenced that the nanoparticles on the surface of acid-treated PP and in the bulk of LDPE/MgO nanocomposites improve charge trapping capacity of the respective material and prevent further charge injection and transport and that the enhanced charge trapping capacity makes PP and LDPE/MgO nanocomposites potential materials for both electret and electrical insulation applications. As for PVDF and VDF-based copolymers, the remanent spatial polarization distribution depends critically on poling method as well as specific parameters used in the respective poling method. In this work, homogeneous polarization poling of P(VDF-TrFE) copolymers with different VDF-contents have been attempted with hysteresis cyclical poling. The behaviour of remanent polarization growth and spatial polarization distribution are reported and discussed. The Piezoelectrically-

generated Pressure Steps (PPSs) method has proven as a powerful method for the charge storage and transport characterization of a wide range of polymer material from nonpolar, to polar, to polymer nanocomposites category.

Keywords: electro-acoustic electric-charge and polarization profiling, space charge, polypropylene, polyethylene nanocomposites, magnesium oxide, polymer electrets, ferroelectrets, electrical insulation, piezoelectricity, ferroelectricity, poly(vinylidene fluoride), hysteresis

Zusammenfassung
Elektroakustische Abtastung von elektrischen Ladungs- und Polarisationsprofilen in Polymerfolien für Elektret- und Isolations-Anwendungen

Elektrete sind Dielektrika mit quasi-permanenter elektrischer Ladung und/oder quasi-permanent ausgerichteten elektrischen Dipolen - das elektrische Analogon zu einem Magneten. Seit der Entdeckung der besonders hohen Stabilität negativer Raumladungen in Polytetrafluorethylen (PTFE, Handelsname Teflon) und der Erfindung des Elektretmikrofons ist aus der spannenden wissenschaftlichen Fragestellung nach den Ursachen der hervorragenden Ladungsspeicherung in Elektreten auch eine wichtige technische Anwendung geworden. In der Geschichte der Elektretforschung und der Elektretanwendungen geht es neben der Ursachenklärung auch immer um die Suche nach neuen Materialien mit besserer Ladungsspeicherung und/oder Dipolpolarisation.

Elektretmaterialien müssen in der Regel elektrisch aufgeladen oder gepolt werden, um die gewünschten elektroaktiven Eigenschaften zu erhalten. Dabei werden entweder elektrische Ladungen auf der Oberfläche oder im Volumen des Elektretmaterials deponiert und/oder elektrische Dipole im Material ausgerichtet. Genaue Informationen über die räumliche Verteilung der elektrischen Ladungen und/oder der Dipolpolarisation sowie deren Entwicklung im Laufe der Zeit sind entscheidend für eine gezielte Verbesserung der Elektretstabilität.

Dielektrika, die zur elektrischen Isolierung von Hochspannungsanlagen eingesetzt werden, können ebenfalls elektrische Raumladungen und/oder Dipolpolarisationen enthalten, deren Verteilungen entscheidend für die Beherrschung der damit einhergehenden Eigenschaftsänderungen sind. Traditionell gelten Raumladungen und Dipolpolarisationen in elektrischen Isolierungen als unerwünscht und schädlich, da sie zu erheblichen Verlusten und zu Verzerrungen der inneren elektrischen Felder führen können. Hohe lokale Felder können Alterungsprozesse auslösen und die Lebensdauer der isolierenden Dielektrika erheblich verkürzen. Mit dem Aufkommen der Hochspannungs-Gleichstromübertragung und des Hochspannungskondensators zur Energiespeicherung in den letzten Jahren hat sich die Situation jedoch grundlegend geändert, da Raumladungen prinzipiell nicht mehr vermeidbar sind und bei entsprechender Gestaltung der Isolierung möglicherweise sogar von Vorteil sein können.

Hier ergeben sich nun Überschneidungen und Synergien zwischen Elektreten und elektrischen Isoliermaterialien, zumal in beiden Fällen hohe elektrische Gleichfelder auftreten. Während quasi-permanent gespeicherte elektrische Ladungen und/oder stark quasi- permanente oder remanente Dipolpolarisationen das wesentliche Merkmal von Elektreten sind, können stabil gespeicherte elektrische Ladungen in elektrischen Isolierungen dazu beitragen, den schädlichen Ladungstransport und damit die effektive elektrische Leitfähigkeit der Dielektrika zu reduzieren. Ein kontrolliertes Einbringen von Raumladungen kann die Injektion und die Anhäufung weiterer Ladungen verhindern, während stark Dipolpolarisationen die Kapazität von elektrischen Energiespeichern wesentlich erhöhen können.

In der vorliegenden Arbeit wurden piezoelektrisch erzeugte Druckstufen (Piezoelectrically generated Pressure Steps oder PPSs) eingesetzt, um die Verteilung elektrischer Ladungen und/oder ausgerichteter elektrischer Dipole in relativ dünnen polymeren Dielektrika (Mikrometerbereich) zu untersuchen. Wesentliche Probenmaterialien waren Polypropylen (PP), Komposite aus Polyethylen mit Magnesiumoxid-Nanopartikeln in geringen Mengen (LDPE/MgO) sowie Poly(vinyliden fluorid-trifluorethylen)-Copolymere (P(VDF-TrFE)). PP-Folien, die mit Phosphorsäure oberflächenbehandelt wurden, um voneinander isolierte

Nanostrukturen an der Oberfläche zu erzeugen, sind ein Beispiel für ein zweidimensionales (2-D) Nanokomposit, während LDPE/MgO ein dreidimensionales (3-D) Nanokomposit darstellt. Es konnte nachgewiesen werden, dass die Nanopartikel auf der Oberfläche von säurebehandeltem PP und im Volumen von LDPE/MgO-Nanokompositen die Ladungsspeicherfähigkeit des jeweiligen Materials entscheidend verbessern. Damit werden weitere Ladungsinjektionen und der Ladungstransport verhindert, was die 2-D PP- und die 3-D LDPE/MgO-Nanokomposite zu geeigneten Kandidaten sowohl für Elektret- als auch für Isolationsanwendungen macht. Bei Polyvinylidenfluorid (PVDF) und Copolymeren auf der Basis von Vinylidenfluorid (VDF) hängt die remanente räumliche Polarisationsverteilung entscheidend von der jeweiligen Polungsmethode sowie von den Parametern des jeweiligen Polungsvorgangs ab. Hier wurde versucht, eine homogene Polung von P(VDF-TrFE)-Copolymeren mit unterschiedlichen VDF-Gehalten mit dem Verfahren der zyklischen Polung (sogenannte Hysterese-Polung) zu erzeugen. Das Entstehen der remanenten Polarisation und deren räumliche Verteilung konnten erfasst und interpretiert werden, um Hinweise für eine optimale Polung zu erhalten.

An den genannten Beispielen konnte gezeigt werden, dass die Methode der piezoelektrisch erzeugten Druckstufen (PPS) ein leistungsfähiges Verfahren zur Charakterisierung der Ladungsspeicherung und des Ladungstransports in Dielektrika ist und dass damit ein breites Spektrum von unpolaren Polymeren über polare Polymerdielektrika bis hin zu polaren Nanokompositen sinnvoll untersucht werden kann. Es wurden wesentliche Erkenntnisse zur Ladungsspeicherung und zur remanten Polarisation in den untersuchten Polymeren gewonnen.

Schlüsselwörter: elektroakustische Abtastung elektrischer Ladungen und Dipolpolarisationen, elektrische Raumladung, Polypropylen, Polyethylen-Nanokomposite, Magnesiumoxid, Polymerelektrete, Ferroelektrete, elektrische Isolierung, Piezoelektrizität, Ferroelektrizität, Poly(vinylidenfluorid), Hysterese

Acknowledgements

First and foremost, I would like to express my sincere gratitude to Professor Gerhard for accepting me as his PhD student and starting my journey in Germany. His immense knowledge and humble manner impressed me deeply and corrected in me many misconceptions. I also wish to thank Prof. Gerhard and his wife Christine Ludwig for the time I spent with them from Germany to Brazil and to China. Their knowledge, humor, kindness, patience and helpful advice to me to all matter of life is precious. I thank Professor Plath from TU Berlin for his hospitality and his willingness to be my second supervisor. A special thank goes to Professor Rychkov for his kind and direct, and friendly style as a mentor.

I am grateful to acknowledge the Vietnamese International Education Department (VIED) for providing funding for my PhD research in Germany. The support of the World University Service (WUS) and Welcome Center (University of Potsdam) during the time I am studying in Germany is undeniably important.

Many thanks to staff and colleagues at the Institute of Physics and Astronomy (University of Potsdam) for creating a pleasant working environment to all of us.

I sincerely thank Professor Gubanski from Chalmers University of Technology (Sweden) for providing the LDPE nanocomposites used in this thesis and I am indebted to my friend and former colleague, Dr. Anh T. Hoang (now at NKT) for our fruitful collaboration in studying the LDPE/Al_2O_3 nanocomposites, for COMSOL simulation of the piezoelectric quartz and for his true friendship and care. I am grateful to Professor Altafim and his group at the University of Sao Paulo (Brazil) for hosting my wonderful trip to Sao Carlos.

I really appreciate Dipl.-Ing Werner Wirges and Manuel Schulze for their technical competencies and funny stories during our daily exchanges and lunch together. I am grateful to Dr. Wolfgang Künstler and Dipl.-Ing Andreas Pucher, the PPS setup would not work without your help. I will remember our discussions every morning then. Many thanks to Dr. Xunlin Qiu (now at TU Chemnitz) and his wife for their kindness and supportive and for reading the manuscript of my thesis. Thank you for our football time and introducing me to many other good Chinese friends. I have enjoyed good time with you. I thank M.Sc. Jingwen Wang for preparing the chemically treated PP films and M.Sc. Thulasinath Raman Venkatesan for our work in development of hysteresis data processing and to both of you for our fruitful collaboration as well as many stimulating discussions. Other former colleagues in the group of "Applied Condensed-Matter Physics" (ACMP) at the University of Potsdam are thanked for their support and the happy time we shared together: Beatrice Unger, Hülya Ragusch, Dr. Fan He, M.Sc Junzhe Song, Dr. Gunnar Gidion, Dipl.-Phys. Matthias Kollosche.

I truly thank Dr. Thinh H. Pham, my former colleague at the Department of Electric Power Systems (HUST, Vietnam) (now in the US) for his companion. He is truly my senior friend and guider whom I can consult on all life issues and who really cares.

Other friends: M.Sc. Hiep H. Nguyen, anh M.Sc. Nang V. Pham, Dr. Hoai-Thu Nguyen, Dr. Nelli Elizarov, M.Eng. MBA. Dien X. Pham, Minh D. Nguyen, Anh V. Nguyen, Tam Le, Ninh Q. Tran, em Phong T. Tran, M.Sc. Thanh D. Nguyen, Nhuan D. Nguyen, Trang T. H. Mai, Huy Q. Pham and M.Sc. Tam T. Mai: thanks to you all for your friendship and importance to me in many ways. Many other friends and relatives that are surely importance but I could not name all of them here due to my sloppy memories and the limited space.

I am indebted to my parents Cuong T. Nguyen and Nguyet T. Doan, di Ninh T. Doan, chi Loan T. Tran, em Thang N. Nguyen for their unconditional love, great support and patience to me. And the last but surely not the least, I thank my beloved wife Dr. Anh T. P. Tran for always being on my side and her encouraging manner. We have ups and downs but we can do it.

Abbreviations

AC	Alternating Current
DC	Direct Current
FEP	fluorinated ethylene propylene
HV	High Voltage
HVAC	High-Voltage Alternating Current
HVDC	High-Voltage Direct Current
ITSD	Isothermally-Stimulated Discharge
IEC	International Electrotechnical Commission
IEEE	Institute of Electrical and Electronics Engineers
LDPE	low-density polyethylene
LDPE/MgO	low-density polyethylene/magnesium oxide
LIPP	Laser-Induced Pressure Pulse
LIMM	Laser Intensity Modulation Method
MCEG	Monocharged Electret Generator
MgO	magnesium oxide
PPS	Piezoelectrically-generated Pressure Step
PP	polypropylene
PE	polyethylene
PETP	poly(ethylene terephthalate)
PVC	poly(vinyl chloride)
PVDF	poly(vinylidene fluoride)
P(VDF-TrFE)	poly(vinylidene fluoride-co-trifluoroethylene)
P(VDF-TFE)	poly(vinylidene fluoride-co-tetrafluoroethylene)
P(VDF-HFP)	poly(vinylidene fluoride-co-hexafluoropropylene)
PWP	Pressure Wave Propagation
PTFE	polytetrafluoroethylene
RT	Room Temperature
SEM	Scanning Electron Micrograph
SPD	Surface Potential Decay
TSD	Thermally-Stimulated Depolarization
XLPE	cross-linked polyethylene

Symbols

c_Q	longitudinal speed of sound in piezoelectric quartz crystal
c_S	longitudinal speed of sound in dielectric sample
E	electric field
ε	relative dielectric permitivity coefficient
ε_0	dielectric constant of vacuum
t_P	pulse duration of voltage-step (square pulse) (100 ns)
t_Q	transit time of pressure step in piezoelectric quartz crystal
t_S	transit time of pressure step in dielectric sample

1 Introduction

Space charge literally means charges in space, i.e., in a region where there is a concentration of charges and/or ions of one polarity [6]. Space charge in dielectrics can be divided into free (or real) charge and bound (or polarization) charge. These real charges maybe mobile electrons, holes, localized inonized impurities whereas bound charges are charges associated with molecular dipoles, which move with the mobility of the molecules. When a dielectrics is put under an applied electric field, various processes take place in the dielectric bulk and at the interface that contribute to a charge distribution in the dielectric, namely dipole orientation, ion migration and charge transfer at the interfaces. The three basic processes are shown in Figure 1 with their typical characteristic of charge distribution (charge spreading and polarity comparing with the one of poling electrodes). The act of putting charge and dipole polarization in insulator (deliberately or indeliberately) can be beneficial or harmful to the dielectric, depending on application at hand, whether it is electret or electrical-insulation application [7]. Detailed knowledge of space charge distribution (real charge and/or dipole polarization) is highly beneficial in understanding the underlying physical processes in order to control and optimize them for respective purposes in electret or electrical-insulation applications [8].

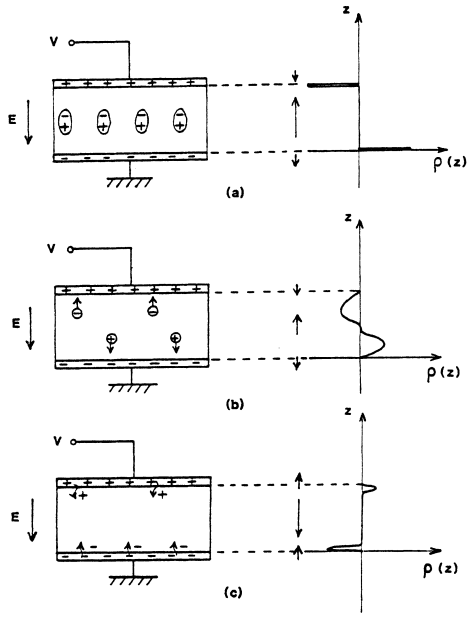

Figure 1: Basic processes contributing to a charge distribution $\rho(z)$ in a dielectric material subjected to an electric field with (a) dipole orientation, (b) ion migration and (c) charge transfer at the interface. After Ref. [8].

1.1 Space-charge and dipole-polarization are prerequisite in electret applications

The word "Electret" was first devised in 1885 by Oliver Heaviside in which he used in "strict analogy to the word magnet only for materials with a permanent dipole polarization" [9]. Modern electret research started in Japan with pioneering work by Mototaro Eguchi [9–11] whose definition of electrets is generally accepted today: Electrets is "quasi-permanent charge as well as quasi-permanent dipole polarization in insulators" [9]. Electrets research history and development was thoroughly reviewed in several review articles [9, 12] and book chapters [13–15] and especially in two comprehensive books on the subject [16, 17]. Figure 2 presents main milestones achieved in the development of electrets research (adapted from Ref. [14]).

Electrets is now an established field surrounding the charge-spring concept [18] that span the so-called "electrets universe" (Figure 3) comprising 6 groups/categories, depending on material structure, namely:

- Space-Charge Electret;
- Polymer Ferro- or Piezo-Electret;
- Molecular-Dipole Electret;
- Piezo- and Pyroelectric Crystal or Ceramic (Electret);
- Piezo- and Pyroelectric Composite Electret;
- Electro-Electret (or Dielectric Elastomer).

Latest development in this field is the introduction of liquid electret [19] that extends the group of electret materials from solid to liquid phase.
Although the concept of electrets is simply dielectrics that can retain electric charge and electric polarization for an extensive amount of time, this implies important applications as electret material could exhibit piezo-, pyro- and ferroelectricity, which is indispensable in transducing purposes. Piezoelectric materials are materials in which electricity can be generated by an applied mechanical stress or vice versa, a mechanical stress can be produced by an applied electric field [13]. Pyroelectricity means heat-generated electricity. This effect is also reversible. This implies that heat can be generated by electricity resulting from the change of the state of electric polarization, such as electro-thermal and electro-calorie effects [13]. Ferroelectric materials are materials which exhibit a spontaneous electric polarization below the Curie temperature, a hysteresis loop and an associated mechanical strain [13]. Electrets is widely used in scientific and technical applications. The first application of polymer electrets is electret microphone in which the microphone membrane was produced out of PTFE or FEP material [20]. This invention eliminates the need of a DC bias (Figure 4) required in the classical electrostatic transducers and brings electret research from a scientific curiosity to important scientific and technological applications. Since then, a multitude of electret applications have been suggested and realized that utilized piezoelectricity [16,21–23], pyroelectricity [16,24,25] and ferroelectricity [26].

Electret materials can be divided into two groups of inorganic and organic material. Polymer is an important group of organic material for electrets and has several advantages compared to inorganic electret material such as: (i) they are flexible and tough; (ii) they can be made very thin with a large area; (iii) they have a low mechanical impedance and hence exhibit a good acoustic coupling to water and biological systems [13, 21, 27].

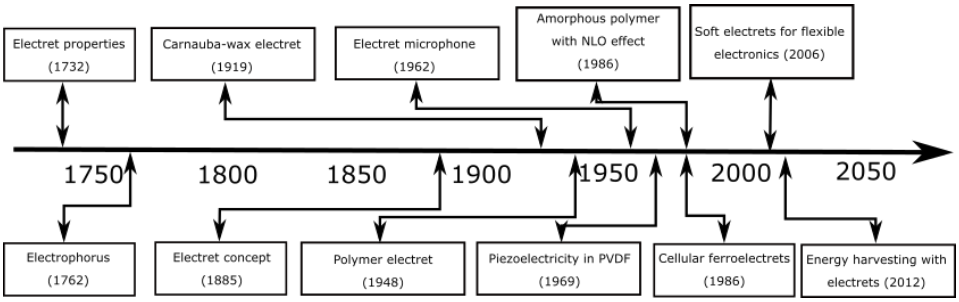

Figure 2: Milestones in electret research history, adapted from Ref. [14].

In some applications the use of polymer electrets (instead of inorganic electret materials) is required as in tactile sensing applications [21]. There was a misconception that piezoelectricity can only be found in polar polymer materials. It was a complete surprised that it also appears in non-polar polymer materials [28]. The trick is to prepare heterogeneous polymer-structure containing porous foam structure with open or closed cells. These open or closed cells were trapped with positive and negative electric charge at their opposite surfaces (Figures 5 and 7). These trapped electric charge at voids' surface form macroscopic dipoles that break the centro-symmetry structure of the nonpolar polymer to render the overall polymer-structure electro-active. Those polymer-systems with electrically charged voids/cavities are now usually called ferro-electrets or piezoelectrets [14, 18, 28–35].

Typical value for piezoelectric activity of ferroelectrets (optimized cellular PP) is 600 pC/N, compared to 2 of crystal (quarzt, silicon dioxide) (d_{11}); 170 – 600 of ceramics (lead zirconate titanate, PZT) and 20 of ferroelectric polymer (β-phase PVDF) [36]. It can be seen that the piezoelectric activity of ferro-electrets are on par with piezoelectric ceramics plus several advantages of organic materials mentioned above. Polymer ferroelectrets could be in the form of cellular polymer foam or polymer-film system (soft- and hard-polymer layers or polymer-layers featuring regular cavities) [15]. Cellular polymer foam ferro-electrets was initially prepared from closed cell polypropylene foam. Following the earlier example of cellular PP, materials could be used for making polymer ferroelectrets have been greatly expanded to comprise groups of polyolefin (PP, PE); polyester (PET, PEN); cyclo-olefin polymer (COP) and copolymer (COC); polycarbonate (PC) and fluoropolymer (PTFE, FEP, PFA and amorphous Teflon) [15].

Selected applications of ferro-electrets could be mentioned as hydrophones, air-borne transducers, microphones, musical pickups, control panels, keyboards, tactile sensors, intruder detectors, wearable energy harvester, etc. [15, 28, 37]. In Figure 6 it is presented the material structure and working cycle of the Monocharged Electret Generator (MCEG) for shoe insole energy harvesters. It is demonstrated that the maximum output voltage of the device is 178 V and current of 2.85 µA during people walking. The maximum harvested power is ca. 35.63 µW under a resistor load and is enough to light up 55 light-emitting diodes (LEDs) with a single step of walking [38].

Cellular polypropylene (PP) is currently the workhorse material for cellular polymer foam ferroelectrets. Various procedures are used to produce polymer foam with conventional way is stretching filler-loaded polymers under suitable conditions. Tiny mineral particles are frequently used as fillers that serves as stress concentrators for microcracks during stretching of the film. Consequently, stretching of the films in two perpendicular directions results in films with lens-like cavities [15]. Typical structure of cellular polypropy-

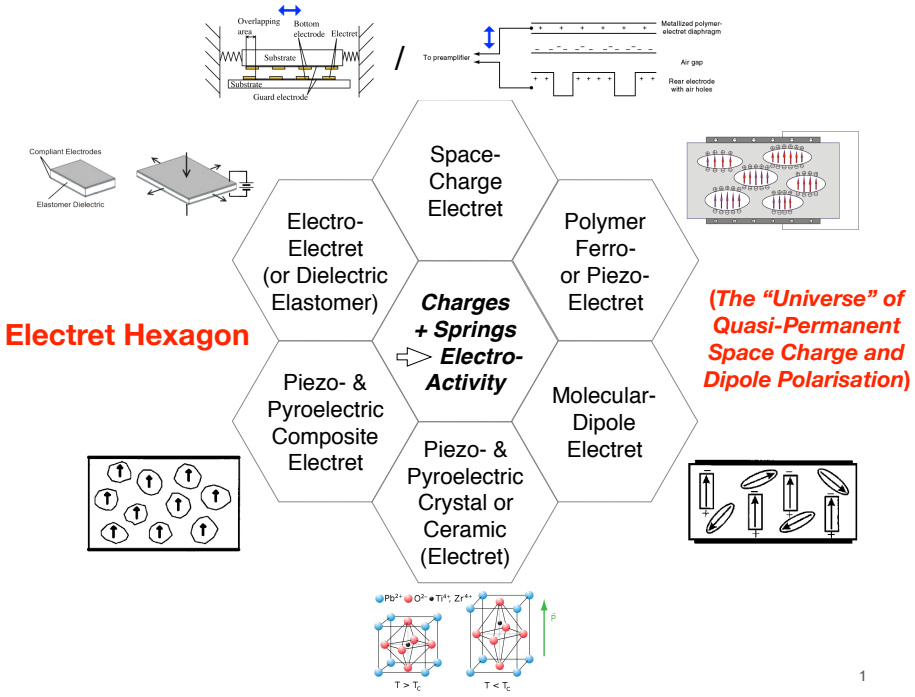

Figure 3: The electret hexagon and the electret universe: An overview of various types of electrets (Courtesy of Professor R. Gerhard, updated version of Fig. 1 in Ref. [18]).

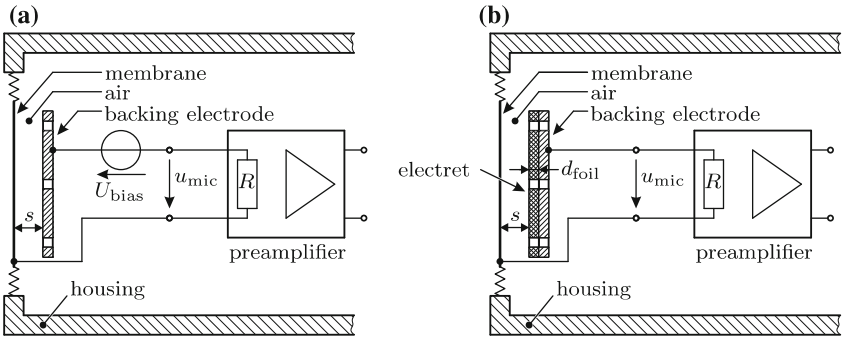

Figure 4: (a) Classical Electrostatic microphone and (b) Electret microphone - a classical application of electric-charges trapped on the surface of electret film – externally surface-charge electrets) (from Ref. [23])

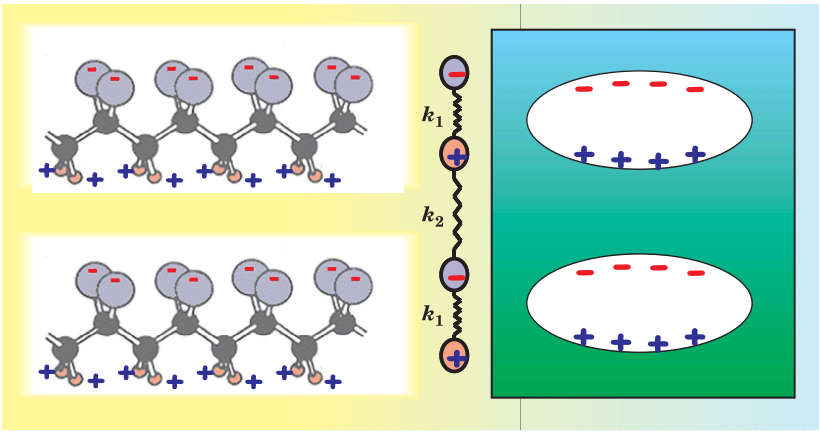

Figure 5: Ferroelectric versus Ferroelectret material structure (internally surface-charge electrets) [29].

lene films is shown in Figure 7 [23].

Cellular PP films are commercially available by the company Emfit Ltd. [39]. To render the cellular PP films electroactive, they are exposed to high electric field to create micro plasma discharge within voids (air cells/cavities) within the PP films. Such micro discharge activity leads to electric charge trapped at inner opposite surfaces of the voids forming macroscopic dipoles. Such macroscopic dipoles, together with the mechanical inhomogeneity of the voids and PP matrix, are responsible for the electroactive properties of cellular PP films. Cellular PP films after charging show high value of piezoelectricity (ca. 600 pC/N or higher). The prominent disadvantage of PP ferroelectrets is its limited working temperature range, which is up to 60 °C [15, 28, 40, 41].

The thermal stability of electromechanical properties of cellular PP ferro-electrets depends on the thermal stability of the less stable charges of the two types (positive and negative charges trapped at the void/channel gas-polymer interface). To improve the thermal stability, there are several routes suggested, comprising of incorporating suitable additives or blending different compounds; physical aging to introduce physical traps for electric charges; chemical defects or traps can also be introduced by surface modification of polymer electrets by reactive gases or chemical solvents [15]. For PE, the surface modification of PE film with H_3PO_4 brings about significant improvement of charge stability. The thermal stability of both positively and negatively charged PE samples was enhanced by about 60 °C with the modification using H_3PO_4 [42]. Similar procedure of surface treatment with H_3PO_4 is also suggested for PP polymer films for enhancement of thermal stability of trapped electric charges at PP film surfaces [43]. The thermal stability enhancement is still rather asymmetry with enhancement of about 34 °C and 50 °C for positively and negatively charged PP films, respectively. The thermal stability enhancement of the chemical treated PP films is suggested to come from “foreign” chemical structures on the treated PP film surface. Such foreign structures are suggested to create deep chemical traps/defects for electric charge trapping and improvement of thermal stability.

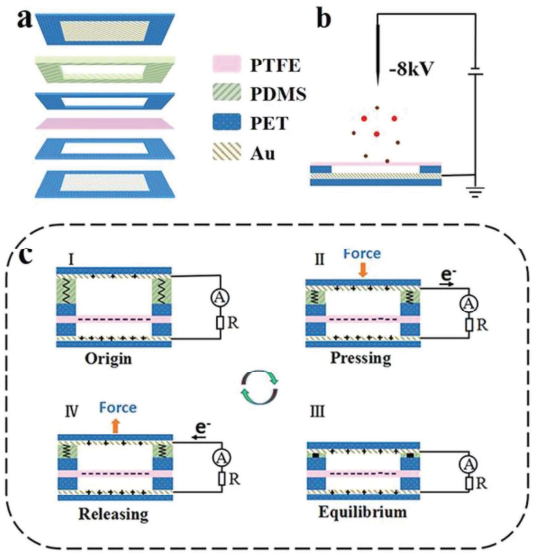

Figure 6: Structure, charging and working mechanism of the Monocharged Electret Generator [38].

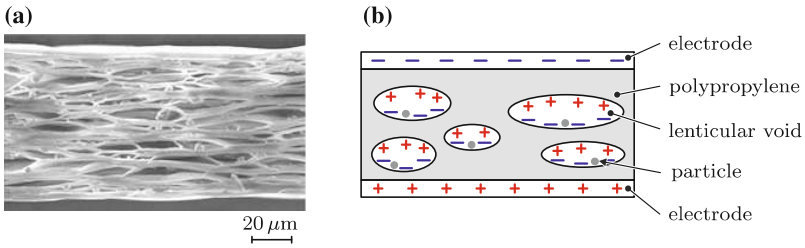

Figure 7: (a) Scanning electron micrograph of PP film; (b) Charge distribution inisde PP ferroelectret film ((internally surface-charge electrets)) [23].

1.2 Space-charge and dipole-polarization are (traditionally) undesirable in electrical-insulation applications

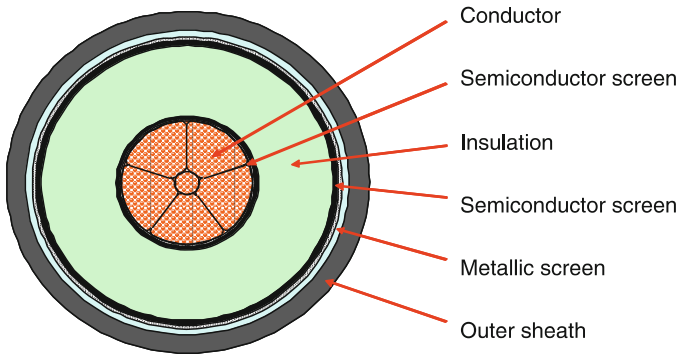

Figure 8: Typical structure of an extruded electric power cable. After Ref. [44].

Electrical insulator is material which prevents free flow of electric charge within its internal insulating wall [45]. The development of electrical insulator material was born out of telecommunication needs and follows the demands of telecommunication cable and electric power cable [46]. Figure 8 depicts a typical structure of a single-core extruded high voltage power cable, a state-of-the-art "optimum" design for a HV power cable which satisfies both economic and technical criteria (electrical, mechanical, thermal requirements, compactness, ease of production, transport and laying, etc.). It comprises of a metal conductor core (commonly used aluminum or copper), an inner semiconductor screen layer, a main extruded insulation layer, outer semiconductor screen and maybe further layer of sheaths and jackets for moisture/water absorption prevention and mechanical protection. Tremendous research and development efforts have been devoting to the development of semiconductor [47] and main insulation material [48, 49] for the ever-increasing rated voltage of high voltage power cable. Global generation of electricity is expected to reach 37 trillion kWh in 2040 from current value of 22 trillion kWh in 2012 [50]. Booming of electricity consumption demand, together with concerns about tragic impact of climate change [51] lead to consideration of global electricity network [52–54] for better utilization of the world's resources [55], increased usage of renewable energy, less dependence on fossil fuel and reduction of CO_2 and other greenhouse gases emission. The global electricity grid calls for long geographical distance HV transmission line for intercontinental and offshore renewable-energy farm connection, favouring HVDC transmission lines [56, 57]. By 2030, HVDC power cable rated voltage of 1 MV should be in needed [58] from current highest rated voltage of 640 kV [59].

The development of electrical insulation research field concerns mainly with improving the design of telecommunication and electric power cable, as well as improved insulating material. Main milestones are selected and presented in Figure 9. It started with the cultivation of gutta-percha by John Tradescant the Younger in 1656 after his travelling to the Far East [60]. The tree, known as "Mazer Wood", grew unnoticedly until it was reintroduced again to the West in 1834 by William Montgomerie [46] and provided material

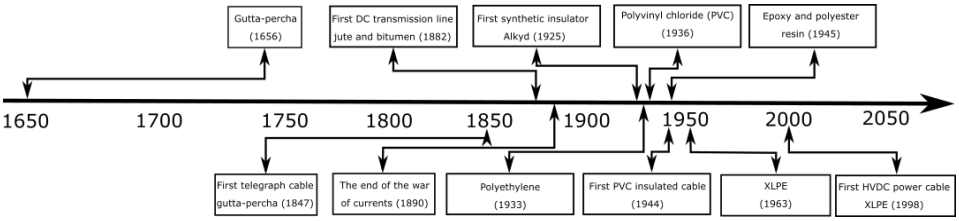

Figure 9: Milestones in electrical-insulation research history.

for manufacturing first telegraph cable in 1847 [46]. First DC transmission line with jute and bitumen insulation was introduced in 1882 [61] together with commercial DC lighting system by Thomas Edison downtown New York City. The year of 1890 marks the end of the war of the currents AC/DC [62] and set course for development of AC power system and devices. In 1925, first synthetic insulator alkyd (saturated polyester) was introduced [63], followed by polyethylene in 1933 [64], PVC in 1936 [65] (replacing natural rubber), epoxy and polyester resin in 1945 [65] and XLPE in 1963 [66]. First polymer-extruded power cable with PVC was first laid in Germany in 1944 [46]. First HVDC power cable with extruded XLPE insulation was commissioned in 1998 [67]. Since then HVDC power cable with extruded XLPE insulation has been considered adequate for transmission of large amount of electrical power over long geographical distances, especially in the context of renewable energy integration and discrete electricity networks connection.

As already mentioned at the beginning of Section 1, various electric charge processes take place when a dielectric is put under high electric filed (see Figure 10). At metal/insulator interfaces, electron can be injected/extracted to/from the insulator, or can be trapped near these regions to form homo- or heterocharge; it can combine with hole or cation for charge annihilation or neutral species for charge-carrier-generation. Similar processes are possible for hole at metal/insulator interface. Deep in the insulator bulk, charge-carrier species can diffuse, drift under external or internal electric field and be trapped at regions in the inner bulk; interfacial polarization (Maxwell-Wagner-Sillars polarization), molecular dipole orientation can take place to form electric polarization; charge-carrier generation or recombination can be excited following aborption or resulting in emission of light (electromagnetic waves). These electric charge processes could lead to space-charge accumulation in insulator that distorts internal electric field, creates local field enhancement, accelerates aging processes and reduces lifetime of cable insulating system [67–71] (relationship of space charge and electrical breakdown in electrical insulation is not always causal, however [72]).

For polymer dielectrics, space charge accummulation depends not only on intensity of applied electric field, but also on its frequency. Figure 11 shows variation of total accumulated space charge in the bulk of XLPE in response to varied frequency. Total accumulated charge decreases monotonously with frequency. Very less charge accumulates at 50 Hz and charge patterns at low frequencies are very similar to the one at DC electric field [74]. Charge accumulation also depends on types of dielectrics under electric field. For polymer dielectrics which are not optimized for use under DC electric field, large accumulation could take place (see Figure 12b). Most notable characteristic of polymer dielectric material for HV power cable application is the so-called ”stress inversion” [76] where electric field gradient in the bulk of of the dielectric reverses after certain period of field application (see Figure 12a) [75]. Maximum electric stress location changes from the inner semiconductor layer to the outer semiconductor layer.

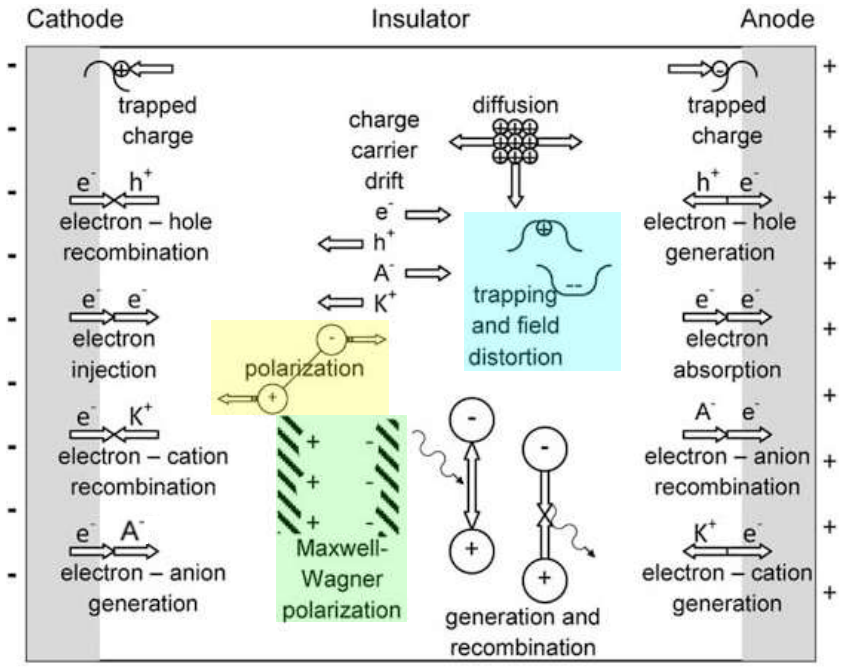

Figure 10: Electric charge processes in an insulator or at an insulator-electrode interface. Adapted from Ref. [73] and by courtesy of Prof. Gerhard.

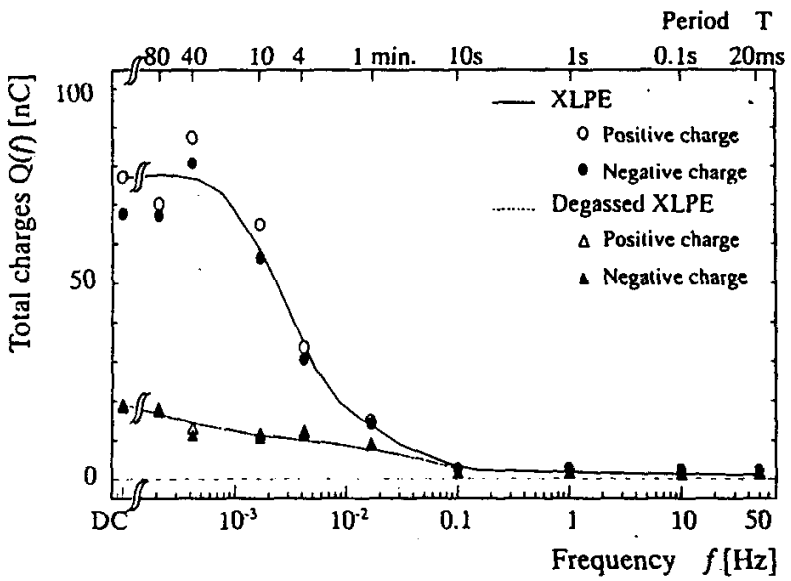

Figure 11: Total space charge accummulation in the bulk of XLPE versus frequency of the applied electric field. After Ref. [74].

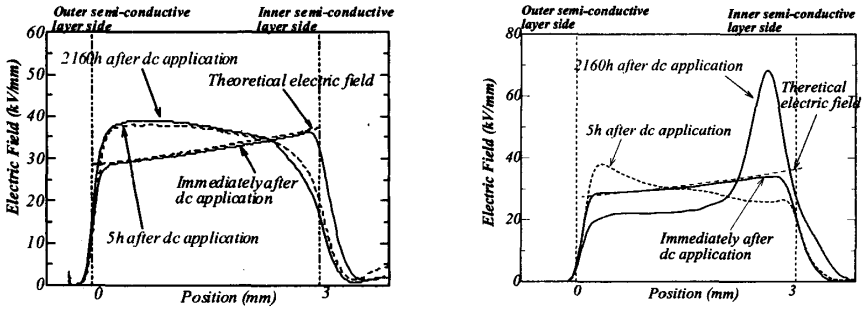

(a) DC XLPE cable, under DC voltage *(b) AC XLPE cable, under DC voltage*

Figure 12: (a) Electric field distribution in DC XLPE cable under DC voltage and (b) Electric field distribution in AC XLPE cable under DC voltage. After Ref. [75].

For HVAC power cable applications, although large space charge accumulation in the insulation bulk is minimized due to effect of alternating electric field direction (50/60 Hz), the possibility of charge injection and extraction in each half-cycle of electric field at protrusion points at the semiconductor/insulation interfaces could bring about mechanical fatigue and accelerated aging to the insulating structure [77]. For HVDC power cable applications, space charge accummulation and its effects are a major drawback and need to be addressed in the research and development of new cable system [67, 76, 78]. Space charge accumulation test on full-sized cable model is recommended, as least by cable manufacturer, when developing new HVDC power cable system as reflected in CIGRE technical brochure (TB) 496 [79], IEEE Standard 1732-2017 [80]. Pressure Wave Propagation (PWP) [81–84], a straight-forward method for electric field distribution measurement in dielectrics (planar or cylindrical form) is particularly suitable for applying to full-sized cable specimen and was specified in an IEC technical report (IEC TR 62836:2013) [85]. Thermal-Pulse Tomography (TPT) is also a promising method although it has been applied to signal cables (PVDF) so far [86–88].

1.3 Organization of the thesis

Electrets are dielectrics with quasi-permanent electric charge and/or dipoles, sometimes can be regarded as an electric analogy to a magnet. Since the discovery of the excellent charge retention capacity of poly(tetrafluoro ethylene) and the invention of the electret microphone, electrets have grown out of a scientific curiosity to an important application both in science and technology. The history of electret research goes hand in hand with the quest for new materials with better capacity at charge and/or dipole retention. To be useful, electrets normally have to be charged/poled to render them electro-active. This process involves electric-charge deposition and/or electric dipole orientation within the dielectrics ' surfaces and bulk. Knowledge of the spatial distribution of electric charge and/or dipole polarization after their deposition and subsequent decay is crucial in the task to improve their stability in the dielectrics.

Likewise, for dielectrics used in electrical insulation applications, there are also needs for accumulated space-charge and polarization spatial profiling. Traditionally, space-charge accumulation and large dipole polarization within insulating dielectrics is considered undesirable and harmful to the insulating dielectrics as they might cause dielectric loss and could lead to internal electric field distortion and local field enhancement. High local elec-

tric field could trigger several aging processes and reduce the insulating dielectrics' lifetime. However, with the advent of high-voltage DC transmission and high-voltage capacitor for energy storage, these are no longer the case [89]. There are some overlapped between the two fields of electrets and electric insulation. While quasi-permanently trapped electric-charge and/or large remanent dipole polarization are the requisites for electret operation, stably trapped electric charge in electric insulation helps reduce electric charge transport and overall reduced electric conductivity. Controlled charge trapping can help in preventing further charge injection and accumulation as well as serving as field grading purpose in insulating dielectrics whereas large dipole polarization can be utilized in energy storage applications.

Several techniques have been suggested on the measurement of charge and dipole polarization in dielectrics. Broadly, they can be divided into destructive and nondestructive measurement methods. Most commonly used destructive methods can be mentioned as sectioning and planing method (which utilizes cutting and shaving tools to extract thin layer of dielectrics combining with other charge density measurement methods), solvent diffusion method and compensation method (which employs a particle beam (electron beam) to sweep through sample thickness and create a propagating layer of higly conductive region in sample bulk to collect information of space charge distribution). The destructive probing methods are detailed in Ref. [16] and references therein. Destructive methods, as their names suggest, neccessitate the destruction of space charge profile within the dielectrics after their charge distribution measurement and therefore do not permit the following of charge evolution over time or the change of applied electrical stress. Since the late 1970s, several methods for non-destructive probing of charge and dipole polarization profiles were developed. They can be conveniently divided into two broad group of acoustical methods (which employ a propagating pressure wave as a virtual probe) and thermal methods (which utilizes the diffusion of heat wave in sample bulk). Several review papers were devoted on the topic of non-destructive methods of probing charge and polarization profiles in dielectrics [8, 9, 90–92], especially Table 1 in Ref. [9] which comprehensively surveys all the non-destructive methods, together with their detecting principle, typical resolution, sample thickness and original references. There are also recent review papers which focus on acoustical methods [82, 93] and thermal methods [88, 94]. Recent development in the acoustical method group is the development of the Electro-Acoustic Reflectometry (EAR) method in extending the spatial resolution to the submicrometer range [95].

In this thesis, the Piezoelectrically-generated Pressure Steps (PPSs) were employed as a nondestructive method to probe the electric-charge and dipole polarization distribution in a range of thin film (several hundred μm) polymer-based materials, namely polypropylene (PP), low-density polyethylene/magnesium oxide (LDPE/MgO) nanocomposites and poly(vinylidene fluoride-co- trifluoro ethylene) (P(VDF-TrFE)) copolymer. PP film surface-treated with phosphoric acid to introduce surfacial isolated nanostructures serves as example of 2-dimensional nano-composites whereas LDPE/MgO serves as the case of 3-dimensional nano-composites with MgO nano-particles dispersed in LDPE polymer matrix. It is evidenced that the nanoparticles on the surface of acid-treated PP and in the bulk of LDPE/MgO nanocomposites improve charge trapping capacity of the respective material and prevent further charge injection and transport and that the enhanced charge trapping capacity makes PP and LDPE/MgO nanocomposites potential materials for both electret and electrical insulation applications. As for PVDF and VDF-based copolymers, the remanent spatial polarization distribution depends critically on poling method as well as specific parameters used in the respective poling method. In this work, homogeneous

polarization poling of P(VDF-TrFE) copolymers with different VDF-contents have been attempted with hysteresis cyclical poling. The behaviour of remanent polarization growth and spatial polarization distribution are reported and discussed.

The thesis is organized as follows. Section 1 gives a brief introduction on the role of space (real) charge and dipole polarization in two seemingly mutually-exclusive applications in electrets and electrical insulation, the role of space-charge profiling method in finding better electret materials, better poling methods or controlling undersirable physical processes in electrical insulation systems. Several destructive and nondestructive charge profiling methods are briefly reviewed. The scope of the work, the PPS measurement method and polymer materials studied are mentioned. Section 2 presents the Piezoelectrically-generated Pressure Steps (PPSs) employed in this thesis for charge and dipole polarization profiling together with its working principle and main features. Typical PPS response signal will be shown together with its peculiar characteristic that needs to be noticed when acquiring the PPS signal. The result of PPS studies on several types of polymer materials will be presented from Section 3 to Section 6 which are based on 4 peer-review publications published on international conference proceedings and focus on three groups of materials studied, namely: charge storage and transport in polypropylene (PP) surface treated with phosphoric acid, low density polyethylene/magnesium oxide (LDPE/MgO) nanocomposites and spatial polarization profiling of poly(vinylidenefluoride-co-trifluoroethylene) (P(VDF-TrFE)) poled with hysteresis cyclical poling method (the Bauer cyclical poling method). Specifically,

- Section 3 is based on Publication I: “Piezoelectrically-generated Pressure Steps (PPSs) for studying charge distributions on corona-charged polypropylene (PP) films”
- Section 4 is based on Publication II: “Depth profile and transport of positive and negative charge in surface (2-D) and bulk (3-D) nanocomposite film”
- Section 5 is based on Publication III: “LDPE/MgO nanocomposite dielectrics for electrical-insulation and ferroelectret-transducer applications”
- Section 6 is based on Publication IV: “Non-uniform polarization profiles in PVDF copolymers after cyclical poling”

General conclusions and future work will conclude the thesis in Section 7.

2 Probing charges and dipoles in polymer dielectrics with Piezoelectrically-generated Pressure Steps (PPSs) - The PPS method and its features

The Piezoelectrically-generated Pressure Steps (PPSs) method was invented by Professor Eisenmenger and colleagues in 1982 [96, 97]. It belongs to the group of nondestructive testing method to probe electric charge and/or dipole polarization distribution in thin polymer films and slabs. The idea of this nondestructive testing is to irradiate pressure-waves propagating in the dielectric bulk. This travelling pressure wave acts as a virtual probe to collect information about electric charge or field distribution within the dielectric bulk. Original idea of using travelling pressure waves to detect charge or electric field distribution was suggested in 1977 by Collins [98] and Laurenceau, Dreyfus and Lewiner [99]. Several implementations of the method were suggested, differ in the way used to generate the pressure wave, namely a shock-tube [99], a high-voltage spark [100], a ruby-laser, a CO_2 laser [81] and a Nd:YAG laser (LIPP (Laser-Induced Pressure Pulse) method) [101]. All the previous methods generate pressure wave in the form of pulse of short-duration and fast rising time. For the LIPP method, the laser pulse duration is in picosecond range which contribute to the high spatial resolution of the method, down to 1 μm, depending on material properties [101]. The PPS method, instead generates pressure steps travelling to the bulk of the measured sample/specimen which induces a uniform deformation of the sample volume behind the propagating step, instead of a travelling compressed layer through the measured sample/specimen volume like in the case of LIPP method [101]. Another implementation of PPS method to generate a pressure pulse (not step), so-called Piezoelectrically-generated Pressure Pulse (PPP) is also suggested in which a shorter-step duration is created by using a shorter electric square pulse by utilizing a shorter cable-length in the cable-discharge generator [101].

The working principle of PPS method is presented in Figure 13. The PPS setup comprises of a step-voltage generator, a piezoelectric crystal (x-cut quartz crystal with thickness of 3 mm and 25 mm diameter), a preamplifier (with gain of ca. 38 dB and 1 GHz bandwidth) and an oscilloscope (Tektronix DPO5204 with maximum of 2 GHz bandwidth). Laying out diagram of the PPS setup is shown in Figure 14. The cable-discharge generator [101] capable of generating a square voltage pulse of ca. 100 ns duration and a rising time of < 1 ns). Upon applying a square voltage pulse to the piezoelectric crystal, a series of alternating pressure steps [97,101] is coupled to the sample under measurement through a thin layer of silicon oil (coupling oil). This silicon oil layer is squeezed to a thickness of 100 – 200 nm upon applying a moderate static pressure from the rubber electrode (a disk of 5 mm in diameter) and the preamplifier on top of the sample (Figure 14) [97]. The coupling oil layer increases the amplitude of pressure-step coupled to sample and also avoids the rise-time deteriorating resulting from dust particles, the softness of the measured dielectric film and the nonfavourable interfacing of the piezoelectric quartz crystal surface and the dielectric film.

Compared to the LIPP method, the amplitude of pressure-step coupled to sample is at least ten time smaller (ca. 50 kPa) [101]. However, with better reproducibility of pressure step from the piezoelectric crystal, it is advantageous of the PPS method to use sampling and signal averaging method to improve the signal-to-noise ratio of each measurement. Depending on signal amplitude of each measurement at hand, the number of averaging can be chosen accordingly. Typical value is in the range of 500 – 3000 and up to 10 000 averages in this thesis.

Figure 15 shows diagram of a series of pressure steps travel back-and-forth in the quartz

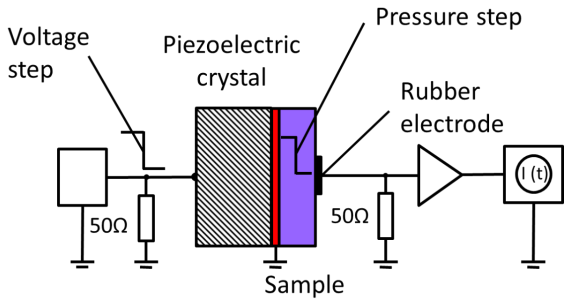

Figure 13: The working principle of Piezoelectrically-generated Pressure Steps (PPSs) method. Adapted from Ref. [102].

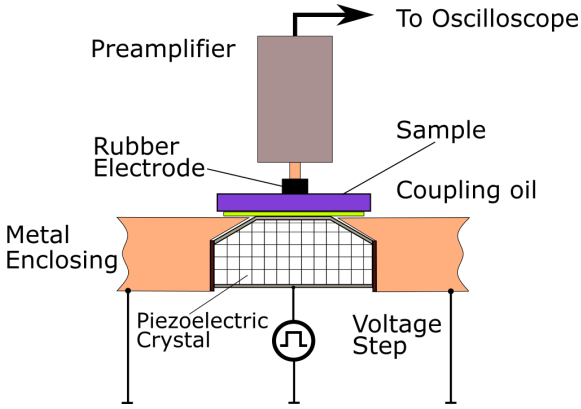

Figure 14: The layout of PPS method.

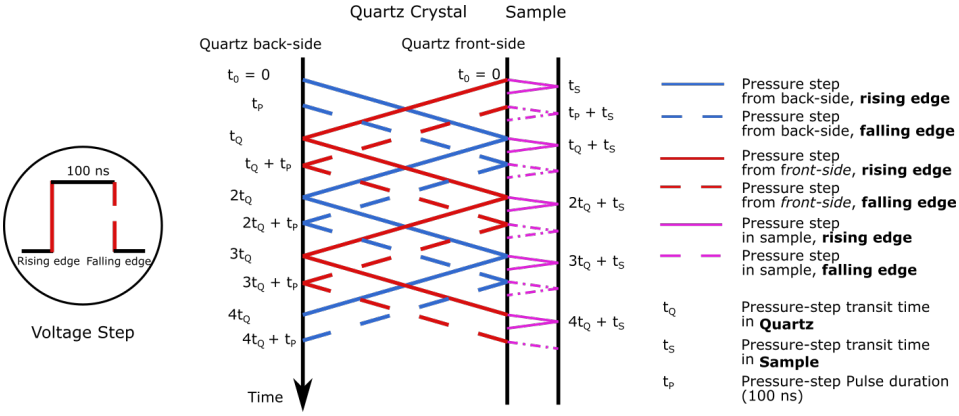

Figure 15: Diagram of a series of pressure reflection in the quartz crystal and sample upon application of a single voltage-step (square pulse voltage) with rising- and falling-edge is in according to the rising- and falling-edge of the voltage-step (or accordingly the pressure-step), respectively. See also Figures 14 and 16.

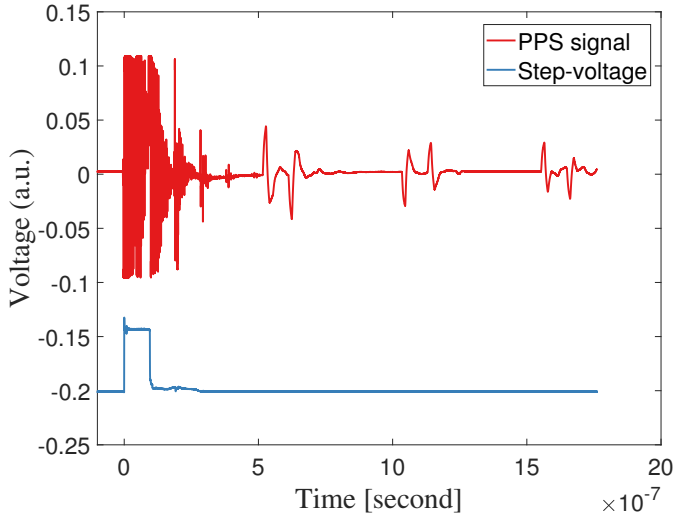

Figure 16: Typical PPS response signal and step-voltage.

crystal and couple into sample upon application of a single square voltage pulse to the quartz crystal. Immediately at the rising edge of the voltage square pulse, two pressure-step pulses start propagating in opposite directions from the front- and back-side of the quartz-crystal (Figures 14 and 15). The pressure-step at the front-side release the first pressure-step pulse into sample with no time delay [97] due to the initial squeezing static pressure applied to sample/quartz front-side interface by the mass of the amplifier, the rubber electrode, etc. and thus create the first response signal from the sample (t_0 = 0 in Figure 15, red solid line). It takes a transit time of t_Q for the pressure-step from the back-side to travel through the thickness of the quartz crystal and to arrive at the front-side quartz/sample interface and to couple into sample another pressure-step and accordingly another sample response signal (at instance t_Q, blue solid line). At this interface, the pressure-step from the back-side is reflected and travels back to the back-side and reaches there at instance $2t_Q$. There, it is again reflected and travels again back to the quartz front-side and couples another pressure-step into sample and another sample response signal (at instance $3t_Q$, blue solid line). Further process of reflection and transit of pressures-step pulses between the quartz front- and back-side carries on similarly to the one described above. For the pressure-step started at the quartz front-side (t_0 =0, red solid line), it takes a transit time of t_Q to reach the quartz back-side, reflects there, travels backward to the front-side and couples a pressure-step to sample and thus another sample response signal at instance of $2t_Q$. There, it is again reflected, travels backward back-side, is reflected at the back-side and travels backward to front-side and creates another sample response signal (at instance $4t_Q$, red solid line), etc. These sample response signal at instances of t = 0, t_Q, $2t_Q$, $3t_Q$, $4t_Q$... are in accordance to the resulting pressure-steps coupled to sample by the two travelling pressure-steps created at the front- and back-side of the quartz at the rising-edge of the voltage-step.

However, the voltage-step from the step-voltage generator is a square voltage pulse of duration t_P (t_P = 100 ns in this thesis) (Figure 16). So, at the falling-edge of the square voltage pulse, another two travelling pressure-steps are created at the quartz front-side and

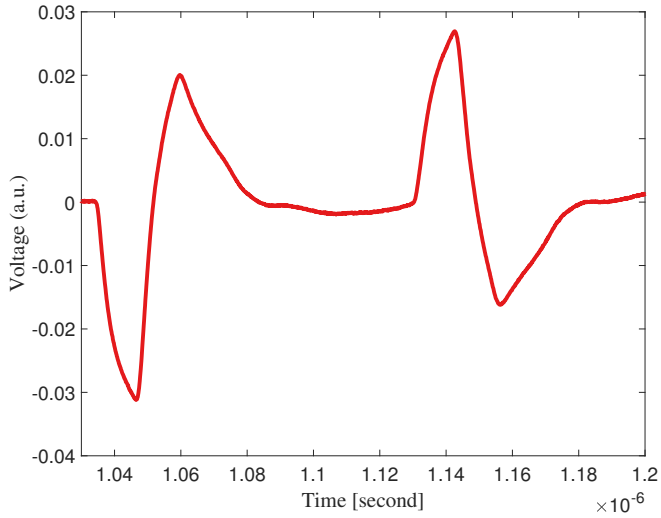

Figure 17: Inverting PPS response signals according to rising- and falling-edge of pressure step. They belong to the third response signal group in Figure 16, separated by ca. 100 ns.

back-side, at instance t_P ($t_P \ll t_Q$) (blue and red dashed line in Figure 15). These two travelling pressure-steps (falling-edge) start to behave similarly to the two travelling pressure-steps (rising-edge) above but delay by the time amount of t_P and create sample response signal at instances of t = t_P, $t_Q + t_P$, $2t_Q + t_P$, $3t_Q + t_P$, $4t_Q + t_P$, etc. These intertwined pressure-steps from the front and back-side of the quartz crystal according to the rising-edge and falling-edge of the voltage square pulse (different by the amount of voltage step duration t_P) release a series of pressure-steps coupling into sample and creating sample response signal with inverting waveforms. The further the time elapses, the further the pressure-step is distorted and attenuated from the initial "ideal step waveform" with fast rising or falling-edge and the further the distortion and attenuation of the sample response signal.

Typical PPS signal is presented in Figure 16. As can be seen from Figure 16, in the PPS response signal (red), there are several groups of sample signal (four in this case, with the first signal group is covered under large noise) with each group of signal is separated from each other by about 500 ns. These signal groups are in response to a series of pressure-steps coupled to sample from the front and acoustically-free back side of the piezoelectric quartz crystal [97] (Figures 14 and 15) upon application of the rising-edge and the falling-edge of the voltage step. 500 ns is the transit time (t_Q) of a pressure-step between the two faces of the quartz crystal of thickness 3 mm with c_Q = 5960 m/s is the longitudinal sound velocity in fused quartz [103] :

$$t_Q = \frac{x_Q}{c_Q} = \frac{3mm}{5960m/s} = 503.3ns \tag{1}$$

Sample response signal according to the rising-egde and the following falling-edge of the voltage-step (pressure-step) is shown in Figure 17. The two inverting response signal are separated by ca. 100 ns in according to the time duration of the rising-edge and falling-edge of the step-voltage. Most of the sample PPS response signal shown in this thesis

was taken in the range of ca. 1 μs (the third group of sample signal) (Figures 16 and 17) according to pressure-step of the voltage-step rising-edge, starting from the front-side of the quartz crystal, after travelling back and forth one cycle in the quartz crystal and coupling to sample (transit time of 2 * 503.3 ns = 1006.6 ns).

Pressure step coupling from the quartz to sample propagates in the sample bulk and creates a compression of the sample volume behind the pressure step wave-front, which travels with the sample's speed of sound c_S. For sample contains real charge and/or dipole polarization, the inhomogeneous compression of the sample created by the travelling pressure-step creates a temporary rearrangement of induced charge and manifests itself as a short-circuit current on sample electrodes. This recorded short-circuit current is a direct image of electric field or polarization distribution profile in sample bulk [8, 9, 83, 84, 101, 102, 104, 105]. For the case of dielectric sample with charge-compensated polarization [96, 97, 106, 107] the short-circuit current is given as [105]

$$I(t) = \frac{A}{L}\frac{p}{\rho_0 c_S}\left[P_r(z = c_S t) - e_i(z = c_S t)\right] \tag{2}$$

in which p, ρ_0, c_S, P_r and e_i are the pressure amplitude, the dielectric sample mass density, the sample longitudinal sound velocity, the remanent polarization and the intrinsic piezoelectric constant, respectively. A, L, z are the sample effective electrode area, the sample thickness and the thickness spatial coordinate, respectively. If the intrinsic piezoelectric constant is either known or negligible, the polarization distribution $P_r(z)$ could be measured directly. For the case of a pure real charge distribution, the current $I(t)$ is given as [105]

$$I(t) = \frac{A}{L}\frac{p}{\rho_0 c_S}(1+\gamma)\,\varepsilon_0 \varepsilon E\,(z = c_S t) \tag{3}$$

where γ, $E(z)$ is the electrostriction constant and the sample spatial electric field intensity, respectively. The charge distribution $\rho(z)$ can be obtained with $dI(t)/dt$ (Poisson's equation). The PPS method does not require a numerical deconvolution procedure. Due to the fact that the voltage square pulse (and accordingly the pressure square pulse) has limited pulse duration (100 ns in this thesis), the PPS method is only suitable for measurement of thin film dielectrics (up to several hundred of micrometer depending on the sound velocity of travelling pressure wave in sample, as long as the transit time of sound in sample is less than 100 ns). The spatial resolution of the method is defined as the distance travelled by the pressure wave during the risetime (ca. 1 ns) of the pressure step [108] and can be as low as 2 μm depending on material properties (material longitudinal sound velocity).

The PPS method had been mostly used by its inventor, Professor Eisenmenger and his colleagues working in related field of electret research (see Section 1.1 for review). Materials which have been studied with PPS are listed in Table 1, mostly focus on PVDF and its copolymers. From the PPS studies of PVDF and its copolymers, the following observations for PVDF and its copolymers have been documented:

- Thermal poling of PVDF at moderate electric field usually leads to inhomogeneous polarization distribution with polarization peak positing near the anode (positive electrode) during thermal poling process [96, 105] while increasing the poling field (> 100 MV/m) tends to improve the inhomogeneities [109]. Similarly, homogeneous poling of PVDF at room temperature is usually attainable only with strong field (> 100 MV/m) [109–111]. It is noted that the inhomogeneous distribution of PVDF could not be improved - even by poling at very high electric field - if it had been initially poled with moderate electric field at room temperature (around the coercive field) [111] and such a behaviour could be related to charge injection from

poling electrodes and trapped at the boundary of the ferroelectric crystallites [96, 97, 106, 107, 111, 112]. It is stressed that polarization and piezoelectricity distribution in PVDF depend critically on the poling method and the specific parameters used in that method [109]. With the help of charge profiling method like PPS it is possible for the optimization of poling parameters of PVDF in transducer applications [109, 113, 114]. A route to homogeneous poling of ferroelectric polymer can also be achived with ferroelectric crystal as electrodes [115] or with polarization hysteresis cycling method (see Section 6).

- The Eisenmenger model [96, 107, 116] of space-charge trapped at the interface of the oriented ferroelectric domains facilitating the retention of these aligned ferroelectric dipoles due to the suppression of the depolarization field. This trapped space-charge at the ferroelectric domain interface stabilizes there aligned dipoles and contributes to the superior thermal stability of ferroelectric polarization in PVDF and its copolymer. This trapped space-charge at the ferroelectric domains model is suggested to be universal to all semicrystalline ferroelectric polymers. However, this model is still under debate [112, 117] and it is still unclear about the role and interaction between space-charge and dipoles in the poling and switching process of PVDF and its copolymers [117].

Table 1: Materials have been studied with PPS method compiled from literature.

Materials	References	Notes
PVDF	[96, 118, 119]	Charge injection trapped at crystallites surface and stabilizing these oriented dipoles
	[101]	Comparing PPS and LIPP measurement results
	[120]	Charge carrier transport causes inhomogeneous spatial polarization
	[121]	β crystallites reduce the mobility of negative charge carriers compared to α crystallites
	[122]	Patterned polarization using focused electron beam; charateristic "thermal profiles" in PVDF
	[123]	Reduction of remanent polarization in poled PVDF immersed in different solvents
	[110]	The necessity of combination of polarization distribution measurements with nonlinear optical measurements
	[124]	H_2, F_2 and HF gas emission in poling of PVDF
	[125]	Time evolution of polarization zones in PVDF
	[126]	In-situ PPS measurement with heat-pulse depolarization
	[111]	Space charge injection and trapping prevent homogeneous poling at moderate electric field intensities
P(VDF-TrFE)	[127]	Charge injection trapped at crystallites surface and stabilizes these oriented dipoles
	[128]	Evidence of injected charges participate in the development of remanent polarization and stabilization of oriented crystallites
	[129]	Domain-wall motion observed with video-STM in epitaxial P(VDF-TrFE)
	[130]	Poling-parameters optimization for piezoelectric polymer cables
P(VDF-TFE)	[108]	Poling of single and multilayer films; uniform polarization at high electric field as charge injection is suppressed
	[131]	In-situ PPS measurement of poled film under TSD
P(VDF-HFP)	[132]	Relatively uniform spatial polarization distribution at poling field higher than 150 MV/m
PVDF, FEP	[105]	Comparing PPS and LIMM measurement results
FEP, PETP	[102]	PPS measurements of real-charged electrets
FEP, PTFE, PFA	[133]	Uniform charge distribution in thermally charged PFA and FEP
PETP	[134]	Space charge and dipole interaction of thermally poled PETP
PTFE	[135]	Decay of surface charge in PTFE treated with $TiCl_4$
LDPE, XLPE	[136]	Space charge formation and migration in different types of PE material

3 Publication 1 - Piezoelectrically-generated Pressure Steps (PPSs) for studying charge distributions on corona-charged polypropylene (PP) films

Q. D. Nguyen, J. Wang, D. Rychkov and R. Gerhard
doanguyen@uni-potsdam.de
Institute of Physics and Astronomy, Faculty of Science
University of Potsdam, Karl-Liebknecht-Strasse 24-25, 14476 Potsdam, Germany

Abstract

Charge distributions on thin corona-charged polypropylene (PP) films have been probed by means of non-destructive piezoelectrically generated pressure steps (PPSs). For higher charging levels which lead to higher electric fields between the corona-deposited charges and the charges on the aluminium/chromium (Al/Cr) electrodes, there are some indications of charge injection into the PP films. Additional results will be presented and analyzed with respect to charge injection and other possible influences on the observed charge profiles.

Keywords:

Electro-acoustical probing of charge profiles, Piezoelectrically generated Pressure Steps (PPSs), Polypropylene (PP), Corona charging, Charge storage and transport

Introduction

We investigate charge profiles on one-side Al/Cr metallized PP films (OPP-TSS from Puetz-Folien) (thickness approx. 50 μm) after corona charging at room temperature for ca. 15 s at several different corona voltages. Different surface potentials result in average electric fields between 19 and 90 MV/m. Charge profiles were obtained by means of the PPS method [96, 102]. Overviews of the PPS and other charge-probing methods are found in [83, 84]. In order to preserve the surface charge on the PP sample, a second uncharged, but otherwise identical PP film was inserted between the PPS-generating quartz crystal and the conducting-rubber electrode.

Result

Charge profiles for positively and negatively charged samples are shown in Figures 18 and 19, respectively. It is obvious that the corona-deposited charges are approximately twice as large as the image charges in the front electrode because the other image charges are at the rear electrode on the second uncharged PP film. It also seems that there is some charge injection at higher electric fields.

Conclusion

During the relatively short charging time at room temperature, there may already be some charge injection from the corona-charged surface into the bulk of the film for both polarities, while there seems no injection from the electrode. Further details and possible artefacts will be discussed.

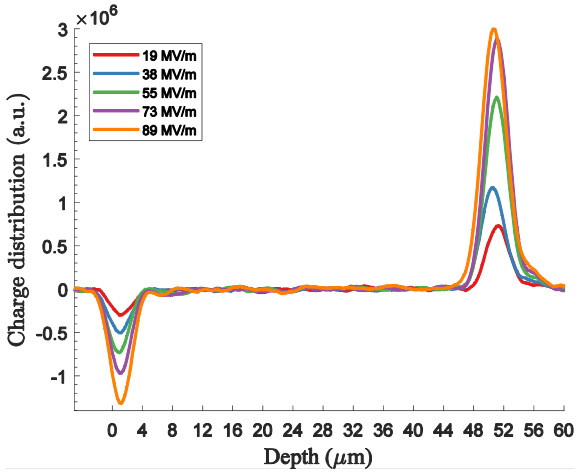

Figure 18: Charge profiles in positively corona-charged PP films. Left: Surface with Al/Cr electrode. Right: Corona-charged film surface.

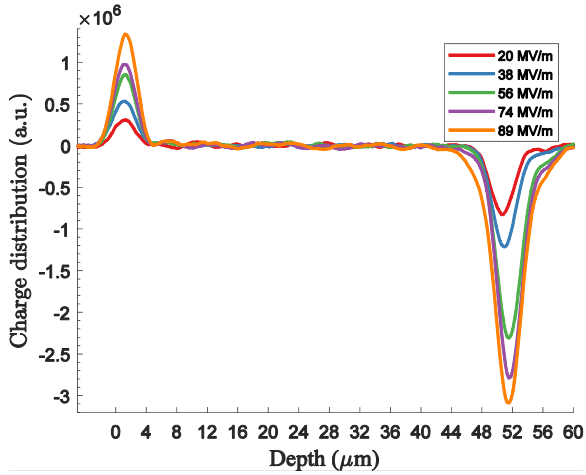

Figure 19: Charge profiles in negatively corona-charged PP films. Left: Surface with Al/Cr electrode. Right: Corona-charged film surface.

Acknowledgements

Q. D. Nguyen gratefully acknowledges funding for his Ph.D. project in Germany from the Vietnamese Ministry of Education and Training (MOET/VIED).

Published in: IEEE 16th International Symposium on Electrets (ISE) Book of Abstracts, 2017, page 145.

3.1 Introduction

In this work, we investigate charge injection and transport in Polypropylene (OPP-TSS from Puetz-Folien) films charged at room temperature (RT) to high initial surface potentials. Some films were linearly heated to elevated temperature levels for partial discharge of corona-deposited charges. The non-destructive Piezoelectrically generated Pressure Step (PPS) method was employed for charge profiling. No charge injection could be detected on PP films charged for short periods of time (ca. 15 sec) with a positive corona discharge. Charge injection can be facilitated via charging with a negative corona discharge or through thermally-assisted charge injection from both film surfaces under the internal electric field.

3.2 Sample

Propypropylene films with a nominal thickness of 50 μm provided by Puetz-Folien (OPP-TSS) were used in this work. They were metallized on one side with 10 nm cromium followed by 100 nm aluminum to provide electrode for better contact in corona-charging, Thermally-stimulated Discharge (TSD) and PPS measurements.

3.3 Experimental method

Corona-charging with corona triode

The samples were cut into circular shapes to be fitted into a sample holder comprising of a metal (aluminum) compact disk (thickness 5 mm) and a metal outer ring (diameter ca. 30 mm). The samples (in sample holder) have been charged by means of a corona discharge in air [137]. The corona voltage was V_c = $\pm$ 12 kV for needle voltage and the control-grid voltage V_g was from $\pm$ 1 kV up to $\pm$ 5 kV.

Thermally-stimulated Discharge

Some samples (in the sample holder) were linearly heated (3 K/min) from RT to different set temperatures in the range of 40 – 120 °C for a partial discharge. Heating plate was computer-controlled. Surface potential was recorded with a non-contacting electrostatic probe (TREK instrument model 341).

Piezoelectrically-generated Pressure Steps (PPSs)

Sample surface charges were first removed by means of liquid ethanol, then charge distributions were measured by means of PPS method [83, 84, 96, 102]. The recorded signal $I(t)$ is proportional to electric-field distribution inside the sample. Charge distribution was obtained by taking the derivative of $I(t)$.

3.4 Result and Discussion

Charge injection to polypropylene sample under corona charging was observed by examining the corresponding charge profile and were experimented in two cases of corona-charging at RT: (i) short charging time (of ca. 15 seconds) and (ii) extended charging time (several hours) . Charge profile was obtained with the PPS measurements.

Figure 20 shows charge profiles of PP sample negatively charged at RT for ca. 15 seconds with final electric-field intensities ranges from 19 MV/m to 92 MV/m. As can be seen from the figure, negative-corona charging with electric field at and higher than 39 MV/m leads to negative charge injection into PP film even at relatively short charging time (right side of the figure). The positive parts of the curves on the right side correspond to pos-

itive image-charge on the rubber electrode of the PPS setup (see Figure 14). The higher the charging electric field intensity, the higher the amount of charge injection into the PP's free surface. Positive charge injection, however, could not be observed at the Al/Cr/PP interface (left side of the figure) even at electric-field intensity as high as 92 MV/m. Similar experiments with positive-corona charging of PP samples (not shown) could not observe the phenomenon of charge injection into PP bulk from the free surface and Al/Cr/PP interface.

The situation is different when PP film is charged under extended charging time (of several hours). Figure 21 presents charge profiles of PP samples corona-charged at RT (electric field intensity of ca. 40 MV/m) both negatively and positively for extended charging time of ca. 17 - 18 hours. As evidence in the figure, electric-charge was injected from both sides of PP film under both charging polarities.

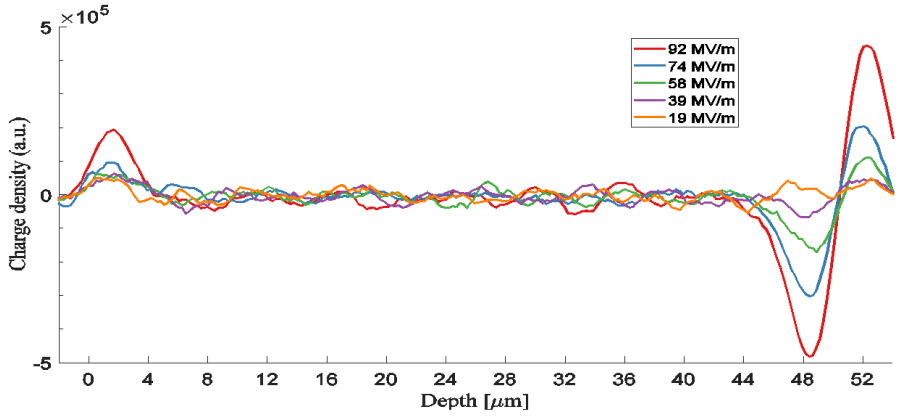

Figure 20: Charge distributions in PP samples negatively corona-charged at RT for ca. 15 seconds with final electric-field intensities as indicated. Each curve corresponds to one sample. Charges are injected from the free surface (right), but blocked at the aluminum/cromium electrode (left).

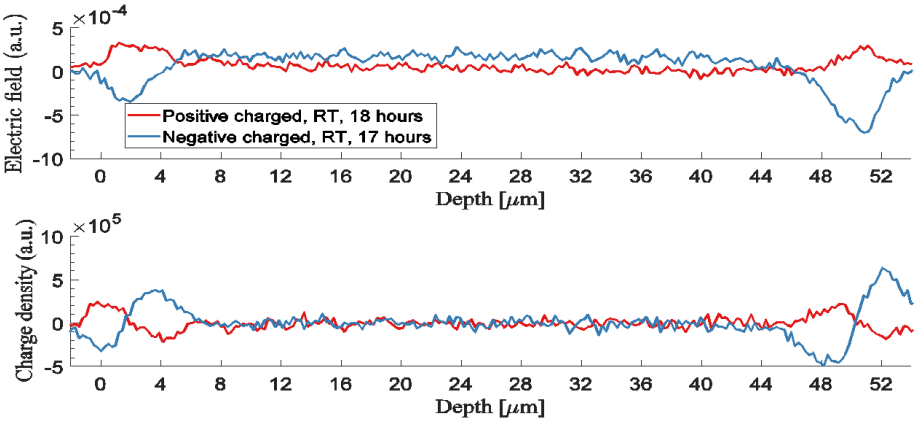

Figure 21: Charge distributions in PP samples negatively (blue) and positively (red) charged at RT for time periods as indicated with a final under electric field of approximately 40 MV/m. Charges are injected from both, the electroded surface (left) and the free surface (right).

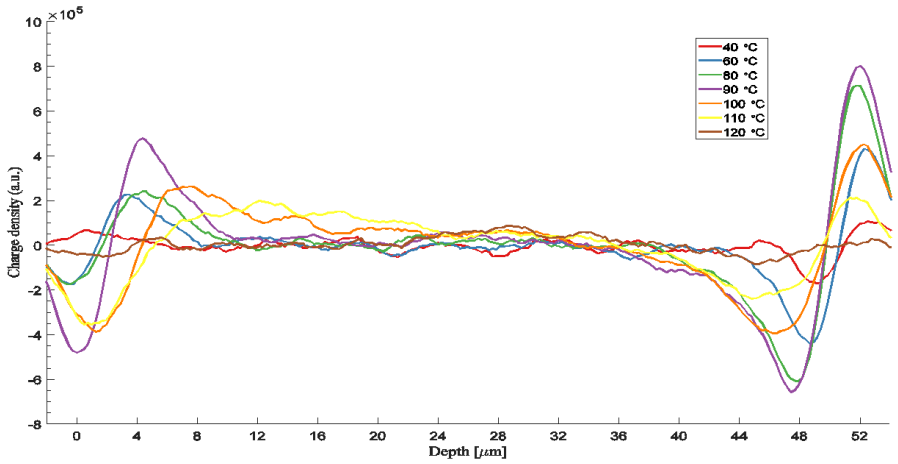

Figure 22: Charge distributions in PP samples negatively corona-charged at RT for ca. 15 seconds with a final electric field of ca. 40 MV/m and linearly heated to temperature levels as indicated for a partial discharging. Each curve corresponds to a different single sample. Charges are injected from both, the electroded surface (left) and the free surface (right).

The transport of corona-deposited charge on PP film was facilitated by thermal energy in TSD measurement. PP samples were charged by negative corona-discharge at RT for 15 seconds at electric field intensity of ca. 40 MV/m. As is shown in Figure 20, negative charge is trapped on the surface and near surface region of the non-metallized side and positive charge on the electrode of the Al/Cr/PP side of the film. Under TSD measurements, by heating the PP sample (in sample holder) to several elevated temperature from 40 — 120 °C, at appropriated temperature, the trapped charges on both PP sides are detrapped from their traps and drift further to the bulk under internal electric field. Following rapid quenching to RT, these drifted charges are retrapped inside the bulk and can be observed by PPS experiment. Figure 22 shows the charge profiles of the negative corona-charge PP films after the above TSD measurements. It should be noted here that before PPS measurement, suface charge layer on the free-surface of each PP film was removed by rinsing with ethanol to prevent unwanted electric field gradient between the PP surface charge and the rubber electrode of PPS (as the rubber electrode diameter is ca. 5 mm, much smaller than sample area of ca. 30 mm). Starting from 40 °C and up to 90 °C, the higher the heating temperature, the higher the amount of charge is injected into the PP bulk from both sides and the deeper the injected depth. Further heating of the sample to higher temperatures leads to reduced amplitude of charge peaks, probably due to neutralization of the two approaching charge clouds of opposite polarities. Upon heating of up to 120 °C, almost no bulk charges present in the sample bulk.

3.5 Conclusion

For Polypropylene film (OPP-TSS from Puetz-Folien) we find:

- Short-time charging (ca. 15 sec), RT, positive corona (electric field of up to approx. 90MV/m): No charge injection from sample surfaces.
- Short time charging (ca. 15 sec), RT, negative corona (electric field higher than ca. 40MV/m): Charge injection from sample free surface only.

- Much longer charging (at ca. 40MV/m) or charging and heating to high temperature levels: Charge injection from both sample surfaces.

Published in: Poster session of the IEEE 16th International Symposium on Electrets (ISE), 2017.

Further detail can be found in Appendix 1.

4 Publication 2 - Depth Profile and Transport of Positive and Negative Charge in Surface (2-D) and Bulk (3-D) Nanocomposite Films

Quyet D. Nguyen, Jingwen Wang, Dmitry Rychkov and Reimund Gerhard
Institute of Physics and Astronomy, Faculty of Science, University of Potsdam
Karl-Liebknecht-Strasse 24-25, 14476 Potsdam, Germany

Abstract

In the present study, the charge distribution and the charge transport across the thickness of 2- and 3-dimensional polymer nanodielectrics was investigated. Chemically surface-treated polypropylene (PP) films and low-density polyethylene nanocomposite films with 3 wt % of magnesium oxide (LDPE/MgO) served as examples of 2-D and 3-D nanodielectrics, respectively. Surface charges were deposited onto the nonmetallized surfaces of the one-side metallized polymer films and found to broaden and to thus enter the bulk of the films upon thermal stimulation at suitable elevated temperatures. The resulting space-charge profiles in the thickness direction were probed by means of Piezoelectrically-generated Pressure Steps (PPSs). It was observed that the chemical surface treatment of PP which led to the formation of nano-structures or the use of bulk nanoparticles from LDPE/MgO nanocomposites enhance charge trapping on or in the respective polymer films and also reduce charge transport inside the respective samples.

Keywords:

LDPE nanocomposites, MgO nanoparticles, Space charge, Charge transport, Charge stability, Acoustic probing of electric-field profiles, Piezoelectrically generated Pressure Steps (PPSs)

4.1 Introduction

The observed reduction of the electrical conductivity in many nanocomposites was suggested to originate from the interface between the nanoparticles/ nanostructures and the polymer matrix [58, 138, 139]. The interface is thought to provide deep traps for charge carriers and to thus prevent further charge injection and/or transport in the nanocomposite bulk [58, 139, 140]. In this paper, charge distribution and transport in "2-D nanocomposites" (PP films surface-treated with phosphoric acid (H_3PO_4)) and "3-D nanocomposites" (LDPE/MgO nanocomposites) are studied. Charge layers were deposited on the nonmetalized surfaces of the polymer films and found to move from the surface into the bulk of the films during thermal stimulation. The resulting charge profiles were obtained by means of Piezoelectrically-generated Pressure Steps (PPSs). The measurements provide further evidence that the surface nanostructures/nanoparticles contribute to the enhanced space charge trapping and reduced charge transport observed in the nanocomposite films.

4.2 Samples and Measurement Methods

A. Samples

1) Oriented polypropylene films: Oriented-polypropylene (PP) commercial films with a nominal thickness of 50 μm were provided by Puetz Folien and were metalized first with 10-nm of chromium (Cr) and then with 100-nm of aluminum (Al) on one side of the films.

The other side of the film was left unmetallized. On surface-treated films, the open surface was brought in contact with H_3PO_4 solution (Carl Roth® 85 %) for 24 hours at 120 ° C. Afterwards the surface-treated samples were thoroughly washed with water and dried before further experiments. Two groups of polypropylene films were used: (i) as-received samples (no treatment; reference group) and (ii) chemically surface-treated samples. Further information about the two groups of polypropylene films can be found in Ref. [43].

2) Low-density polyethylene/magnesium oxide nanocomposite films: LDPE/MgO films (ca. 75 μm thick) were obtained by compression moulding of LDPE/MgO pellets containing LDPE powder doped with 200 ppm of the antioxidant Irganox 1076 and 3 wt % of MgO nanoparticles (crystallites of ca. 10 nm in size [141]). The LDPE/MgO nancomposite films were prepared by the polymer technology group at the Royal Institute of Technology (KTH) in Stockholm and kindly provided by Professor Gubanski (Chalmers University of Technology, Sweden) to us for further investigation. Additional information on the LDPE/MgO nanocomposite films and their preparation can be found in Ref. [141]. Commercial LDPE films (ca. 52 μm thick) from Goodfellow were used as reference samples. LDPE (Goodfellow) and LDPE/MgO 3 wt % films were evaporated first with 10 nm Cr and then with 100 nm Al on the rear side. The front side of the films was left unmetallized.

B. Measurement methods

1) Corona discharge in air: The polymer films were mounted in a sample holder consisting of a compact aluminum disk (thickness ca. 5 mm) and an outer ring with a diameter of ca. 30 mm. Surface charges were deposited on the non-metalized surfaces of polymer samples by means of a corona discharge in air (corona triode system) [142] at room temperature (RT). The charging time was 15 seconds. The point electrode voltage was $\pm$ 12 kV while the grid electrode voltage was varied between $\pm$ 1 and $\pm$ 3 kV. For negative corona charging of PP films, the grid electrode voltage was set to $-$ 2 kV; for corona charging of LDPE/MgO films, the grid electrode voltage was chosen to yield an average electric field of approx. 26 kV/mm across a film.

2) Thermally-stimulated Surface-Potential Decay: A sample in its sample holder was heated at 80 ° C for 4 hours and the surface potential was recorded as a function of time. The surface potential was measured with a non-contact electrostatic voltmeter (TREK model 341) with an accuracy of $\pm$ 5 V. The partial discharging of the corona-deposited charges on polymer films was done by combining Thermally-Stimulated Discharge (TSD) with rapid quenching of the polymer sample back to room temperature. For TSD, the polymer sample (and its sample holder) was heated from room temperature to several elevated temperatures at a heating rate of 3 K/min. When the sample temperature reached the desired elevated temperature, the sample (and sample holder) was quickly transferred to a large metal surface nearby (at room temperature) for rapid quenching back to room temperature.

3) Piezoelectrically-generated Pressure Steps (PPSs): PPS [81, 83, 84, 96, 102] were used to probe the electric-field profile across a polymer film. In this work, the PPS signal has not been calibrated so that the electric-field distribution across the thickness of a polymer film is obtained only in arbitrary units. Two different configurations were used for the PPS measurements in this work: (i) single-layer configuration (for PP films) and (ii) double-layer configuration (for LDPE/MgO films). In the single-layer configuration, a single PP film was investigated with the rubber electrode [102, 133] directly applied to the PP-film surface. Upon application of the rubber electrode (diameter ca. 5 mm) to the PP-film surface (diameter ca. 30 mm), a portion of the surface charge (if any) on the PP film is destroyed [133]. To avoid unwanted electricfield gradients between the rubber electrode and the PP film surface, the charge layer on the PP-film surface was removed by washing the

surface thoroughly with ethanol before the PPS measurement. In the double-layer configuration used on the LDPE/MgO films, the surface-charge layer was protected by putting another non-metalized commercial LDPE (Goodfellow) film on top of the LDPE/MgO film free surface before application of the rubber electrode. This configuration allows for the probing of bulk and surface charges on the LDPE/MgO films.

4.3 Result and Discussion

A. Charge distribution and transport in as-received and in chemically treated PP films
Figures. 23 a and b present the charge profile in as-received and chemically surface-treated PP films, respectively, charged in a negative corona and discharged at elevated temperatures. Upon heating of the as-received PP samples to elevated temperatures, surface charges start to move from the open surface and/or from the metal/polymer interface into the polymer bulk. For the chemically treated films, negative charges at the chemically treated surface tend to stay at the surface or in the region near the treated surface. When heated to 120 $^\circ$ C, these deeply trapped negative charges still stay at the near-surface region and force injected positive charge from the metal/polymer interface to advance further and to be more broadly distributed in the bulk of the PP film.

B. Charge distribution and transport in LDPE/MgO nanocomposite films

Being different from the 2-dimensional nanocomposites [43] of the PP films after chemical surface treatment with H_3PO_4, LDPE/MgO nanocomposites possess a truly 3-dimensional composite structure with MgO nanoparticles dispersed in the LDPE polymer matrix. Figure 24 shows Isothermal Surface-Potential Decay (ISPD) curves of as-received LDPE films (Goodfellow) and of LDPE/MgO nanocomposite films charged by means of positive and negative corona discharges. The initial surface potentials were chosen to result in initial average bulk electric fields of approx. 26 kV/mm. Measurements of charge distribution in the nanocomposite films after the above ISPD measurements are shown in Figure 25. From Figure 25 it can be seen that except for a small portion of space-charge in the near-surface regions on both side of the nanocomposite films, no charge is present in a large portion of the nanocomposite bulk.

4.4 Conclusion

In this work, charge distribution and transport in 2- and 3-dimensional polymer nanodielectrics was studied (chemically surface-treated PP and bulk nanocomposite LDPE/MgO, respectively). Confined layers of electric charge were deposited onto the non-metallized surfaces of the polymer films and broadened during thermally-stimulated discharge. It was found that the surface treatment of PP and the nanoparticles in LDPE/MgO films enhance charge trapping and reduce charge transport. On PP films, chemical treatment enhances the negative charge retention at the surface and yields deep negative traps in or near the suface region, while charges are injected from the metal/PP interface on the other side of the film when heated to elevated temperatures. For LDPE/MgO films, when heated to elevated temperatures, originally confined layers of deposited charge stay close to the near-surface region on both sides with no space-charge deeply inside the nanocomposite bulk.

Acknowledgement

Quyet D. Nguyen is indebted to Vietnam's International Education Cooperation Department (VIED) for kindly providing funding towards his PhD project at the University of Pots-

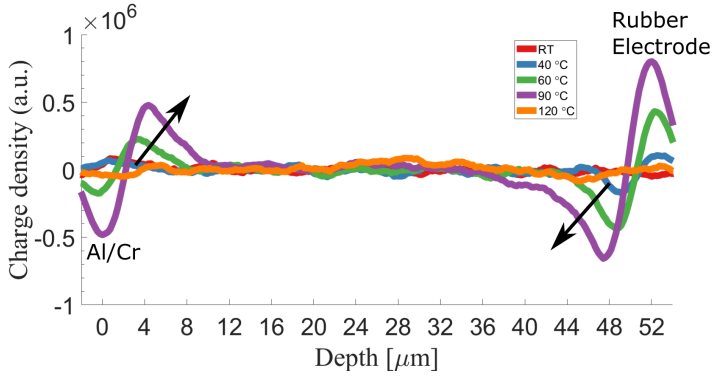

(a) As-received PP

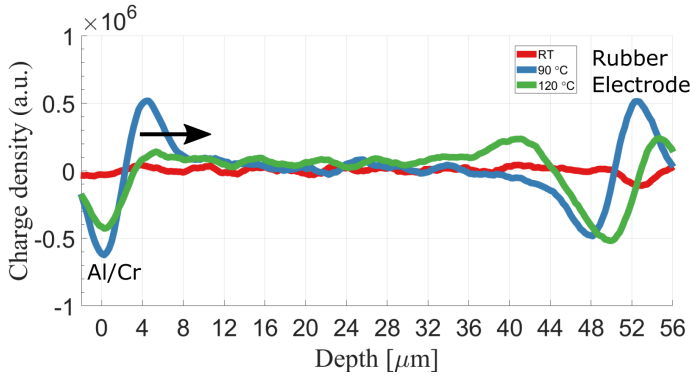

(b) Chemically surface-treated PP

Figure 23: Charge distribution of polypropylene films charged in a negative corona discharge in air at room temperature and partial reduction of deposited charges by heating at 3 K/min to several elevated temperatures followed by rapid quenching back to room temperature for (a) as-received PP films and (b) PP films chemically surface-treated with phosphoric acid.

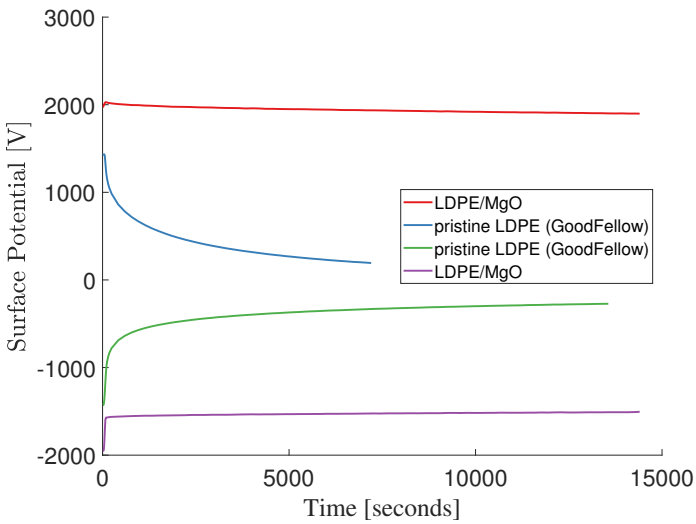

Figure 24: Isothermal Surface-Potential Decay (ISPD) (80 ° C, 4 hours) of as-received LDPE and of LDPE/MgO nanocomposite films. Samples were charged in a corona discharged to an initial surface potential that yield an average electric field of approx. 26 kV/mm in the samples. The thicknesses of the LDPE (Goodfellow) and LDPE/MgO films are ca. 52 and 77 µm, respectively.

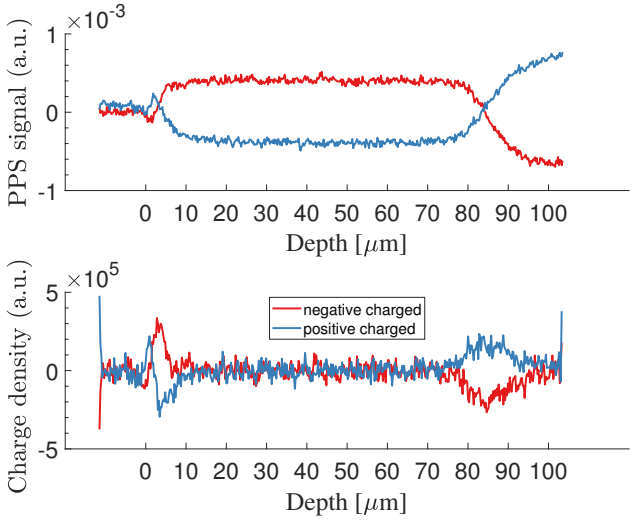

Figure 25: Electric-field and charge distributions in LDPE/MgO nanocomposite films after the Isothermal Surface Potential Decay (ISPD) (80 ° C, 4 hours). The charge layer on non-metalized sample surface was protected with another non-metalized as-received LDPE film. The metalized and the free surface of the LDPE/MgO nanocomposite film are on the left and right side of the figure, respectively. The upper figure shows the electric-field distribution; the lower figure depicts the corresponding charge distribution (the derivative of the electric-field distribution).

dam in Germany.

Published in: © [2019] IEEE. Reprinted, with permission, from Q. D. Nguyen, J. Wang, D. Rychkov, and R. Gerhard, "Depth profile and transport of positive and negative charge in surface (2-d) and bulk (3-d) nanocomposite films," in 2nd IEEE International Conference on Electrical Materials and Power Equipment (ICEMPE), 2019, pp. 300-302.
DOI: 10.1109/ICEMPE.2019.8727256

5 Publication 3 - LDPE/MgO Nanocomposite Dielectrics for Electrical-Insulation and Ferroelectret-Transducer Applications

Q. D. Nguyen and R. Gerhard
doanguyen@uni-potsdam.de
Institute of Physics and Astronomy, Faculty of Science
University of Potsdam, Karl-Liebknecht-Strasse 24-25, 14476 Potsdam, Germany

Abstract

Published results on LDPE/MgO nanocomposites (3 wt%) show that they promise to be good electrical-insulation materials. In this work, the nanocomposites are examined as a potential (ferro-)electret material as well. Isothermal surface potential decay measurements show that charged LDPE/MgO films still exhibit significant surface potentials after heating for 4 hours at 80 °C, which suggests good capabilities of LDPE/MgO nanocomposites to hold electric charges of both polarities. Open tubular-channel ferroelectrets prepared from LDPE/MgO nanocomposite films show significant piezoelectricity with d_{33} coefficients of about 20 pC/N after charging and are stable up to temperatures of at least 80 °C. Thus LDPE/MgO nanocomposites may become available as a new ferroelectret material. To increase their d_{33} coefficients, it is desirable to optimize the charging conditions and the ferroelectret structure.

Keywords:

ferroelectrets, LDPE nanocomposites, electroacoustic probing, space-charge and polarization profiles, thermally stimulated discharge

5.1 Introduction

Differences in technical and economical requirements often lead to large geographical distances between electric-power generation centers and regions of high power consumption. Such situations require power transmission over long geographical distances. With increasing constraints against new overhead electric transmission lines and concerns about environmental impact, electric power-cable transmission lines are more and more often required. To reduce power loss during transmission, transmission voltages need to be high. These requirements lead to a constant need to find new or to improve existing insulation materials so that they can withstand higher operating voltages. Low-density polyethylene (LDPE) has been successfully applied in high-voltage AC (HVAC) power-cable insulation [46] and it is tempting to use LDPE also in high voltage DC (HVDC) power-cable insulation. Essential requirements on HVDC insulation are high dielectric breakdown strength, low electrical conductivity and negligible space-charge accummulation [65]. For HVDC power cable with a nominal operating voltage of 1 MV, the electrical conductivity of new insulating media must be lower by at least a factor of 10 than the current value in cross-linked polyethylene (XLPE) [141]. Adding a small percentage of nanoparticles to the polymer system is a promising approach to develop new polymer composites with enhanced electrical, mechanical and thermal properties.

Insulating materials with very low electrical conductivity usually have a good capability to capture and retain electric charge and to thus promote space-charge accumulation which can lead to distortion of internal electric fields. The field distortion will often cause local electric-field enhancements that can yield accelerated aging processes and even premature failure of insulating systems.

Electrets [9], on the other hand, are materials that have the capability to retain quasi-permanent electric charge and/or electric polarization. The implanted charge and/or oriented polarization are utilized in transducer applications. Ferroelectrets [28, 29] are a new class of electrets that have a foam-like structure with cavities that contain electric charges of both polarities on opposite surfaces and form macroscopic dipoles. Ferroelectrets show quasi-ferroelectric characteristics. Current ferroelectret research is concerned with finding new materials that have better charge-retaining capability, with improving existing materials in their charge-trapping properties [43, 135, 143] or with optimizing the design of ferroelectret systems [36, 41] to attain higher piezoelectricity and/or thermal stability. Polymers that simultaneously show electrical insulation characteristics and electret properties are promising as multifunctional materials. In this work, we studied films of an LDPE/MgO nanocomposite with 3 wt% of magnesium oxide (MgO) nanoparticles. The possibility of the nanocomposite to be both an electrically insulating material and a ferroelectret are presented and discussed.

5.2 Samples and Experiments

LDPE/MgO nanocomposite (3 wt% of MgO nanoparticles) films were provided by Professor Gubanski (Chalmers University of Technology, Sweden) for our study. The nanocomposite films were the result of a research cooperation between the polymer technology groups at the Royal Institute of Technology (KTH) in Stockholm and Chalmers University of Technology in Gothenburg (Sweden) within a project financed by the Swedish Foundation for Strategic Research and Chalmers' Areas of Advance in Energy and in Material Science [144]. The MgO nanoparticles had been produced in the laboratory and mixed with LDPE powder to form LDPE/MgO nanocomposite films. The aim is to achieve precise control of the nanocomposite composition and the level of chemical impurity in order to correlate the composition and the structure with the corresponding macroscopic properties of the nanocomposite film.

MgO nanoparticles were prepared by means of aqueous precipitation of $Mg(OH)_2$ and subsequent calcination at 400 °C for 1 hour. The platelet-shaped MgO nanoparticles (3 wt%) were then thoroughly mixed with ground LDPE powder (Borealis) containing 200 ppm antioxidant (Irganox 1076) dissolved in n-heptan. Pellets were prepared from the LDPE/MgO nanocomposite by extrusion at 150 °C for 6 min at 100 rpm, and final films with a thickness of ca. 80 μm were obtained through compression molding in ambient atmosphere at 130 °C for 10 min under contact pressure and for another 10 min at a compression force of 200 kN. Compressed films were cooled down to 30 °C under the final pressure. More details on the preparation procedure may be found in [141].

Commercial LDPE (without antioxidants or nanoparticles) films from GoodFellow Ltd. (England) were used as reference samples. Films for Thermally-Stimulated Discharge (TSD) and Piezoelectrically-generated Pressure-Steps (PPSs) measurements were metallized on one side with Chromium/Aluminum electrodes (10 nm/ 50 nm thickness, respectively). Ferroelectret [28, 29, 33] film systems assembled from LDPE/MgO films were metallized with the same electrode specifications on both sides for dynamic piezoelectric d_{33} measurements.

5.2.1 Thermally-Stimulated Discharge (TSD)

As-received LDPE (GoodFellow) and LDPE/MgO nanocomposite films were charged at room temperature (RT) in a corona triode system with needle and grid electrode [145] for ca. 15 seconds (with either positive or negative polarities). The needle (point) voltage was $\pm$ 12 kV. The grid-electrode voltage was chosen to achieve initial average electric fields of ap-

prox. 26 kV/mm in the sample bulk. Heating during TSD measurement comprises linear heating from RT to 80 °C (heating rate of ca. 0.67 °C/sec) plus isothermal heating at 80 °C for 4 hours (Isothermal surface-potential decay).

5.2.2 Piezoelectrically-generated Pressure Steps (PPSs)

After TSD, the LDPE/MgO nanocomposite samples were measured with the PPS method [83, 84, 96, 101, 102] to probe their charge distributions. A second non-metallized as-received LDPE film (GoodFellow) of ca. 50 μm thickness was put on top of the LDPE/MgO sample (free, non-metallized surface) to protect its surface charge layer. Pressure steps always entered from the electroded side of the LDPE/MgO nanocomposite film. The longitudinal sound velocity of the LDPE/MgO nanocomposite was estimated as 2.3 km/s. The spatial resolution of the PPS measurement was ca. 3–4 μm.

5.2.3 Open-tubular-channel ferroelectrets

Ferroelectret samples were prepared from LDPE/MgO nanocomposite films with the method of heat fusing around a template (perfluoroalkoxy alkane (PFA) film of 100 μm thickness) plus cutting-off and pulling-out the template [33]. The samples were metallized (10 nm Cr/ 50 nm Al) with circular electrodes (diameter 1.5 cm) on both sides. They were then charged by one of two methods:

- Contact charging at RT for 10 minutes. Charging voltage is $+$ 5 kV.
- Thermal ferroelectret charging at 80 °C for 15 minutes with a contact-charging voltage of $-$ 5 kV [146]. After charging under both electric field and elevated temperature, samples were cooled down to RT under the applied charging voltage.

The piezoelectricity of LDPE/MgO ferroelectret samples after charging was measured by means of the dynamic method [147]. The thermal stability of the piezoelectric d_{33} coefficient was checked by heating nanocomposite ferroelectret samples at 80 °C for 1 or 2 hours. The piezoelectric d_{33} coefficient was then measured again.

5.3 Result and Discussion

5.3.1 LDPE/MgO as electrical insulation

The inclusion of MgO nanoparticles into an LDPE polymer matrix leads to improvements in the observed electrical and thermal properties of the nanocomposite film. The electrical bulk conductivity calculated from charging-current measurement on LDPE/MgO nanocomposite films is ca. 1×10^{-15} S/m after 11 hours under an applied electric field of 32.5 kV/mm at a temperature of 60 °C (UN-MgO 3 wt% according to Fig. 5 of Ref. [141]. The value is 30 times smaller than that of as-received LDPE (3×10^{-14} S/m) and even smaller than that of pure MgO crystals (1×10^{-13} to 1×10^{-12} S/m [141]).

From thermogravimetry, it is known that LDPE/MgO nanocomposite shows a temperature shift of the onset of thermal degradation by ca. $+$ 100 °C compared to that of pristine LDPE (from 250 to 350 °C) [141]. Such a material with very low conductivity usually exhibits very good charge retention, which is a desired property of ferroelectrets and will be assessed and discussed in the following. One drawback of LDPE/MgO nanocomposites is the amount of water uptake connected with the introduction of MgO nanoparticles into the LDPE polymer matrix [58,148]. The amount of water in LDPE/MgO nanocomposites can be as high as 7 times of that in as-received LDPE [58], which may limit the use of LDPE/MgO nanocomposites in electrical insulation for HVDC power cables, unless measures of complete sealing against water/moisture penetration (during manufacturing and operating

full-scale power cables) are adopted [58]. With regard to the ferroelectret application discussed below, the high level of water uptake is also detrimental to the long-term stability of the deposited charge at or near the surfaces of the internal cavities or open channels of the ferroelectret systems, which means reduced service-life of their transducing behavior.

5.3.2 LDPE/MgO as ferroelectret transducer

Figure 26 shows TSD measurements of as-received LDPE (GoodFellow) and of LDPE/MgO nanocomposites charged by means of positive and negative corona discharges. Initial surface potentials were chosen to result in initial average bulk electric fields of approx. 26 kV/mm. For films charged at both polarities, the surface potential decays much faster on as-received LDPE than on LDPE/MgO films. After 30 minutes of heating at 80 °C, only about 30 % of the initial surface potential is left. LDPE/MgO samples retain charges much better. At the end of 4 hours of heating, there is almost no surface potential decay for samples charged at positive polarity. For negatively charged sample, after the initial drop from -2 to -1.5 kV due to the initial fast linear heating, the surface potential remains stable until the end of the isothermal period. The charge distribution in LDPE/MgO samples after 4 hours of heating at 80 °C was measured with the PPS method. From the result in Figure 27, it can be seen that charges of both polarities have been injected from the electrode up to the depth of ca. 5 μm, leaving a layer of induced image charges of opposite polarity on the electrode. Charge injection from the free surface into the bulk is difficult to conclude in this case due to possible errors in the film-thickness measurement (measured with a micrometer screw), film-thickness reduction due to Maxwell stress caused by electric charges of opposite polarity on the surfaces of the LDPE/MgO film under measurement, etc. Nevertheless, it is clear that there is almost no charge present in the film bulk.

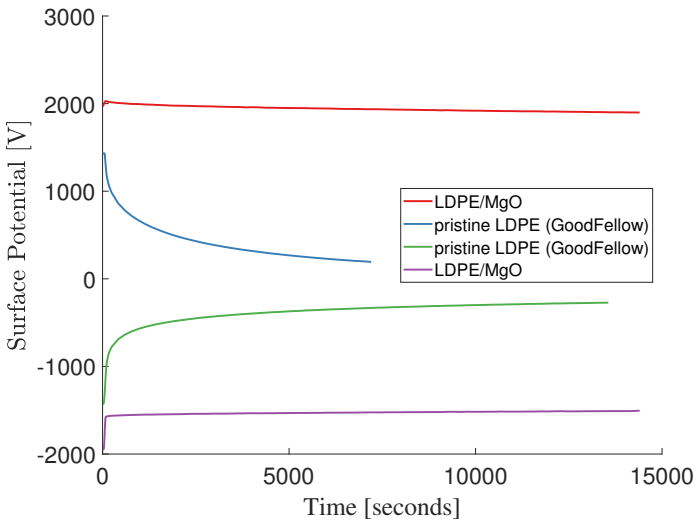

Figure 26: Thermally-Stimulated Discharge (TSD) measurement of LDPE/MgO nanocomposite and as-received LDPE from GoodFellow. The thicknesses of the LDPE/MgO and LDPE films are ca. 77 and 52 μm, respectively. Samples were charged to an initial surface potential that generates an average bulk electric field of approx. 26 kV/mm.

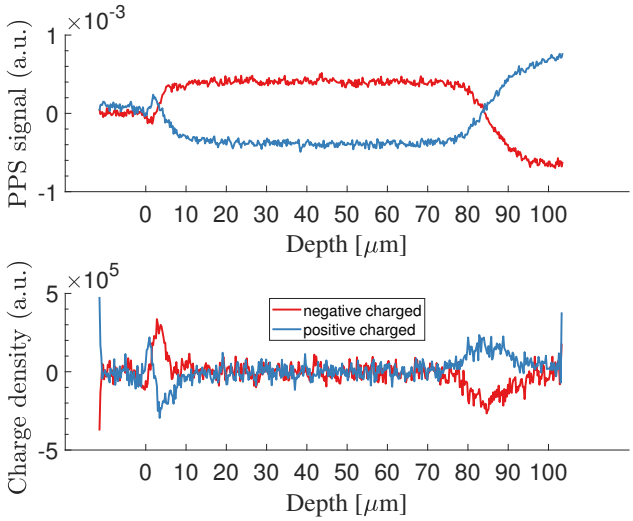

Figure 27: Piezoelectrically-generated Pressure Steps (PPSs) measurements of LDPE/MgO nanocomposite after Thermally-stimulated Discharge (TSD) measurement (80 ° C, 4 hours). The surface charge layer on LDPE/MgO free surface was protected with another non-metallized as-received LDPE sample. Metallized and free surface (protected with as-received LDPE film) are on the left and right side of the figure, respectively. The longitudinal sound velocity in the LDPE/MgO film was estimated as 2.3km/s. The spatial resolution of the current PPS measurement is ca. 3−4 μm. Upper plot shows bulk electric field distribution. Lower plot presents charge distribution, the derivative of the electric-field distribution (Poisson's equation).

Table 2: Remaining piezoelectric coefficient d_{33} [pC/N] of LDPE/MgO nanocomposite ferroelectrets. Heating time is presented in brackets.

Charging temperature	After charging	Charged and heated at 80 °C
RT	35	21 (1 hour)
Therm. charg. 80 °C	30	25 (2 hours)

The good charge retention of LDPE/MgO nanocomposites for both charge polarities suggests a possible ferroelectret material. LDPE/MgO nanocomposite material was also used to prepare open-tubular-channel ferroelectrets with the method presented in [33]. Preliminary thermal-stability measurements of the quasi-static piezoelectric coefficient d_{33} on the LDPE/MgO nanocomposite ferroelectret is shown in Table 2. Together with the TSD result in Figure 26, it can be seen that the piezoelectricity of the tubular-channel ferroelectret sample is quite stable up to temperatures of at least 80 °C. Thus, LDPE/MgO nanocomposites have the potential to be a good electrets.

5.4 Conclusion

The following conclusions can be drawn:

- Electrical-conductivity and thermogravimetry measurements reveal significantly improved electrical and thermal properties of LDPE/MgO nanocomposite films compared to those of as-received LDPE samples. Thus the nanocomposites are promis-

ing as electrical insulation media for high voltage DC or AC power cables.

- LDPE/MgO nanocomposites could also be potential (ferro-)electret materials as evidenced by TSD, PPS and piezoelectric-coefficient (d_{33}) measurements.
- One drawback of LDPE/MgO nanocomposites is the higher amount of water that may diffuse into the nanocomposite system and that can be detrimental to its applications as electrical insulation or electret material. The issue needs to be addressed in future work.

Acknowledgements

Quyet D. Nguyen thanks Vietnam's International Education Department for providing funding for his PhD research in Germany. Professor Gubanski from Chalmers University of Technology (Sweden) is gratefully acknowledged for providing the LDPE/MgO nanocomposite films used in this work.

6 Publication 4 - Non-uniform polarization profiles in PVDF copolymers after cyclical poling

Q. D. Nguyen, T. Raman Venkatesan, W. Wirges and R. Gerhard
Institute of Physics and Astronomy, Faculty of Science
University of Potsdam, Karl-Liebknecht-Strasse 24-25, 14476 Potsdam, Germany

Abstract

Poly(vinylidene fluoride-trifluoroethylene) (P(VDF-TrFE)) copolymers, probably the most often used electro-active polymers, are rendered ferro-, pyro-, and piezoelectric via poling under high electric fields. Uniform polarization profiles across the sample thickness are advantageous or even necessary for most device applications. Here, we attempted to obtain spatially uniform polarization profiles in commercial P(VDF-TrFE) copolymer films with 50/50, 72/28 and 75/25 mol% of VDF/TrFE by means of cyclical hysteresis poling. The polarization profiles were mapped with Piezoelectrically generated Pressure Steps (PPSs), and the resulting depth profiles were correlated with the corresponding hysteresis curves. In addition, Fourier-Transform Infrared (FTIR) spectroscopy was used to identify the β-phase fractions in the P(VDF-TrFE) compositions. 75/25 mol% copolymer samples show the most uniform polarization profiles and the highest remanent polarization of 70 mC/m^2 (as seen from the hysteresis curves) – corresponding to the highest β-phase fraction in comparison (as observed in FTIR measurements).

Keywords:

P(VDF-TrFE) copolymer; ferroelectric polymer; cyclical hysteresis poling (a.k.a. “Bauer poling”); Piezoelectrically generated Pressure Steps (PPSs); spatial polarization profiles

6.1 Introduction

Since the discovery of piezoelectricity in Polyvinylidene fluoride (PVDF) in 1969 [149], there has been extensive research with the aim of improving its piezo-, pyro- and ferroelectric properties. PVDF is utilized in many applications ranging from transducers to memory devices [26]. It is a semicrystalline polymer and exists in at least 5 different crystalline phases, namely the α-, β-, γ-, δ- and ε-phase [138, 150]. Out of the 5 phases, the inherently polar β-phase PVDF has the highest (monomer) molecular dipole moment of 2.1 D. In the β phase, the polymer chains are arranged in a planar zig-zag (all-trans) conformation with all its molecular dipoles in the crystal lattice aligned in the same direction, leading to a rather high net electric polarization [151,152]. The non-polar α-phase is, however, the thermodynamically most stable crystalline modification when prepared by means of normal solution casting at room temperature. It was discovered that copolymerization of vinylidene fluoride (VDF) with trifluoroethylene (TrFE) monomers with a VDF molar content between 50 and 80 mol% leads to a copolymer of P(VDFTrFE) that always crystallizes in the β conformation [151, 153] which is desired in many practical applications owing to its easy preparation and its high piezo- and pyroelectricity. P(VDF-TrFE) copolymer has also been employed in several device applications, especially as transducers, energy-storage capacitors [138, 150] and organic field-effect transistors (OFET) for memory applications [154].

P(VDF-TrFE) film still needs to be poled under high electric fields to render it electroactive (i.e. piezo-, pyro-, and ferroelectric). The most common method to pole ferroelectric polymer electrets is corona poling. However, it is only suitable for applications which do not require high-precision poling [22], as corona poling does not always lead

to uniform distribution of the electrical polarization throughout the poled polymer films [101,155]. Non-homogeneously poled PVDF and P(VDF-TrFE) films exhibit ill-defined transducer properties in particular with respect to their frequency behaviour – as highlighted in PVDF hydrophone [156] and second-harmonic generation applications [110]. One approach for homogeneous poling of ferroelectric polymer films is the so-called "Bauer cyclical poling method" [22, 157, 158]. It was done by forcing the film polarization through several hysteresis cycles, until a reproducible polarization hysteresis is achieved and extra space charge in the poled samples has been "drained off" [22, 110, 157]. The homogeneous distribution of polarization throughout the bulk of the poled film was proven with the pressure-wave propagation method (PWP) [81,157]. In the present paper, a similar procedure to Bauer cyclic hysteresis poling was used on commercial P(VDF-TrFE) films with different compositions.

The resulting polarization profiles were probed by means of Piezoelectrically generated Pressure Steps (PPSs) [96] to ascertain the effectivity of hysteresis poling. Hysteresis loops and polarization depth profiles of successfully poled P(VDFTrFE) copolymer samples will be presented and discussed.

6.2 Samples and Measurement methods

6.2.1 Poly(vinylidene-trifluoroethylene) copolymer samples

Commercial P(VDF-TrFE) copolymer films with molecular compositions of 50/50, 72/28 and 75/25 mol% VDF/TrFE were provided by Piezotech SA in the form of thin films with a thickness of 30, 27 and 48 μm, respectively. All films were metalized on both sides with circular aluminum electrodes (diameter ca. 12-15 mm, thicknesses 50-60 nm) for the polarization-hysteresis (Sawyer-Tower circuit), polarization-distribution and piezoelectric-coefficient measurements.

6.2.2 Polarization hysteresis with a Sawyer-Tower circuit

For poling of the P(VDF-TrFE) films with the Bauer cyclical poling method [22, 157, 158], polarization-hysteresis (*P-versus-E curves*) monitoring in a Sawyer-Tower circuit was used [159]. A sequence of unipolar sinusoidal voltage curves (positive and negative direction) at a frequency of 1 Hz with maximum electric fields of 80 MV/m and 100 MV/m was used for hysteresis poling (cyclical poling process) [160]. The sample was subjected to the first 50 cycles at 80 MV/m, followed by another 50 cycles at 100 MV/m in order to achieve polarization saturation at the respective electric fields.

6.2.3 Spatial polarization-distribution measurements

Piezoelectrically-generated Pressure Steps (PPSs) [81, 83, 84, 96, 102] were used to probe the spatial distribution of the electric polarization inside the sample film. Figure 13 shows the working principle of the PPS method. In this work, the PPS signals are not calibrated (arbitrary units for the ordinate) so that only information about the polarization distribution along the thickness direction of polymer films is obtained. Comparison of the PPS signals from different samples with different thicknesses is thus not possible, since different sample thicknesses would require appropriate scaling of the overall PPS signal amplitudes. Each P(VDF-TrFE) copolymer film was equipped with aluminum electrodes (diameter ca. 12-15 mm) on both sides, which significantly increases the RC-time constant of the PPS signal [102]. In order to reduce the RC-time constant and to increase the signal bandwidth, an additional (non-electroded) poly(ethylene terephthalate) (PET) film with a thickness of ca. 12 μm was inserted between sample and rubber electrode in the PPS measurement [102]. The observed PPS signal is a direct image of the polarization distribution in

Table 3: Table of sample thicknesses, β phase contents (before poling), remanent polarization (P_r) values and calculated piezoelectric (d_{33}) coefficients at the end of the cyclical poling for the diferrent compositions of the P(VDF-TrFE) copolymer.

P(VDF-TrFE)	50/50 mol%	72/28 mol%	75/25 mol%
Sample thickness (μm)	30	27	48
β-phase content (%) (from FTIR)	81	85	87
Remanent polarization (P_r) (mC/m^2)	35	34	70
Piezoelectric (d_{33}) coefficient (pC/N)	-20	-10	-27

the thickness direction of the film under measurement [96]. For P(VDF-TrFE) copolymer films, a longitudinal sound velocity of 2.4 km/s was assumed [161].

6.2.4 Dynamical piezoelectric coefficient (d_{33}) measurements

After cyclical poling (Section 6.2.2), the copolymer films were subjected to dynamic piezoelectric coefficient (d_{33}) measurements [147]. A static force of ca. 4-10 N was applied in order to ensure stable mechanical contact with the metal-plate electrodes of the dynamical piezoelectricity measuring setup. A measuring frequency of 2 Hz was used, and the average value of 6 consecutive measurements was recorded as the d_{33} coefficient of the respective sample.

6.2.5 Fourier-Transformed Infrared (FTIR) Spectroscopy and crystalline phases in the P(VDF-TrFE) copolymers

A Bruker Alpha-P ® FTIR spectrometer operated in the ATR (Attenuated Total Reflection) mode at room temperature was used to investigate the chain conformations and the crystalline phases present in the P(VDF-TrFE) copolymer films with different molar compositions not only qualitatively, but also quantitatively.

6.3 Result and Discussion

The FTIR spectra of the unpoled P(VDF-TrFE) copolymer samples with the three different compositions are shown in Figure 28. The characteristic peaks corresponding to the different crystalline conformations of the copolymer chains are found in the 1500-400 cm^{-1} wavelength section of the FTIR spectra. According to the relevant literature [162–164], the wavenumbers of 1284, 879 and 842 cm^{-1} have been assigned to the polymer chains that are predominantly in the β phase. We can clearly see from the figure that the copolymer shows a strong absorption at these bands - indicating a dominant β phase in all three copolymers, as expected. Subsequently, the wavenumbers at 803, 763 and 613 cm^{-1} [150,165] usually associated with the crystalline fraction in the α phase do not manifest in the form of clear peaks in the spectra. The presence of a certain amount of γ phase is, however, observed via the peak at 505 cm^{-1} [166].

The fraction of the β phase in the individual copolymers with different compositions can be quantified by means of the procedure suggested by Gregorio and Cestari [167]. The values that were observed in our comparative study are found in Table 3. From the table, we can see that the copolymer with 25 mol% TrFE has the highest β-phase content of 87%, while the smallest β-phase fraction is seen in the copolymer with 50 mol% TrFE

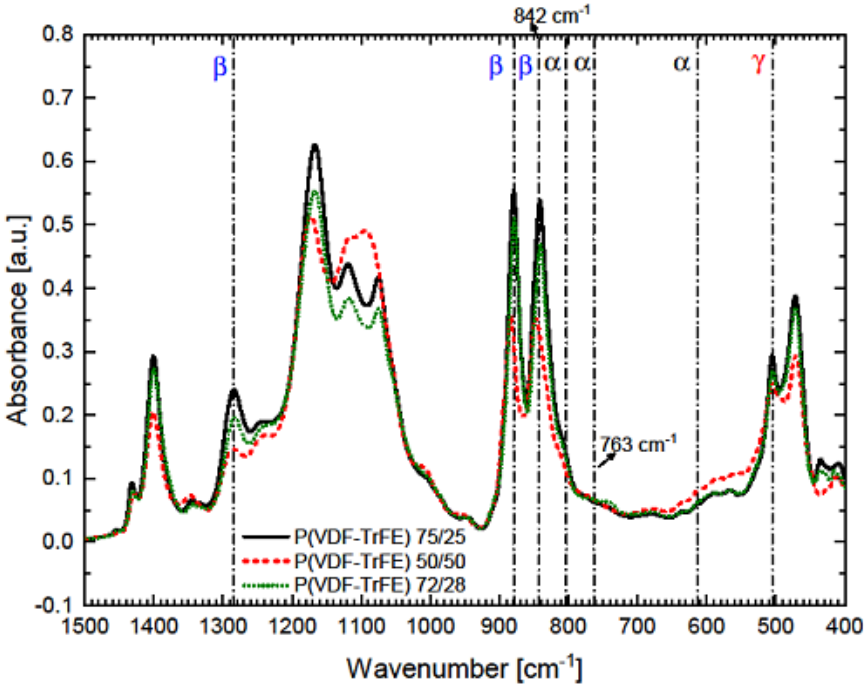

Figure 28: FTIR absorption spectra of P(VDF-TrFE) copolymer films with different molar compositions.

content. The higher fraction of β phase suggests that the 75/25 mol% should also possess superior electrical properties than the other compositions.

Figures 29(a), 30(a) and 31(a) depict the polarization hysteresis of the P(VDF-TrFE) copolymer samples with 50/50, 72/28 and 75/25 mol% composition of VDF/TrFE, respectively, after 50 cycles of poling at 100 MV/m. It can be seen that all three compositions show a clear polarization hysteresis, although with different temporal behaviour. Out of the three compositions, the P(VDF-TrFE) copolymer with 75/25 mol% exhibits the highest remnant polarization (P_r) value of ca. 70 mC/m^2 at the end of the cyclical poling procedure – as shown in Table 3, which corresponds to the fact that this composition shows the highest fraction of β phase and which also leads to a higher d_{33} coefficient (Table 3). The P_r values obtained for the 50/50 and 75/25 mol% compositions are comparable to the values found in the literature [153, 168] for similar compositions.

During cyclical poling at 80 MV/m, the hysteresis curves still continued to grow for all the three compositions at the end of 50 cycles. On increasing the field to 100 MV/m, the hysteresis curves for the 50/50 and 75/25 mol% samples saturated after poling for 10 cycles (Figures 29 and 31), while the hysteresis curve still continued to grow for the 72/28 mol% composition up to the 50th cycle (Figure 30). Following this, the 72/28 mol% sample was poled for additional 50 cycles at 100 MV/m, which again led to further growing hysteresis loops. The P_r values increased from 34 mC/m^2 at the end of 50 cycles to 44 mC/m^2 at the end of 100 cycles at 100 MV/m.

Furthermore, looking at the ferroelectric properties of the P(VDF-TrFE) films with 72/28 mol% as listed in Table 3, and comparing it with the other two compositions, we observe that its properties are between those of the 50/50 and the 75/25 mol% compositions. It

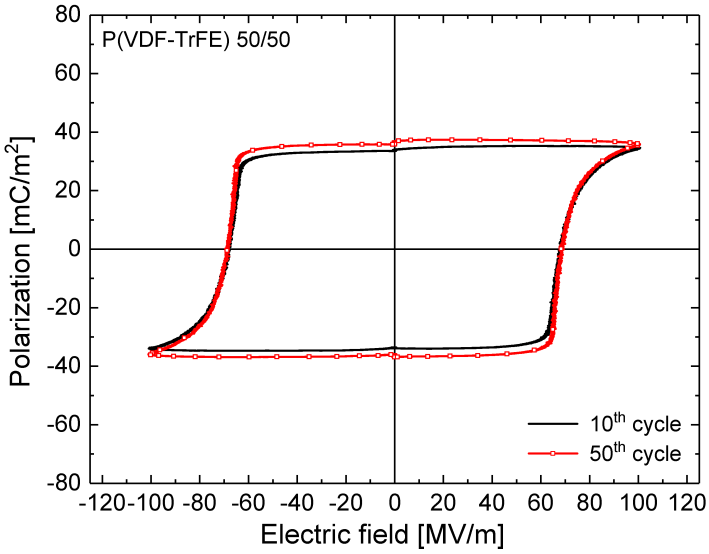

(a) Polarization-vs.-electric-field hysteresis

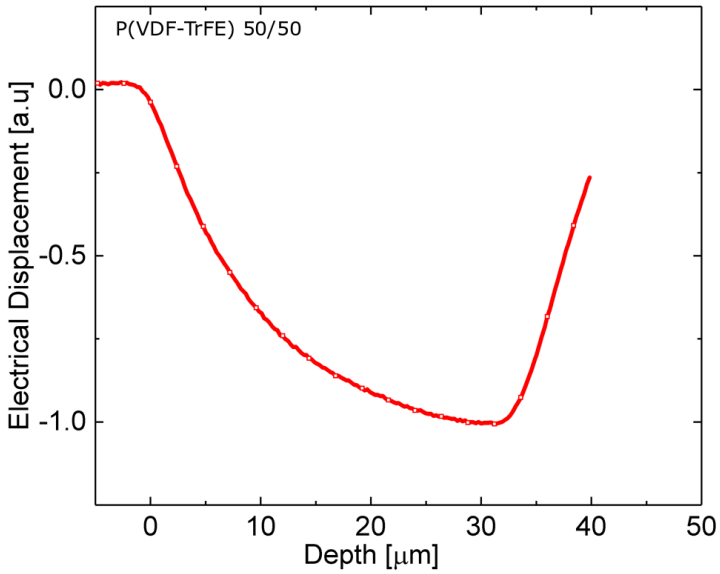

(b) Spatial Polarization Profile

Figure 29: (a) Polarization-vs.-electric-field hysteresis curves for P(VDF-TrFE) copolymer samples with 50/50 mol% composition (tenth and fiftieth poling cycles) and (b) typical spatial polarization profile with the pressure step entering the sample at the electrode that was biased during poling.

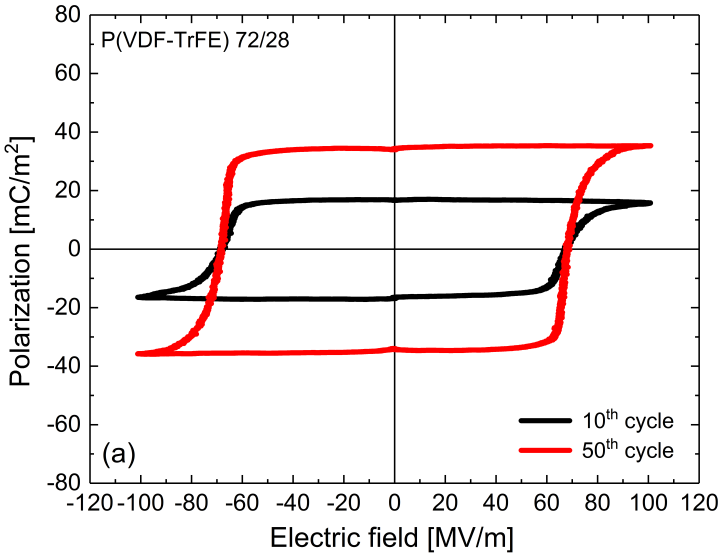

(a) Polarization-vs.-electric-field hysteresis

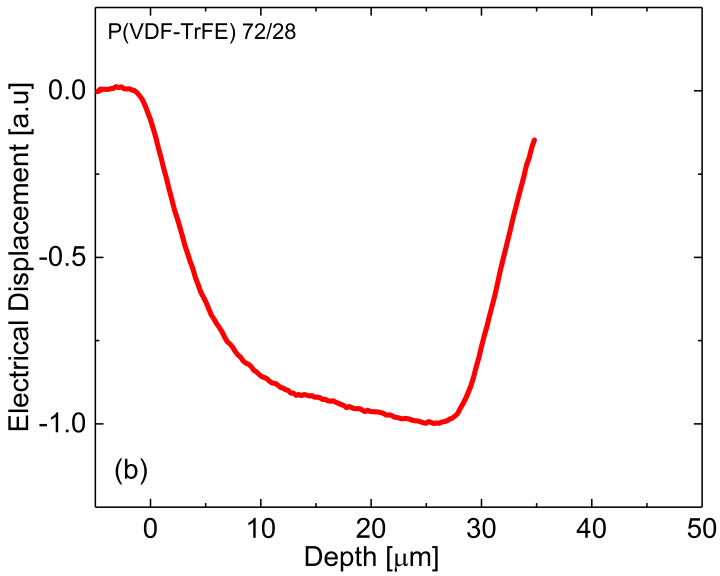

(b) Spatial Polarization Profile

Figure 30: (a) Polarization-vs.-electric-field hysteresis curves for P(VDF-TrFE) copolymer samples with 72/28 mol% composition (tenth and fiftieth poling cycles) and (b) typical spatial polarization profile with the pressure step entering the sample at the electrode that was biased during poling.

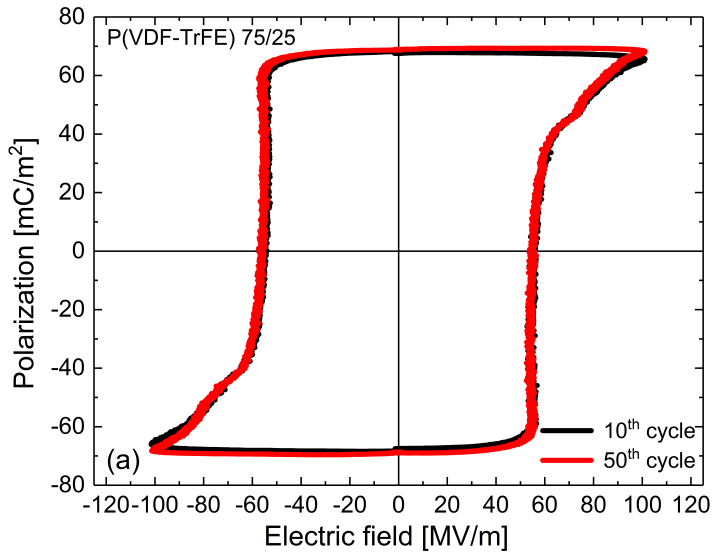

(a) Polarization-vs.-electric-field hysteresis

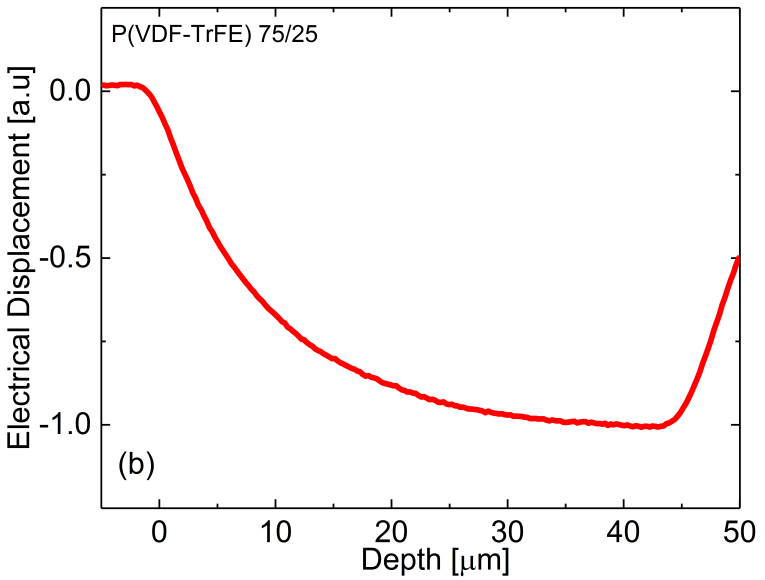

(b) Spatial Polarization Profile

Figure 31: (a) Polarization-vs.-electric-field hysteresis curves for P(VDF-TrFE) copolymer samples with 75/25 mol% composition (tenth and fiftieth poling cycles) and (b) typical spatial polarization profile with the pressure step entering the sample at the electrode that was biased during poling.

has been shown before that the ferroelectric properties increase with the increase in the TrFE ratio when the molar composition of TrFE is between 50 and 80 mol% [26]. All these findings seem to suggest that the ferroelectric polarization in the 72/28 mol% sample has not yet saturated and that a significantly higher number of cycles might be needed for this particular composition in order for the ferroelectric polarization to saturate and for the sample to arrive at similar d_{33} and P_r values as that of 75/25 mol%. However, one has to take into account also the fatigue behavior in the hysteresis curves when samples are poled for a higher number of cycles in the range of 100-1000 cycles [152, 169, 170].

Figures 29(b), 30(b) and 31(b) show the spatial polarization profiles measured with the PPS method for the 50/50, 72/28 and 75/25 mol% compositions, respectively, at the end of poling the samples at 100 MV/m for 50 cycles. From the figures, we observe that all three compositions show fairly non-uniform polarization distributions throughout their sample thickness. Especially for the 50/50 and 75/25 mol% compositions, even though the P_r saturates at the end of cyclical poling at 100 MV/m, the samples still show an inhomogeneous polarization profile. Again, out of the three compositions, the P(VDF-TrFE) samples with 75/25 mol% composition show a better spatial polarization distribution. Thus, we observe that the TrFE content not only influences the ferroelectric properties, but also the uniformity of the polarization across the sample thickness.

6.4 Conclusion

Commercial P(VDF-TrFE) copolymers with VDF/TrFE ratios of 50/50, 72/28 and 75/25 mol% were poled with the Bauer cyclical poling method where the samples have been subjected to 50 hysteresis cycles at an electric field of 80 MV/m, followed by additional 50 cycles at 100 MV/m. The PPS method was used to investigate the uniformity of the polarization distribution across the sample thickness after poling for all three compositions, and the results were compared with the corresponding hysteresis loops. In addition, the ferroelectric sample properties were studied by calculating the β-phase content from FTIR measurements and by measuring the dynamic piezoelectric d_{33} coefficients. Among the three compositions, the 75/25 mol% P(VDF-TrFE) films showed the highest remanent polarization values and d_{33} coefficients along with essentially uniform polarization distributions across the sample thickness – corresponding to the fact that the respective copolymer possessed the highest fraction of the polar β phase, which indicates that the TrFE content affects the uniformity of the polarization distribution. Though the hysteresis loops quickly saturate after 10 cycles for the 50/50 and 75/25 mol% compositions, the respective PPS curves reveal a polarization distribution that as quite non-uniform across the sample thickness even after 50 cycles of poling at 100 MV/m. This suggests that a higher number of poling cycles might still be needed to achieve uniform polarization. The hysteresis behaviour of P(VDF-TrFE) films with 72/28 mol% which does not show a clear hysteresis saturation needs to be analysed further in order to understand the significant differences to the more optimal polymer films with the rather similar composition of 75/25 mol%.

Acknowledgement

The authors are indebted to Dr.rer.nat.habil. Xunlin Qiu (TU Chemnitz) for stimulating discussions. Quyet D. Nguyen is grateful to Vietnam's International Education Cooperation Department (VIED) for funding his PhD project in Germany.

Accepted to be published in: 2019 IEEE International Symposium on Applications of Ferroelectrics (ISAF), 2019, 4 pages.

7 Conclusions and Outlook

The advancement of the two fields of electrets and electrical insulation go hand in hand with the discovery of new dielectric materials with improved relevant properties. For electret applications such as energy harvesting, sensing or actuating, it is necessary of making use of dielectrics with enhanced charge thermal stability and/or higher charge-storage density. Whereas for electrical insulating applications, with the invention of HVDC transmission, it is necessary to find material with reduced DC conductivity, high DC breakdown strength and reduced charge injection and accumulation. The quest to those novel materials requires better space charge profiling method for the understanding of underlying physical processes of the dielectrics when subjected to high electric field to have a better control of them and to enhance desire properties, mitigate or better suppress adverse ones.

This PhD project utilized the Piezoelectrically-generated Pressure Steps (PPSs) as a method for non-destructive probing of electric (real) charge and dipole polarization profiles in a range of polymers from nonpolar (PP as-received and chemically treated with phosphoric acid), polar (P(VDF-TrFE)) and polymer nanocomposites (LDPE/MgO). We had the chance to study the LDPE/MgO nanocomposites from the research collaboration with Professor Gubanski and his research group in Chalmers University (Sweden) with the aim to examine the hypothesis that nano-particles in LDPE/MgO nanocomposites contribute to the enhanced charge trapping capacity of the nanocomposites and further prevent charge injection and/or transport in the bulk of the nanocomposite material. The LDPE/MgO nanocomposites with MgO nanoparticles dispersed in the bulk of LDPE polymer matrix served as an example of 3-dimensional nanocomposites whereas PP chemically treated on the surface served as 2-dimensional nanocomposites case. The results of the research are as follows.

For as-received polypropylene (PP) films, after negative corona charging, negative charges were deposited on the non-metallized (front) surface and positive charges accumulated on the metal/polymer interface on the rear side of the film. Upon partial discharging of the deposited charge by linear heating to several elevated temperatures (thermally stimulated discharge (TSD)), charge distribution measurements show that surface charges were injected from both sides of the as-received film (upon heating up to 90 °C). For PP film chemically treated on the surface with phosphoric acid, negative corona discharge also deposits negative charge on non-metallized surface and positive charge on the metal/polymer interface but upon partial discharging to elevated temperatures up to 120 °C, negative charges tend to reside at the chemically treated surface or near surface region while positive charges inject from the rear side. Upon heating to 120 °C, the stable negative charges trapped at the nonmetallized surface force positive charges to inject and spread over in the bulk of the treated PP films. PP surface treated with phosphoric acid leads to substantial improvement in thermal stability of the trapped charge (for both cases of negative and positive corona discharge). The acid treatment process creates several isolated nanostructures on the treated surface and can be regarded as a 2-dimensional PP nanocomposite case.

For LDPE/MgO nanocomposite film, this is a true 3-dimensional polymer nanocomposites with MgO nanoparticles dispersed in LDPE polymer matrix. Isothermally-stimulated discharge (80 °C, 4 hours) of the corona-deposited charge (on nonmetallized surface and image charge on metal/polymer interface) and charge profiling measurements showed that those deposited charges tend to reside in the surface or close to surface region on both sides of the film where MgO nanoparticles are present. Tubular-channel ferroelectret films prepared from the above LDPE/MgO films once more confirms the stable charge

trapping capacity of LDPE/MgO on the surface with substantial piezoelectric activity (d_{33} coefficient of ca. 30 pC/N) and is stable up to 80 °C (remaining d_{33} of ca. 2/3 initial values).

It is evidenced that nanoparticles on 2-dimensional nanocomposites of PP and 3-dimensional nanocomposites of LDPE/MgO are effective at improving charge trapping capacity and reduce charge injection and transport in the region where nanoparticles are present. The nanoparticles reduce charge injection and transport on both sides of LDPE/MgO nanocomposite film but fail to do so on the non-treated side of PP films. The above measurements also hint that PP treated with phosphoric acid and LDPE/MgO nanocomposites can potentially be material for both electret (ferroelectret) and electrical insulation applications.

For P(VDF-TrFE) copolymer, three compositions of VDF/TrFE (50/50, 72/28 and 75/25 % mol) have been attempted spatially homogeneous poling with the "Bauer cyclical poling" method. Films of each composition were poled by traversing its polarization hysteresis curve (Polarization vs. Electric field curve) several times (50 times at a field of 80 MV/m followed by 50 times at a field of 100 MV/m). All compositions show clear hysteresis polarization with different remnant polarization values. The VDF/TrFE 75/25 % mol composition showed the highest value of remnant polarization (70 mC/m^2) and best temporal hysteresis behavior with consistent hysteresis curve achieved already at the 10^{th} cycle of the polarization hysteresis at 100 MV/m. Spatial polarization distribution measurements show that all profiles of different compositions are not homogeneous and probably higher number of hysteresis traversing is needed. With the 72/28 % mol composition, much slower tempo of hysteresis growth is shown. At 100 MV/m, remnant polarization value stands 15 mC/m^2 and 34 mC/m^2 at 10^{th} and 50^{th} hysteresis cycle, respectively. The reason for the slow hysteresis growth is currently not clear and will be addressed in future studies.

The future work to be carried for 3 groups of materials are as follows.

- For PP chemically treated with phosphoric acid, charge profiling measurements have so far been carried only with films charged negatively with corona discharge. Similar measurement procedure should be carried out with film positively charged to confirm the role of surface-nanostructures on positive charge retention enhancement. Furthermore, as-received PP film could also be treated on both sides of the film and study the effect of charge retention.

- For LDPE/MgO nanocomposites studied in this thesis, the MgO nanoparticles is not surface-treated and large agglomeration of MgO nanoparticles could be found in the obtained LDPE/MgO nanocomposites (see Figure 6 in Ref. [141]). Surface functionalization of MgO nanoparticle by providing long hydrocarbon functional silsesquioxane coatings (8 or 18 hydrocarbon unit longs) [141] improves dramatically MgO nanoparticles dispersion in the final nanocomposites and further reduces DC conductivity (Figures 5 and 6 in Ref. [141]). Charge retention capacity are thus expected to be superior for those LDPE nanocomposites with surface-functionalized MgO nanoparticles.

- For P(VDF-TrFE) the slow tempo of hysteresis growth in the 72/28 % mol VDF/TrFE composition is currently not clear and will be addressed in future studies.

- The Piezoelectrically-generated Pressure Steps (PPSs) method has proven as a powerful method for study of charge storage and transport and polarization distribution in a range of polymer film from nonpolar, to polar and to polymer nanocomposites. However, throughout this thesis, the PPS signal is not calibrated. Much more valuable information can be obtained with quantified space-charge or polarization distribution PPS signal. This issue will be addressed in future works.

- Through studies of 3 groups of material in this thesis that can bear both electret and electrical-insulation applications (PP, LDPE/MgO nanocomposites and P(VDF-TrFE)), it comes to the observation that space-charge and large dipole polarization is not necessarily harmful to dielectrics in electrical insulation application. In proper utilization, they can bring about great benefit [89,171]. Knowledge, experience and experimental methods developed in electrets research are helpful in electrical insulation research and for bridging the two research fields. Certain research results have been achieved in this direction for example the study of electrical insulating properties of PP ferroelectrets [172] and suggestion on incorporation of space-containing fillers (voids) to XLPE layer in HVAC power cable [173] (which is traditionally suggested to be avoided as cause of partial discharge (PD) within HV insulation bulk).

List of Figures

List of Tables

References

[1] Q. D. Nguyen, J. Wang, D. Rychkov, and R. Gerhard, "Piezoelectrically-generated pressure steps (PPSs) for studying charge distributions on corona-charged polypropylene films," in *2017 IEEE 16th International Symposium on Electrets (ISE) Book of Abstracts*. IEEE, 2017, p. 145.

[2] Q. D. Nguyen, J. Wang, D. Rychkov, and R. Gerhard, "Depth profile and transport of positive and negative charge in surface (2-d) and bulk (3-d) nanocomposite films," in *2019 IEEE 2nd International Conference on Electrical Materials and Power Equipment (ICEMPE)*. IEEE, 2019, pp. 300–302, doi:10.1109/ICEMPE.2019.8727256.

[3] Q. D. Nguyen and R. Gerhard, "LDPE/MgO nanocomposite dielectrics for electrical-insulation and ferroelectret-transducer applications," in *2018 IEEE 2nd International Conference on Dielectrics (ICD)*. IEEE, 2018, 4 pages, doi: 10.1109/ICD.2018.8514713.

[4] Q. D. Nguyen, T. Raman Venkatesan, W. Wirges, and R. Gerhard, "Non-uniform polarization profiles in PVDF copolymers after cyclical poling," in *2019 IEEE International Symposium on Applications of Ferroelectrics (ISAF)*. IEEE, 2019, 4 pages (accepted).

[5] A. T. Hoang, Q. D. Nguyen, W. Wirges, R. Gerhard, Y. V. Serdyuk, and S. M. Gubanski, "Open-circuit thermally stimulated currents in LDPE/Al_2O_3 nanocomposite," in *2016 IEEE Conference on Electrical Insulation and Dielectric Phenomena (CEIDP)*, 2016, pp. 611–614, doi: 10.1109/CEIDP.2016.7785595.

[6] D. K. Das-Gupta, "Space charge and dielectric polarization in polymers," in *Proceedings of the 6th International Conference on Properties and Applications of Dielectric Materials (Cat. No.00CH36347)*, vol. 1, 2000, pp. 24–29 vol.1, doi:10.1109/ICPADM.2000.875622.

[7] J. Lewiner, "Space charge and polarization in insulators: a long history with a promising future," *Dielectrics and Electrical Insulation, IEEE Transactions on*, vol. 17, no. 4, pp. 1096–1105, 2010.

[8] J. Lewiner, "Evolution of experimental techniques for the study of the electrical properties of insulating materials," *IEEE Transactions on Electrical Insulation*, vol. EI-21, no. 3, pp. 351–360, 1986, doi:10.1109/TEI.1986.349076.

[9] R. Gerhard(-Multhaupt), "Electrets: dielectrics with quasi-permanent charge or polarization," *Electrical Insulation, IEEE Transactions on*, vol. EI-22, no. 5, pp. 531–554, 1987, doi:10.1109/TEI.1987.299007.

[10] M. Eguchi, "On dielectric polarisation," *Proceedings of the Physico-Mathematical Society of Japan. 3rd Series*, vol. 1, no. 10, pp. 326–331, 1919.

[11] M. Eguchi, "XX. on the permanent electret," *Philosophical Magazine Series 6*, vol. 49, no. 289, pp. 178–192, 1925, doi: 10.1080/14786442508634594.

[12] G. M. Sessler, "Electrets: recent developments," *Journal of Electrostatics*, vol. 51-52, pp. 137–145, 2001, doi: 10.1016/S0304-3886(01)00091-2.

[13] K.-C. Kao, *Dielectric phenomena in solids: with emphasis on physical concepts of electronic processes*. Academic Press, 2004.

[14] I. Graz and A. Mellinger, "Polymer electrets and ferroelectrets as EAPs: Fundamentals," in *Electromechanically Active Polymers: A Concise Reference*, ser. Polymers and Polymeric Composites: A Reference Series, F. Carpi, Ed. Springer International Publishing, 2016, pp. 551–560.

[15] X. Qiu, "Polymer electrets and ferroelectrets as EAPs: Materials," in *Electromechanically Active Polymers: A Concise Reference*, ser. Polymers and Polymeric Composites: A Reference Series, F. Carpi, Ed. Springer International Publishing, 2016, pp. 1–29.

[16] G. M. Sessler, Ed., *Electrets*, 3rd ed. Laplacian Press, 1998, vol. 1, reprint of Ref. [137].

[17] R. Gerhard(-Multhaupt), Ed., *Electrets*, 3rd ed. Laplacian Press, 1999, vol. 2.

[18] R. Gerhard, "From electrode charges on dielectric elastomers to trapped charges and electric dipoles in electrets and ferroelectrets: fundamental and applications-relevant aspects of diversity in electroactive polymers," in *Electroactive Polymer Actuators and Devices (EAPAD) 2016*, vol. 9798. International Society for Optics and Photonics, 2016, p. 97980T, doi: 10.1117/12.2218300.

[19] A. Ghosh, M. Yoshida, K. Suemori, H. Isago, N. Kobayashi, Y. Mizutani, Y. Kurashige, I. Kawamura, M. Nirei, O. Yamamuro, T. Takaya, K. Iwata, A. Saeki, K. Nagura, S. Ishihara, and T. Nakanishi, "Soft chromophore featured liquid porphyrins and their utilization toward liquid electret applications," *Nature Communications*, vol. 10, p. 4210, 2019, doi:10.1038/s41467-019-12249-8.

[20] G. M. Sessler and J. E. West, "Self-biased condenser microphone with high capacitance," *The Journal of the Acoustical Society of America*, vol. 34, no. 11, pp. 1787–1788, 1962, doi: 10.1121/1.1909130.

[21] K. S. Ramadan, D. Sameoto, and S. Evoy, "A review of piezoelectric polymers as functional materials for electromechanical transducers," *Smart Materials and Structures*, vol. 23, no. 3, p. 033001, 2014, doi: 10.1088/0964-1726/23/3/033001.

[22] S. Bauer and F. Bauer, "Piezoelectric Polymers and Their Applications," in *Piezoelectricity: Evolution and Future of a Technology*, ser. Springer Series in Materials Science, W. Heywang, K. Lubitz, and W. Wersing, Eds. Berlin, Heidelberg: Springer Berlin Heidelberg, 2008, pp. 157–177, doi:10.1007/978-3-540-68683-5_6.

[23] S. Rupitsch, *Piezoelectric Sensors and Actuators: Fundamentals and Applications*, ser. Topics in Mining, Metallurgy and Materials Engineering. Springer Berlin Heidelberg, 2018.

[24] S. Bauer and S. B. Lang, "Pyroelectric polymer electrets," *IEEE Transactions on Dielectrics and Electrical Insulation*, vol. 3, no. 5, pp. 647–676, 1996, doi:10.1109/94.544186.

[25] S. B. Lang and S. Muensit, "Review of some lesser-known applications of piezoelectric and pyroelectric polymers," *Applied Physics A*, vol. 85, no. 2, pp. 125–134, 2006, doi: 10.1007/s00339-006-3688-8.

[26] H. Nalwa, *Ferroelectric Polymers: Chemistry: Physics, and Applications*, ser. Plastics Engineering. Taylor & Francis, 1995.

[27] E. Fukada, "History and recent progress in piezoelectric polymers," *IEEE Transactions on Ultrasonics, Ferroelectrics, and Frequency Control*, vol. 47, no. 6, pp. 1277–1290, 2000, doi: 10.1109/58.883516.

[28] R. Gerhard(-Multhaupt), "Less can be more. Holes in polymers lead to a new paradigm of piezoelectric materials for electret transducers," *IEEE Transactions on Dielectrics and Electrical Insulation*, vol. 9, no. 5, pp. 850–859, 2002, doi:10.1109/TDEI.2002.1038668.

[29] S. Bauer, R. Gerhard(-Multhaupt), and G. M. Sessler, "Ferroelectrets: Soft electroactive foams for transducers," *Physics Today*, vol. 57, no. 2, pp. 37–43, 2004, doi:10.1063/1.1688068.

[30] R. A. C. Altafim, H. C. Basso, R. A. P. Altafim, L. Lima, C. V. d. Aquino, L. G. Neto, and R. Gerhard(-Multhaupt), "Piezoelectrets from thermo-formed bubble structures of fluoropolymer-electret films," *IEEE Transactions on Dielectrics and Electrical Insulation*, vol. 13, no. 5, pp. 979–985, 2006, doi: 10.1109/TDEI.2006.247822.

[31] X. Zhang, J. Hillenbrand, and G. Sessler, "Thermally stable fluorocarbon ferroelectrets with high piezoelectric coefficient," *Applied Physics A*, vol. 84, no. 1, pp. 139–142, 2006, doi: 10.1007/s00339-006-3573-5.

[32] X. Qiu, A. Mellinger, M. Wegener, W. Wirges, and R. Gerhard, "Barrier discharges in cellular polypropylene ferroelectrets: How do they influence the electromechanical properties?" *Journal of Applied Physics*, vol. 101, no. 10, p. 104112, 2007, doi: 10.1063/1.2735410.

[33] R. A. P. Altafim, X. Qiu, W. Wirges, R. Gerhard, R. A. C. Altafim, H. C. Basso, W. Jenninger, and J. Wagner, "Template-based fluoroethylenepropylene piezoelectrets with tubular channels for transducer applications," *Journal of Applied Physics*, vol. 106, no. 1, p. 014106, 2009, doi:10.1063/1.3159039.

[34] Z. Sun, X. Zhang, Z. Xia, X. Qiu, W. Wirges, R. Gerhard, C. Zeng, C. Zhang, and B. Wang, "Polarization and piezoelectricity in polymer films with artificial void structure," *Applied Physics A*, vol. 105, no. 1, p. 197, 2011, doi: 10.1007/s00339-011-6481-2.

[35] Y. Li and C. Zeng, "Low-temperature CO2-assisted assembly of cyclic olefin copolymer ferroelectrets of high piezoelectricity and thermal stability," *Macromolecular Chemistry and Physics*, vol. 214, no. 23, pp. 2733–2738, 2013, doi: 10.1002/macp.201300440.

[36] C. Zeng and Y. Li, "Method of manufacture for polymer foam-based piezoelectric material," U.S. Patent US 2017/0 047 505 A1, Oct., 2017, https://patents.google.com/patent/US20170047505A1/en.

[37] M. Wegener and S. Bauer, "Microstorms in cellular polymers: A route to soft piezoelectric transducer materials with engineered macroscopic dipoles," *ChemPhysChem*, vol. 6, no. 6, pp. 1014–1025, 2005, doi: 10.1002/cphc.200400517.

[38] S. Gong, C. Wang, J. Zhang, C. Zhang, J. E. West, and K. Ren, "Monocharged electret generator for wearable energy harvesting applications," *Advanced Sustainable Systems*, vol. 2, no. 5, p. 1700178, 2018, doi: 10.1002/adsu.201700178.

[39] Emfit Ltd. (2016) Emfit ltd. Https://www.emfit.com/.

[40] G. M. Yang, "Thermally stimulated discharge of electron-beam-and corona-charged polypropylene films," *Journal of Physics D: Applied Physics*, vol. 26, no. 4, p. 690, 1993, doi: 10.1088/0022-3727/26/4/024.

[41] X. Zhang, J. Hillenbrand, G. M. Sessler, S. Haberzettl, and K. Lou, "Fluoroethylene-propylene ferroelectrets with patterned microstructure and high, thermally stable piezoelectricity," *Applied Physics A*, vol. 107, no. 3, pp. 621–629, 2012, doi:10.1007/s00339-012-6840-7.

[42] D. Rychkov, R. Alberto Pisani Altafim, X. Qiu, and R. Gerhard, "Treatment with orthophosphoric acid enhances the thermal stability of the piezoelectricity in low-density polyethylene ferroelectrets," *Journal of Applied Physics*, vol. 111, no. 12, p. 124105, 2012, doi:10.1063/1.4729866.

[43] J. Wang, D. Rychkov, and R. Gerhard, "Chemical modification with orthophosphoric acid enhances surface-charge stability on polypropylene electrets," *Applied Physics Letters*, vol. 110, no. 19, p. 192901, 2017, doi:10.1063/1.4983348.

[44] G. Migliavacca, *Advanced Technologies for Future Transmission Grids*. Springer Science & Business Media, 2012.

[45] Wikipedia. (2020) Insulator (electricity). https://en.wikipedia.org/wiki/Insulator_(electricity) (accessed 05th February 2020).

[46] R. Arrighi, "From Impregnated Paper to Polymeric Insulating Materials in Power Cables," *Electrical Insulation, IEEE Transactions on*, vol. EI-21, no. 1, pp. 7–18, 1986, doi:10.1109/TEI.1986.349036.

[47] K. Jager and L. Lindbom, "The continuing evolution of semiconductor materials for power cable applications," *IEEE Electrical Insulation Magazine*, vol. 21, no. 1, pp. 20–34, 2005, doi:10.1109/MEI.2005.1389267.

[48] T. Worzyk, *Submarine Power Cables: Design, Installation, Repair, Environmental Aspects*, ser. Power Systems. Springer Berlin Heidelberg, 2009.

[49] W. Thue, *Electrical Power Cable Engineering, Third Edition*, ser. Power Engineering (Willis). Taylor & Francis, 2011.

[50] G. C. Montanari, P. H. F. Morshuis, M. Zhou, G. C. Stevens, A. S. Vaughan, Z. Han, and D. Li, "Criteria influencing the selection and design of HV and UHV DC cables in new network applications," *High Voltage*, vol. 3, no. 2, pp. 90–95, 2018, doi:10.1049/hve.2017.0098.

[51] S. A. Kulp and B. H. Strauss, "New elevation data triple estimates of global vulnerability to sea-level rise and coastal flooding," *Nature Communications*, vol. 10, no. 1, pp. 1–12, 2019, doi:10.1038/s41467-019-12808-z.

[52] S. Chatzivasileiadis, D. Ernst, and G. Andersson, "The Global Grid," *Renewable Energy*, vol. 57, pp. 372–383, 2013, doi:10.1016/j.renene.2013.01.032.

[53] J. Yu, K. Bakic, A. Kumar, A. Iliceto, L. Beleke Tabu, J. Ruaud, J. Fan, B. Cova, H. Li, D. Ernst, and others, "Global electricity network-Feasibility study," vol. CIGRE Technical Report 775. Study Committee: C1 WG: C1.35, 2019, https://orbi.uliege.be/handle/2268/239969.

[54] L. Ji, X. Jia, A. S. F. Chiu, and M. Xu, "Global Electricity Trade Network: Structures and Implications," *PloS one*, vol. 11, no. 8, pp. e0 160 869–e0 160 869, 2016, doi:10.1371/journal.pone.0160869.

[55] Resource Watch. (2020) World resource watch. https://resourcewatch.org/ (accessed 06th Feb. 2020).

[56] A. Alassi, S. Bañales, O. Ellabban, G. Adam, and C. MacIver, "HVDC Transmission: Technology Review, Market Trends and Future Outlook," *Renewable and Sustainable Energy Reviews*, vol. 112, pp. 530 – 554, 2019, doi:10.1016/j.rser.2019.04.062.

[57] A. Kalair, N. Abas, and N. Khan, "Comparative study of HVAC and HVDC transmission systems," *Renewable and Sustainable Energy Reviews*, vol. 59, pp. 1653–1675, 2016, doi:10.1016/j.rser.2015.12.288.

[58] A. M. Pourrahimi, R. T. Olsson, and M. S. Hedenqvist, "The Role of Interfaces in Polyethylene/Metal-Oxide Nanocomposites for Ultrahigh-Voltage Insulating Materials," *Advanced Materials*, p. 1703624, 2017, doi:10.1002/adma.201703624.

[59] NKT Group. (2017) 640 kV XLPE HVDC cable system. https://tinyurl.com/y3rtt6y2.

[60] I. Baker, "Gutta Percha," in *Fifty Materials That Make the World*. Cham: Springer International Publishing, 2018, pp. 89–91, doi:10.1007/978-3-319-78766-4_17.

[61] M. Farzaneh, S. Farokhi, and W. A. Chisholm, *Electrical Design of Overhead Power Transmission Lines*. McGraw Hill Professional, 2012.

[62] V. Smil, *Creating the Twentieth Century: Technical Innovations of 1867-1914 and Their Lasting Impact*. Oxford University Press, 2005.

[63] K. N. Mathes, "A brief history of development in electrical insulation," in *[1991] Proceedings of the 20th Electrical Electronics Insulation Conference*, 1991, pp. 147–150, doi:10.1109/EEIC.1991.162590.

[64] A. Peacock, *Handbook of Polyethylene: Structures: Properties, and Applications*, ser. Plastics Engineering. Taylor & Francis, 2000.

[65] G. Teyssedre and C. Laurent, "Advances in high-field insulating polymeric materials over the past 50 years," *IEEE Electrical Insulation Magazine*, vol. 29, no. 5, pp. 26–36, 2013, doi:10.1109/MEI.2013.6585854.

[66] N. Hampton, R. Hartlein, H. Lennartsson, H. Orton, and R. Ramachandran, "Long-Life XLPE Insulated Power Cable," in *Proceedings of the 7th International Conference on Insulated Power Cable*. Jicable, 2007, pp. 1–6.

[67] G. Mazzanti and M. Marzinotto, *Extruded Cables for High-Voltage Direct-Current Transmission: Advances in Research and Development*, ser. IEEE Press Series on Power Engineering. Wiley, 2013.

[68] Y. Zhang, J. Lewiner, C. Alquie, and N. Hampton, "Evidence of strong correlation between space-charge buildup and breakdown in cable insulation," *IEEE Transactions on Dielectrics and Electrical Insulation*, vol. 3, no. 6, pp. 778–783, 1996, doi:10.1109/94.556559.

[69] R. A. Anderson and S. R. Kurtz, "Direct observation of field-injected space charge in a metal-insulator-metal structure," *Journal of Applied Physics*, vol. 56, no. 10, pp. 2856–2863, 1984, doi:10.1063/1.333821.

[70] Y. Cao, G. G. Jiang, and S. Boggs, "Guarded needle for "charge injection" measurement," *Review of Scientific Instruments*, vol. 73, no. 8, pp. 3012–3017, 2002, doi:10.1063/1.1492000.

[71] L. A. Dissado and J. C. Fothergill, *Electrical Degradation and Breakdown in Polymers*. P. Peregrinus, 1992.

[72] S. Boggs, "A rational consideration of space charge," *IEEE Electrical Insulation Magazine*, vol. 20, no. 4, pp. 22–27, 2004, doi:10.1109/MEI.2004.1318836.

[73] J. Nelson, *Dielectric Polymer Nanocomposites*, ser. SpringerLink : Bücher. Springer US, 2009, page 203.

[74] T. Takada, "Acoustic and optical methods for measuring electric charge distributions in dielectrics," *Dielectrics and Electrical Insulation, IEEE Transactions on*, vol. 6, no. 5, pp. 519–547, 1999.

[75] T. Yamanaka, S. Maruyama, and T. Tanaka, "The development of DC+/-500 kV XLPE cable in consideration of the space charge accumulation," in *Proceedings of the 7th International Conference on Properties and Applications of Dielectric Materials (Cat. No.03CH37417)*, vol. 2, 2003, pp. 689–694 vol.2, doi:10.1109/ICPADM.2003.1218511.

[76] M. Salah Khalil, "International research and development trends and problems of HVDC cables with polymeric insulation," *IEEE Electrical Insulation Magazine*, vol. 13, no. 6, pp. 35–47, 1997, doi:10.1109/57.637152.

[77] S. Boggs and J. Kuang, "High field effects in solid dielectrics," *IEEE Electrical Insulation Magazine*, vol. 14, no. 6, pp. 5–12, 1998.

[78] J. Martinez-Vega, Ed., *Dielectric Materials for Electrical Engineering*, ser. ISTE. Wiley, 2013.

[79] "CIGRÉ Recommendations for Testing DC Extruded Cable Systems for Power Transmission at a Rated Voltage up to 500 kV," *CIGRÉ TB 496*, pp. 1–36, 2012.

[80] "IEEE Recommended Practice for Space Charge Measurements on High-Voltage Direct-Current Extruded Cables for Rated Voltages up to 550 kV," *IEEE Std 1732-2017*, pp. 1–36, 2017, doi:10.1109/IEEESTD.2017.7949158.

[81] C. Alquie, G. Dreyfus, and J. Lewiner, "Stress-Wave Probing of Electric Field Distributions in Dielectrics," *Physical Review Letters*, vol. 47, no. 20, pp. 1483–1487, 1981, doi:10.1103/PhysRevLett.47.1483.

[82] J. Lewiner, S. Holé, and T. Ditchi, "Pressure wave propagation methods: A rich history and a bright future," *IEEE Transactions on Dielectrics and Electrical Insulation*, vol. 12, no. 1, pp. 114–126, 2005, doi:10.1109/TDEI.2005.1394022.

[83] R. Gerhard(-Multhaupt), "Analysis of pressure-wave methods for the nondestructive determination of spatial charge or field distributions in dielectrics," *Physical Review B*, vol. 27, no. 4, p. 2494, 1983, doi:10.1103/PhysRevB.27.2494.

[84] G. L. Ferreira and R. Gerhard(-Multhaupt), "Derivation of response equations for the nondestructive probing of charge and polarization profiles," *Physical Review B*, vol. 42, no. 12, p. 7317, 1990, doi:10.1103/PhysRevB.42.7317.

[85] "Measurement of Internal Electric Field in Insulating Materials - Pressure Wave Propagation Method," *IEC TR 62836:2013*, pp. 1–12, 2013.

[86] A. Mellinger, R. Flores-Suárez, R. Singh, M. Wegener, W. Wirges, R. Gerhard, and S. B. Lang, "Thermal-Pulse Tomography of Space-charge and Polarization Distributions in Electret Polymers," *International Journal of Thermophysics*, vol. 29, no. 6, pp. 2046–2054, 2008, doi:10.1007/s10765-008-0532-8.

[87] R. F. Suárez, A. Mellinger, M. Wegener, W. Wirges, R. Gerhard-Multhaupt, and R. Singh, "Thermal-pulse tomography of polarization distributions in a cylindrical geometry," *Dielectrics and Electrical Insulation, IEEE Transactions on*, vol. 13, no. 5, pp. 1030–1035, 2006.

[88] A. Mellinger and R. Singh, "Polarization and Space-Charge Profiling with Laser-Based Thermal Techniques," in *Nanomaterials*. Wiley-VCH Verlag GmbH & Co. KGaA, 2012, pp. 729–758, doi:10.1002/9783527646821.ch13.

[89] R. Gerhard, "Dielectric materials for electro-active (electret) and/or electro-passive (insulation) applications," in *2019 IEEE 2nd International Conference on Electrical Materials and Power Equipment (ICEMPE)*. IEEE, 2019, pp. 94–99, doi:10.1109/ICEMPE.2019.8727276.

[90] G. Sessler, "Charge distribution and transport in polymers," *IEEE Transactions on Dielectrics and Electrical Insulation*, vol. 4, no. 5, pp. 614–628, 1997, doi:10.1109/94.625648.

[91] S. Holé, T. Ditchi, and J. Lewiner, "Non-destructive methods for space charge distribution measurements: What are the differences?" *IEEE Transactions on Dielectrics and Electrical Insulation*, vol. 10, no. 4, pp. 670–677, 2003, doi:10.1109/TDEI.2003.1219652.

[92] R. Fleming, "Space charge profile measurement techniques: Recent advances and future directions," *IEEE Transactions on Dielectrics and Electrical Insulation*, vol. 12, no. 5, pp. 967–978, 2005, doi:10.1109/TDEI.2005.1522190.

[93] S. Hole, "Recent developments in the pressure wave propagation method," *IEEE Electrical Insulation Magazine*, vol. 25, no. 3, pp. 7–20, 2009, doi:10.1109/MEI.2009.4976898.

[94] S. Bauer and S. Bauer-Gogonea, "Current practice in space charge and polarization profile measurements using thermal techniques," *Dielectrics and Electrical Insulation, IEEE Transactions on*, vol. 10, no. 5, pp. 883–902, 2003, doi:10.1109/TDEI.2003.1237336.

[95] L. Hamidouche, E. Geron, and S. Hole, "Very high spatial resolution space charge measurement using electro-acoustic reflectometry (EAR)," *IEEE Electrical Insulation Magazine*, vol. 33, no. 5, pp. 9–16, Sep. 2017, doi:10.1109/MEI.2017.8014386.

[96] W. Eisenmenger and M. Haardt, "Observation of charge compensated polarization zones in polyvinylindenfluoride (PVDF) films by piezoelectric acoustic step-wave response," *Solid State Communications*, vol. 41, no. 12, pp. 917–920, 1982, doi:10.1016/0038-1098(82)91235-2.

[97] M. Haardt and W. Eisenmenger, "High resolution technique for measuring charge and polarization distributions in dielectrics by piezoelectrically induced pressure step waves (PPS)," in *Conference on Electrical Insulation Dielectric Phenomena - Annual Report 1982*, 1982, pp. 46–51, doi:10.1109/CEIDP.1982.7726511.

[98] R. E. Collins, "Measurement of charge distribution in electrets," *Review of Scientific Instruments*, vol. 48, no. 1, pp. 83–91, 1977, doi:10.1063/1.1134854.

[99] P. Laurenceau, G. Dreyfus, and J. Lewiner, "New Principle for the Determination of Potential Distributions in Dielectrics," *Phys. Rev. Lett.*, vol. 38, no. 1, pp. 46–49, 1977, doi:10.1103/PhysRevLett.38.46.

[100] A. Migliori and J. D. Thompson, "A nondestructive acoustic electric field probe," *Journal of Applied Physics*, vol. 51, no. 1, p. 479, 1980, doi:10.1063/1.327347.

[101] R. Gerhard(-Multhaupt), G. M. Sessler, J. E. West, K. Holdik, M. Haardt, and W. Eisenmenger, "Investigation of piezoelectricity distributions in poly (vinylidene fluoride) by means of quartz-or laser-generated pressure pulses," *Journal of applied physics*, vol. 55, no. 7, pp. 2769–2775, 1984, doi:10.1063/1.333284.

[102] R. Gerhard(-Multhaupt), M. Haardt, W. Eisenmenger, and G. M. Sessler, "Electric-field profiles in electron-beam-charged polymer electrets," *Journal of Physics D: Applied Physics*, vol. 16, no. 11, p. 2247, 1983, doi:10.1088/0022-3727/16/11/027.

[103] G. Kino, *Acoustic waves: devices, imaging, and analog signal processing*, ser. Prentice-Hall Signal Processing Series. Prentice Hall PTR, 1987.

[104] R. Gerhard(-Multhaupt), "Poly(vinylidene fluoride): A piezo-, pyro- and ferroelectric polymer and its poling behaviour," *Ferroelectrics*, vol. 75, no. 1, pp. 385–396, 1987, doi:10.1080/00150198708008991.

[105] P. Bloss, M. Steffen, H. Schafer, G. Eberle, and W. Eisenmenger, "Polarization and electric field distribution in thermally poled PVDF and FEP," *IEEE Transactions on Dielectrics and Electrical Insulation*, vol. 3, no. 3, pp. 417–424, 1996, doi:10.1109/94.506215.

[106] M. G. Broadhurst, G. T. Davis, J. E. McKinney, and R. E. Collins, "Piezoelectricity and pyroelectricity in polyvinylidene fluoride—A model," *Journal of Applied Physics*, vol. 49, no. 10, p. 4992, 1978, doi:10.1063/1.324445.

[107] W. Eisenmenger, H. Schmidt, and B. Dehlen, "Space charge and dipoles in polyvinylidenefluoride," *Brazilian Journal of Physics*, vol. 29, no. 2, pp. 295–305, 1999, doi:10.1590/S0103-97331999000200011.

[108] S. N. Fedosov, A. E. Sergeeva, G. Eberle, and W. Eisenmenger, "Polarization profiles in corona poled P (VDF-TFE) copolymer studied by piezoelectrically induced pressure step method," *Journal of Physics D: Applied Physics*, vol. 29, no. 12, p. 3122, 1996, doi:10.1088/0022-3727/29/12/028/.

[109] G. Sessler, "Charge Storage in Dielectrics," *IEEE Transactions on Electrical Insulation*, vol. 24, no. 3, pp. 395–402, 1989, doi:10.1109/14.30879.

[110] S. Bauer, G. Eberle, H. Schlaich, and W. Eisenmenger, "Second-harmonic generation with partially poled polymers," *Optics Letters*, vol. 18, no. 1, pp. 16–18, 1993, doi:10.1364/OL.18.000016.

[111] S. Fedosov and A. Sergeeva, "Distribution of the Ferroelectric Polarization in Polyvinylidene Fluoride During Initial Poling and Polarization Reversal," *Journal of Nano- and Electronic Physics*, vol. 11, no. 1, p. 01012, 2019, doi:10.21272/jnep.11(1).01012.

[112] G. M. Sessler, D. K. Das-Gupta, A. S. DeReggi, W. Eisenmenger, T. Furukawa, J. A. Giacometti, R. Gerhard(-Multhaupt), R. Faria, S. Fedosov, L. Brehmer, and others, "Piezo-and Pyroelectricity in Electrets, Caused by Charges, Dipoles or both," *IEEE Trans. Electr. Insul.*, vol. 27, no. 4, pp. 872–897, 1992.

[113] C. Alquié and J. Lewiner, "A new method for studying piezoelectric materials," *Revue de Physique Appliquée*, vol. 20, no. 6, pp. 395–402, 1985, doi:10.1051/rphysap:01985002006039500.

[114] S. Bauer, "Poled polymers for sensors and photonic applications," *Journal of Applied Physics*, vol. 80, no. 10, pp. 5531–5558, 1996, doi:10.1063/1.363604.

[115] B. Ploss and B. Ploss, "Poling of P(VDF-TrFE) with ferroelectrically applied dielectric displacement," *Ferroelectrics*, vol. 184, no. 1, pp. 107–116, 1996, doi:10.1080/00150199608230250.

[116] G. Eberle, H. Schmidt, and W. Eisenmenger, "Piezoelectric polymer electrets," *IEEE Transactions on Dielectrics and Electrical Insulation*, vol. 3, no. 5, pp. 624–646, 1996, doi:10.1109/94.544185.

[117] H. von Seggern and S. Fedosov, "Importance of screening charge dynamics on polarization switching in polyvinylidene fluoride," *Applied Physics Letters*, vol. 91, no. 6, 2007, doi:10.1063/1.2769402.

[118] M. Womes, E. Bihler, and W. Eisenmenger, "Dynamics of polarization growth and reversal in PVDF films," *IEEE Transactions on Electrical Insulation*, vol. 24, no. 3, pp. 461–468, 1989, doi:10.1109/14.30890.

[119] G. Eberle and W. Eisenmenger, "Dynamics of poling PVDF between 25°C and 120°C," in *[1991 Proceedings] 7th International Symposium on Electrets (ISE 7)*, 1991, pp. 388–393, doi:10.1109/ISE.1991.167242.

[120] K. Holdik and W. Eisenmenger, "Charge and polarization dynamics in polymer films," in *1985 5th International Symposium on Electrets (ISE 5)*, 1985, pp. 553–558, doi:10.1109/ISE.1985.7341537.

[121] E. Bihler, K. Holdik, and W. Eisenmenger, "Polarization Distributions in Isotropic, Stretched or Annealed PVDF Films," *IEEE Transactions on Electrical Insulation*, vol. 24, no. 3, pp. 541–544, 1989, doi:10.1109/14.30902.

[122] D. Schilling, K. Dransfeld, E. Bihler, K. Holdik, and W. Eisenmenger, "Polarization profiles of polyvinylidene fluoride films polarized by a focused electron beam," *Journal of Applied Physics*, vol. 65, no. 1, pp. 269–275, 1989, doi:10.1063/1.342536.

[123] B. Dehlen, G. Eberle, and W. Eisenmenger, "Influence of solvents on the polarization distribution in PVDF," in *[Proceedings] 1992 Annual Report: Conference on Electrical Insulation and Dielectric Phenomena*, 1992, pp. 172–177, doi:10.1109/CEIDP.1992.283230.

[124] G. Eberle, H. Schmidt, and W. Eisenmenger, "Influence of poling conditions on the gas emission of PVDF," in , *Conference on Electrical Insulation and Dielectric Phenomena, 1993. Annual Report*, 1993, pp. 263–268, doi:10.1109/CEIDP.1993.378962.

[125] G. Eberle, B. Dehlen, and W. Eisenmenger, "Time development of multiple polarization zones in PVDF," in *1993 Proceedings IEEE Ultrasonics Symposium*, vol. 1, 1993, pp. 529–532, doi:10.1109/ULTSYM.1993.339554.

[126] B. Dehlen, B. Kussner, G. Eberle, and W. Eisenmenger, "Heat pulse depolarization and short-time pyroelectricity of PVDF and copolymer," in *9th International Symposium on Electrets (ISE 9) Proceedings*, 1996, pp. 925–930, doi:10.1109/ISE.1996.578234.

[127] E. Bihler, G. Neumann, G. Eberle, and W. Eisenmenger, "Influence of charge injection on the formation of remanent polarization in P(VDF-TrFE) copolymers," in *Annual Conference on Electrical Insulation and Dielectric Phenomena*, 1990, pp. 140–145, doi:10.1109/CEIDP.1990.201333.

[128] G. Eberle, E. Bihler, and W. Eisenmenger, "Polarization dynamics of VDF-TrFE copolymers," *IEEE Transactions on Electrical Insulation*, vol. 26, no. 1, pp. 69–77, 1991, doi:10.1109/14.68230.

[129] C. Ludwig, G. Eberle, B. Gompf, J. Petersen, and W. Eisenmenger, "Thermal motion of one-dimensional domain walls in monolayers of a polar polymer observed by Video-STM," *Annalen der Physik*, vol. 505, no. 4, pp. 323–329, 1993, doi:10.1002/andp.19935050402.

[130] M. Wegener and R. Gerhard(-Multhaupt), "Electric poling and electromechanical characterization of 0.1-mm-thick sensor films and 0.2-mm-thick cable layers from poly(Vinylidene Fluoride-Trifluroethylene)," *IEEE Transactions on Ultrasonics, Ferroelectrics, and Frequency Control*, vol. 50, no. 7, pp. 921–931, 2003, doi:10.1109/TUFFC.2003.1214511.

[131] B. Küssner, G. Eberle, W. Eisenmenger, S. Fedosov, and A. Sergeeva, "Thermal stability of polarization in P(VDF-TFE) copolymer," *Journal of Materials Science Letters*, vol. 16, no. 5, pp. 368–370, 1997, doi:10.1023/A:1018598412232.

[132] M. Wegener, W. Künstler, K. Richter, and R. Gerhard(-Multhaupt), "Ferroelectric polarization in stretched piezo- and pyroelectric poly(vinylidene fluoride-hexafluoropropylene) copolymer films," *Journal of Applied Physics*, vol. 92, no. 12, pp. 7442–7447, Dec. 2002, doi:10.1063/1.1524313.

[133] R. Gerhard(-Multhaupt), G. Eberle, X. Zhongfu, Y. Guomao, and W. Eisenmenger, "Electric-field profiles in corona- or electron-beam-charged and thermally treated Teflon PTFE, FEP, and PFA films," in *Conference on Electrical Insulation and Dielectric Phenomena, 1992. Annual Report*, 1992, pp. 61–66, doi:10.1109/CEIDP.1992.283248.

[134] D. Gunter, G. Eberle, E. Bihler, and W. Eisenmenger, "Space charge and polarization in PETP at different temperatures," in *[1991 Proceedings] 7th International Symposium on Electrets (ISE 7)*, 1991, pp. 343–348, doi:10.1109/ISE.1991.167234.

[135] D. Rychkov and R. Gerhard, "Stabilization of positive charge on polytetrafluoroethylene electret films treated with titanium-tetrachloride vapor," *Applied Physics Letters*, vol. 98, no. 12, p. 122901, 2011, doi:10.1063/1.3565166.

[136] G. Eberle, I. Muller, and W. Eisenmenger, "Space charge formation and migration in different PE materials," in , *Conference on Electrical Insulation and Dielectric Phenomena, 1995. Annual Report*, 1995, pp. 85–88, doi:10.1109/CEIDP.1995.483582.

[137] G. M. Sessler, Ed., *Electrets*, second enlarged ed. Springer, 1987.

[138] Prateek, V. K. Thakur, and R. K. Gupta, "Recent Progress on Ferroelectric Polymer-Based Nanocomposites for High Energy Density Capacitors: Synthesis, Dielectric Properties, and Future Aspects," *Chemical Reviews*, vol. 116, no. 7, pp. 4260–4317, 2016, doi:10.1021/acs.chemrev.5b00495.

[139] I. Plesa, P. V. Notingher, C. Stancu, F. Wiesbrock, and S. Schlögl, "Polyethylene Nanocomposites for Power Cable Insulations," *Polymers*, vol. 11, no. 1, p. 24, 2019, doi:10.3390/polym11010024.

[140] G. Chen, M. Hao, Z. Xu, A. Vaughan, J. Cao, and H. Wang, "Review of high voltage direct current cables," *CSEE Journal of Power and Energy Systems*, vol. 1, no. 2, pp. 9–21, 2015, doi:10.17775/CSEEJPES.2015.00015.

[141] L. K. H. Pallon, A. T. Hoang, A. M. Pourrahimi, M. S. Hedenqvist, F. Nilsson, S. Gubanski, U. W. Gedde, and R. T. Olsson, "The impact of MgO nanoparticle interface in ultra-insulating polyethylene nanocomposites for high voltage DC cables," *Journal of Materials Chemistry A*, vol. 4, no. 22, pp. 8590–8601, 2016, doi:10.1039/C6TA02041K.

[142] J. A. Giacometti, S. Fedosov, and M. M. Costa, "Corona charging of polymers: recent advances on constant current charging," *Brazilian Journal of Physics*, vol. 29, no. 2, pp. 269–279, 1999, doi:10.1590/S0103-97331999000200009.

[143] D. Rychkov, R. Gerhard, V. Ivanov, and A. Rychkov, "Enhanced electret charge stability on polyethylene films treated with titanium-tetrachloride vapor," *IEEE Transactions on Dielectrics and Electrical Insulation*, vol. 19, no. 4, pp. 1305–1311, 2012, doi:10.1109/TDEI.2012.6260005.

[144] S. M. Gubanski, "Insulating materials for next generations of HVAC and HVDC cables," in *2016 IEEE International Conference on High Voltage Engineering and Application (ICHVE)*, Sep. 2016, pp. 1–6, doi:10.1109/ICHVE.2016.7800823.

[145] J. Giacometti and O. N. Oliveira Jr, "Corona charging of polymers," *Electrical Insulation, IEEE Transactions on*, vol. 27, no. 5, pp. 924–943, 1992, doi:10.1109/14.256470.

[146] X. Qiu, W. Wirges, and R. Gerhard, "Thermal poling of ferroelectrets: How does the gas temperature influence dielectric barrier discharges in cavities?" *Applied Physics Letters*, vol. 108, no. 25, p. 252901, 2016, doi:10.1063/1.4954263.

[147] M. Kappel, M. Abel, and R. Gerhard, "Characterization and calibration of piezoelectric polymers: In situ measurements of body vibrations," *Review of Scientific Instruments*, vol. 82, no. 7, p. 075110, 2011, doi:10.1063/1.3607435.

[148] C. Zou, J. C. Fothergill, and S. W. Rowe, "The effect of water absorption on the dielectric properties of epoxy nanocomposites," *IEEE Transactions on Dielectrics and Electrical Insulation*, vol. 15, no. 1, pp. 106–117, 2008, doi:10.1109/T-DEI.2008.4446741.

[149] H. Kawai, "The Piezoelectricity of Poly (vinylidene Fluoride)," *Japanese Journal of Applied Physics*, vol. 8, no. 7, p. 975, 1969, doi:10.1143/JJAP.8.975.

[150] P. Martins, A. C. Lopes, and S. Lanceros-Mendez, "Electroactive phases of poly(vinylidene fluoride): Determination, processing and applications," *Progress in Polymer Science*, vol. 39, no. 4, pp. 683–706, 2014, doi:10.1016/j.progpolymsci.2013.07.006.

[151] T. Furukawa, "Ferroelectric properties of vinylidene fluoride copolymers," *Phase Transitions*, vol. 18, no. 3-4, pp. 143–211, 1989, doi:10.1080/01411598908206863.

[152] K. Zaitsu, S. Lee, K. Ishibe, T. Sekitani, and T. Someya, "A field-cycle-induced high-dielectric phase in ferroelectric copolymer," *Journal of Applied Physics*, vol. 107, no. 11, p. 114506, 2010, doi:10.1063/1.3429079.

[153] T. Furukawa, "Structure and functional properties of ferroelectric polymers," *Advances in Colloid and Interface Science*, vol. 71-72, pp. 183–208, 1997, doi:10.1016/S0001-8686(97)90017-8.

[154] J. C. Scott and L. D. Bozano, "Nonvolatile Memory Elements Based on Organic Materials," *Advanced Materials*, vol. 19, no. 11, pp. 1452–1463, 2007, doi:10.1002/adma.200602564.

[155] G. M. Sessler and A. Berraissoul, "LIPP investigation of piezoelectricity distributions in PVDF poled with various methods," *Ferroelectrics*, vol. 76, no. 1, pp. 489–496, 1987, doi:10.1080/00150198708016971.

[156] B. Fay, P. A. Lewin, G. Ludwig, G. M. Sessler, and G. Yang, "The influence of spatial polarization distribution on spot poled PVDF membrane hydrophone performance," *Ultrasound in Medicine & Biology*, vol. 18, no. 6, pp. 625–635, 1992, doi:10.1016/0301-5629(92)90077-N.

[157] F. Bauer, "Ferroelectric Properties of PVDF Polymer and VF2/C2F3H Copolymers: High Pressure and Shock Response of PVDF Gauges," *Ferroelectrics*, vol. 115, no. 4, pp. 247–266, 1991, doi:10.1080/00150193.1991.11876611.

[158] F. Bauer and R. A. Graham, "Very high pressure behavior of precisely-poled PVDF," *Ferroelectrics*, vol. 171, no. 1, pp. 95–102, 1995, doi:10.1080/00150199508018424.

[159] B. Dickens, E. Balizer, A. S. DeReggi, and S. C. Roth, "Hysteresis measurements of remanent polarization and coercive field in polymers," *Journal of Applied Physics*, vol. 72, no. 9, pp. 4258–4264, 1992, doi:10.1063/1.352213.

[160] M. Wegener, "Polarization-electric field hysteresis of ferroelectric PVDF films: Comparison of different measurement regimes," *Review of Scientific Instruments*, vol. 79, no. 10, p. 106103, 2008, doi:10.1063/1.2972169.

[161] H. Ohigashi, K. Koga, M. Suzuki, T. Nakanishi, K. Kimura, and N. Hashimoto, "Piezoelectric and ferroelectric properties of P (VDF-TrFE) copolymers and their application to ultrasonic transducers," *Ferroelectrics*, vol. 60, no. 1, pp. 263–276, 1984, doi:10.1080/00150198408017527.

[162] M. Kobayashi, K. Tashiro, and H. Tadokoro, "Molecular Vibrations of Three Crystal Forms of Poly(vinylidene fluoride)," *Macromolecules*, vol. 8, no. 2, pp. 158–171, 1975, doi:10.1021/ma60044a013.

[163] H.-M. Bao, J.-F. Song, J. Zhang, Q.-D. Shen, C.-Z. Yang, and Q. M. Zhang, "Phase Transitions and Ferroelectric Relaxor Behavior in P(VDF/TrFE/CFE) Terpolymers," *Macromolecules*, vol. 40, no. 7, pp. 2371–2379, 2007, doi:10.1021/ma062800l.

[164] K. J. Kim, G. B. Kim, C. L. Vanlencia, and J. F. Rabolt, "Curie transition, ferroelectric crystal structure, and ferroelectricity of a VDF/TrFE(75/25) copolymer 1. The effect of the consecutive annealing in the ferroelectric state on curie transition and ferroelectric crystal structure," *Journal of Polymer Science Part B: Polymer Physics*, vol. 32, no. 15, pp. 2435–2444, 1994, doi:10.1002/polb.1994.090321501.

[165] S. Zhang, B. Chu, B. Neese, K. Ren, X. Zhou, and Q. M. Zhang, "Direct spectroscopic evidence of field-induced solid-state chain conformation transformation in a ferroelectric relaxor polymer," *Journal of Applied Physics*, vol. 99, no. 4, p. 044107, 2006, doi:10.1063/1.2169659.

[166] K. Tashiro, M. Kobayashi, and H. Tadokoro, "Vibrational spectra and disorder-order transition of poly(vinylidene fluoride) form III," *Macromolecules*, vol. 14, no. 6, pp. 1757–1764, 1981, doi:10.1021/ma50007a028.

[167] R. G. Jr and M. Cestari, "Effect of crystallization temperature on the crystalline phase content and morphology of poly(vinylidene fluoride)," *Journal of Polymer Science Part B: Polymer Physics*, vol. 32, no. 5, pp. 859–870, 1994, doi:10.1002/polb.1994.090320509.

[168] B. Chu, X. Zhou, K. Ren, B. Neese, M. Lin, Q. Wang, F. Bauer, and Q. M. Zhang, "A Dielectric Polymer with High Electric Energy Density and Fast Discharge Speed," *Science*, vol. 313, no. 5785, pp. 334–336, 2006, doi:10.1126/science.1127798.

[169] Y. Mabuchi, T. Nakajima, T. Furukawa, and S. Okamura, "Electric-Field-Induced Polarization Enhancement of Vinylidene Fluoride/Trifluoroethylene Copolymer Ultrathin Films," *Applied Physics Express*, vol. 4, no. 7, p. 071501, 2011, doi:10.1143/APEX.4.071501.

[170] S. Z. Yuan, X. J. Meng, J. L. Sun, Y. F. Cui, J. L. Wang, L. Tian, and J. H. Chu, "Abnormal polarization enhancement effects of P(VDF-TrFE) films during fatigue process," *Physics Letters A*, vol. 375, no. 14, pp. 1612–1614, 2011, doi:10.1016/j.physleta.2011.02.064.

[171] L. Zhu, "Exploring Strategies for High Dielectric Constant and Low Loss Polymer Dielectrics," *The Journal of Physical Chemistry Letters*, vol. 5, no. 21, pp. 3677–3687, 2014, doi:10.1021/jz501831q.

[172] X. Qiu, F. Groth, W. Wirges, and R. Gerhard, "Cellular polypropylene foam films as DC voltage insulation and as piezoelectrets — A comparison," *IEEE Transactions on Dielectrics and Electrical Insulation*, vol. 25, no. 3, pp. 829–834, 2018, doi:10.1109/TDEI.2018.007192.

[173] G. Perego, R. Candela, and D. Parris, “High-voltage electric cable,” US Patent US9 837 183B2, Dec., 2017.

Appendix 1

Publication I

Q. D. Nguyen, J. Wang, D. Rychkov, and R. Gerhard, “Piezoelectrically-generated pressure steps (PPSs) for studying charge distributions on corona-charged polypropylene films,” in *2017 IEEE 16th International Symposium on Electrets (ISE) Book of Abstracts*. IEEE, 2017, p. 145

Piezoelectrically generated Pressure Steps (PPS) for studying charge distributions on corona-charged Polypropylene (PP) films

Q. D. Nguyen[1], J. Wang[1], D. Rychkov[1], and R. Gerhard[1]

doanguyen@uni-potsdam.de (Corresponding e-mail address)

[1]Applied Condensed-Matter Physics, Institute of Physics and Astronomy, Faculty of Science, University of Potsdam, Karl-Liebknecht-Strasse 24-25, 14476 Potsdam, Germany

Abstract: Charge distributions on thin corona-charged polypropylene (PP) films have been probed by means of non-destructive piezoelectrically generated pressure steps (PPS). For higher charging levels which lead to higher electric fields between the corona-deposited charges and the charges on the aluminium/chromium (Al/Cr) electrodes, there are some indications of charge injection into the PP films. Additional results will be presented and analyzed with respect to charge injection and other possible influences on the observed charge profiles.

Keywords: Electro-acoustical probing of charge profiles, Piezoelectrically generated Pressure Steps (PPS), Polypropylene (PP), Corona charging, Charge storage and transport

Introduction

We investigate charge profiles on one-side Al/Cr-metallized PP films (OPP-TSS from Puetz-Folien) (thickness approx. 50µm) after corona charging at room temperature for ca. 15 s at several different corona voltages. Different surface potentials result in average electric fields between 19 and 90 MV/m. Charge profiles were obtained by means of the PPS method [1]. Overviews of the PPS and other charge-probing methods are found in [2]. In order to preserve the surface charge on the PP sample, a second uncharged, but otherwise identical PP film was inserted between the PPS-generating quartz crystal and the conducting-rubber electrode.

Results

Charge profiles for positively and negatively charged samples are shown in Figures 1 and 2, respectively. It is obvious that the corona-deposited charges are approximately twice as large as the image charges in the front electrode because the other image charges are at the rear electrode on the second uncharged PP film. It also seems that there is some charge injection at higher electric fields.

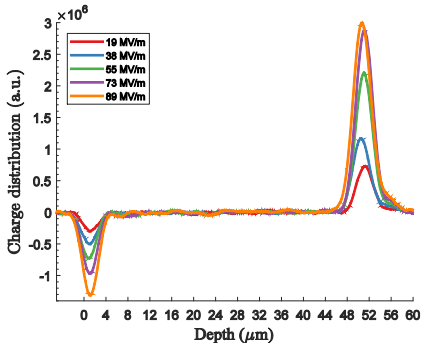

Figure 1: Charge profiles in positively corona-charged PP films. Left: Surface with Al/Cr electrode. Right: Corona-charged film surface.

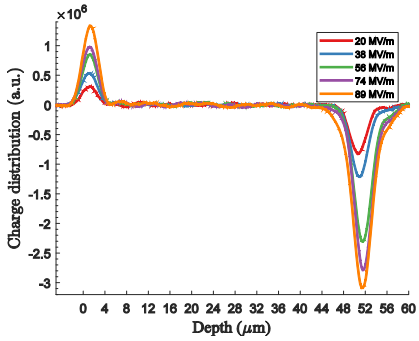

Figure 2: Charge profiles in negatively corona-charged PP films. Left: Surface with Al/Cr electrode. Right: Corona-charged film surface.

Conclusions

During the relatively short charging time at room temperature, there may already be some charge injection from the corona-charged surface into the bulk of the film for both polarities, while there seems no injection from the electrode. Further details and possible artefacts will be discussed.

References

1. W. Eisenmenger and M. Haardt, *Solid State Communications*, Vol. 41, pp. 917–920, **1982**, doi: 10.1016/0038-1098(82)91235-2; R. Gerhard, M. Haardt, W. Eisenmenger and G. M. Sessler, *J. Phys. D: Appl. Phys.*, Vol. 16, pp. 2247-2256, **1983**, doi: 10.1088/0022-3727/16/11/027.
2. R. Gerhard, *Phys. Rev. B*, Vol. 27, pp. 2494-2503, **1983**, doi: 10.1103(PhysRevB.27.2494; G. F. Leal Ferreira and R. Gerhard, *ibid.*, vol. 42, no. 12, pp. 7317–7321, **1990**, doi: 10.1103/PhysRevB.42.7317.

Acknowledgements

Q. D. Nguyen gratefully acknowledges funding for his Ph.D. project in Germany from the Vietnamese Ministry of Education and Training (MOET/VIED).

Piezoelectrically-generated Pressure Step (PPS) for Studying Charge Distribution on Corona-charged Polypropylene (PP) Films

Quyet Doan Nguyen, Jingwen Wang, Dmitry Rychkov, and Reimund Gerhard
Institute of Physics and Astronomy, Applied Condensed Matter Physics,
University of Potsdam, Potsdam, Germany
doanguyen@uni-potsdam.de

Introduction

In this work we investigate the charge injection and transport of Polypropylene (OPP-TSS from Puetz-Folien) film charged at room temperature (RT) to high initial surface potential. Some films were linearly heated to elevated temperature levels for partial discharge of corona-deposited charges. The non-destructive Piezoelectrically-generated Pressure Step (PPS) method was employed for charge profiling. No sign of charge injection with PP film charged at short charging time (ca. 15 sec) with positive corona discharge. Charge injection can be facilitated by charging with negative corona discharge or by thermally-assisted charge injection from both film surfaces under sample internal electric field.

Sample preparation

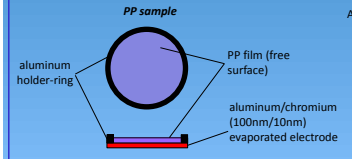

A sketch of bulk charge distribution

(Free-surface charge layer was removed with liquid ethanol)

Measurement procedure

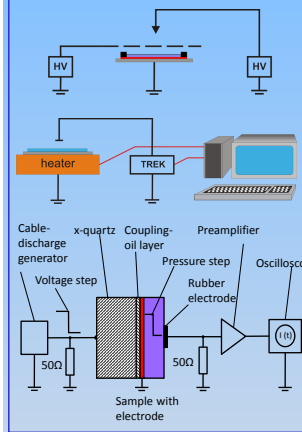

The samples have been charged by corona discharge in air. [1] The corona voltage was V_c=+/-12 kV for needle voltage and the control-grid voltage V_g was from +/-1 kV up to +/-5 kV.

Some samples were linearly (3K/min) heated from RT to different set temperatures in range of (40 – 120) °C to partially discharge. Heating plate was computer-controlled. Surface potential was recorded with a non-contacting electrostatic probe.

Sample surface charges were removed with liquid ethanol, then charge distribution in sample was measured with PPS method.[2-5] Recorded signal I(t) is proportional to electric field distribution in the sample bulk. Charge distribution was obtained by taking the derivative of I(t).

Conclusions

For Polypropylene film (OPP-TSS from Puetz-Folien)

- **Short time (ca. 15 sec), RT, positive corona charge (electric field intensity up to ca. 90MV/m): no charge injection from both sample surfaces.**
- **Short time (ca. 15 sec), RT, negative corona charge (electric field intensity higher than ca. 40MV/m): charge injection from sample free surface only.**
- **Much longer charging time (under ca. 40MV/m) or charged and heated to high temperature levels: charge injection from both sample surfaces.**

Acknowledgement

Q. D. Nguyen gratefully acknowledges funding for his Ph.D. Project in Germany from the Vietnamese Ministry of Education and Training (MOET/VIED).

Experimental results I

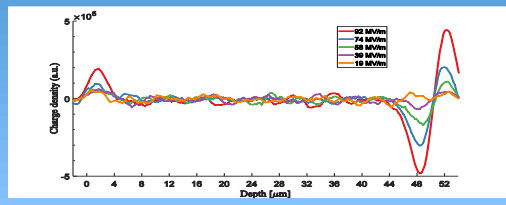

Charge distribution of PP samples charged (RT, ca. 15 sec) under negative-corona discharge with electric field intensity as indicated. Each curve corresponds to individual sample. Charges are injected from free surface (right) but blocked at aluminum/cromium electrode.

Experimental results II

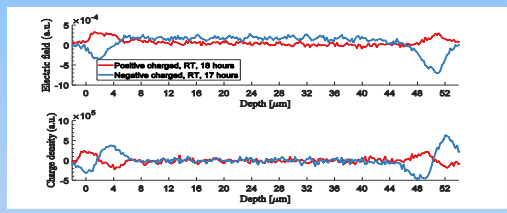

Charge distribution of PP samples charged (RT) under electric field ca. 40 MV/m negatively (blue) and positively (red) for time period as indicated. Charges are injected from both electroded surface (left) and free surface (right).

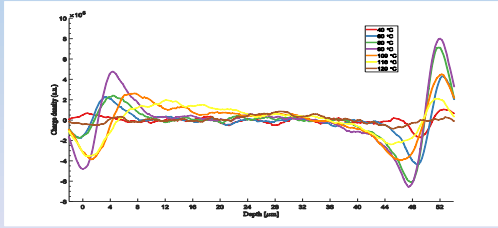

Charge distribution of PP samples charged (RT, ca. 15 sec) under negative-corona discharge (electric field intensity ca. 40 MV/m) and linearly heated (to temperature levels as indicated) to partially discharge. Each curve corresponds to individual sample. Charges are injected from both electroded surface (left) and free surface (right).

References

[1] G. M. Sessler (Ed.), Electrets, 2nd edition Berlin Heidelberg, Germany: Springer-Verlag, 1987.
[2] W. Eisenmenger and M. Haardt, "Observation of charge compensated polarization zones in polyvinylindenfluoride (PVDF) films by piezoelectric acoustic step-wave response," *Solid State Communications*, vol. 41, no. 12, pp. 917–920, 1982, doi:10.1016/0038-1098(82)91235-2.
[3] R. Gerhard-Multhaupt, M. Haardt, W. Eisenmenger, and G. M. Sessler, "Electric-field profiles in electron-beam-charged polymer electrets," *J. Phys. D: Appl. Phys.*, vol. 16, no. 11, p. 2247, 1983, doi:10.1088/0022-3727/16/11/027.
[4] R. Gerhard-Multhaupt, "Analysis of pressure-wave methods for the nondestructive determination of spatial charge or field distributions in dielectrics," *Physical Review B*, vol. 27, no. 4, p. 2494, 1983, doi:10.1103/PhysRevB.27.2494.
[5] G. L. Ferreira and R. Gerhard-Multhaupt, "Derivation of response equations for the nondestructive probing of charge and polarization profiles," *Physical Review B*, vol. 42, no. 12, p. 7317, 1990, doi:10.1103/PhysRevB.42.7317.

Appendix 2

Publication IV

Q. D. Nguyen, T. Raman Venkatesan, W. Wirges, and R. Gerhard, “Non-uniform polarization profiles in PVDF copolymers after cyclical poling,” in *2019 IEEE International Symposium on Applications of Ferroelectrics (ISAF)*. IEEE, 2019, 4 pages (accepted)

Non-uniform polarization profiles in P(VDF-TrFE) copolymer films after cyclical poling

Quyet D. Nguyen, Thulasinath Raman Venkatesan, Werner Wirges, and Reimund Gerhard
Institute of Physics and Astronomy, Faculty of Science, University of Potsdam, Germany
thuraman@uni-potsdam.de

***Abstract*— Poly(vinylidene fluoride-trifluoroethylene) (P(VDF-TrFE)) copolymers, probably the most often used electro-active polymers, are rendered ferro-, pyro-, and piezo-electric via poling under high electric fields. Uniform polarization profiles across the sample thickness are advantageous or even necessary for most device applications. Here, we attempted to obtain spatially uniform polarization profiles in commercial P(VDF-TrFE) copolymer films with 50/50, 72/28 and 75/25 mol% of VDF/TrFE by means of cyclical hysteresis poling. The polarization profiles were mapped with Piezoelectrically generated Pressure Steps (PPSs), and the resulting depth profiles were correlated with the corresponding hysteresis curves. In addition, Fourier-Transform Infrared (FTIR) spectroscopy was used to identify the β-phase fractions in the P(VDF-TrFE) compositions. 75/25 mol% copolymer samples show the most uniform polarization profiles and the highest remanent polarization of 70 mC/m^2 (as seen from the hysteresis curves) – corresponding to the highest β-phase fraction in comparison (as observed in FTIR measurements).**

Keywords*— *P(VDF-TrFE) copolymer; ferroelectric polymer; cyclical hysteresis poling (a.k.a. "Bauer poling"); Piezoelectrically generated Pressure Steps (PPSs); spatial polarization profiles

I. INTRODUCTION

Since the discovery of piezoelectricity in Polyvinylidene fluoride (PVDF) in 1969 [1], there has been extensive research with the aim of improving its piezo-, pyro- and ferroelectric properties. PVDF is utilized in many applications ranging from transducers to memory devices [2]. It is a semicrystalline polymer and exists in at least 5 different crystalline phases, namely the α-, β-, γ-, δ- and ε-phase [3,4]. Out of the 5 phases, the inherently polar β-phase PVDF has the highest (monomer) molecular dipole moment of 2.1 D. In the β phase, the polymer chains are arranged in a planar zig-zag (all-trans) conformation with all its molecular dipoles in the crystal lattice aligned in the same direction, leading to a rather high net electric polarization [5,6]. The non-polar α-phase is, however, the thermodynamically most stable crystalline modification when prepared by means of normal solution casting at room temperature. It was discovered that copolymerization of vinylidene fluoride (VDF) with trifluoroethylene (TrFE) monomers with a VDF molar content between 50 and 80 mol% leads to a copolymer of P(VDF-TrFE) that always crystallizes in the β conformation [5,7] which is desired in many practical applications owing to its easy preparation and its high piezo- and pyroelectricity. P(VDF-TrFE) copolymer has also been employed in several device applications, especially as transducers, energy-storage capacitors [3,4] and organic field-effect transistors (OFET) for memory applications [8].

P(VDF-TrFE) film still needs to be poled under high electric fields to render it electroactive (*i.e.* piezo-, pyro-, and ferroelectric). The most common method to pole ferroelectric polymer electrets is corona poling. However, it is only suitable for applications which do not require high-precision poling [9], as corona poling does not always lead to uniform distribution of the electrical polarization throughout the poled polymer films [10,11]. Non-homogeneously poled PVDF and P(VDF-TrFE) films exhibit ill-defined transducer properties in particular with respect to their frequency behaviour – as highlighted in PVDF hydrophone [12] and second-harmonic generation applications [13]. One approach for homogeneous poling of ferroelectric polymer films is the so-called "Bauer cyclical poling method" [9,14,15]. It was done by forcing the film polarization through several hysteresis cycles, until a reproducible polarization hysteresis is achieved and extra space charge in the poled samples has been "drained off" [9,13,14]. The homogeneous distribution of polarization throughout the bulk of the poled film was proven with the pressure-wave propagation method (PWP) [14,16]. In the present paper, a similar procedure to Bauer cyclic hysteresis poling was used on commercial P(VDF-TrFE) films with different compositions.

The resulting polarization profiles were probed by means of Piezoelectrically generated Pressure Steps (PPSs) [17] to ascertain the effectivity of hysteresis poling. Hysteresis loops and polarization depth profiles of successfully poled P(VDF-TrFE) copolymer samples will be presented and discussed.

II. SAMPLES AND MEASUREMENT METHODS

A. Poly(vinylidene-trifluoroethylene) copolymer samples

Commercial P(VDF-TrFE) copolymer films with molecular compositions of 50/50, 72/28 and 75/25 mol% VDF/TrFE were provided by Piezotech SA in the form of thin films with a thickness of 30, 27 and 48 μm, respectively. All films were metalized on both sides with circular aluminum electrodes (diameter ca. 12-15 mm, thicknesses 50-60 nm) for the polarization-hysteresis (Sawyer-Tower circuit), polarization-distribution and piezoelectric-coefficient measurements.

B. Polarization hysteresis with a Sawyer-Tower circuit

For poling of the P(VDF-TrFE) films with the Bauer cyclical poling method [9,14,15], polarization-hysteresis (*P-versus-E*

curves) monitoring in a Sawyer-Tower circuit was used [18]. A sequence of unipolar sinusoidal voltage curves (positive and negative direction) at a frequency of 1 Hz with maximum electric fields of 80 MV/m and 100 MV/m was used for hysteresis poling (cyclical poling process) [19]. The sample was subjected to the first 50 cycles at 80 MV/m, followed by another 50 cycles at 100 MV/m in order to achieve polarization saturation at the respective electric fields.

C. Spatial polarization-distribution measurements

Piezoelectrically-generated Pressure Steps (PPSs) [16,17, 20-22] were used to probe the spatial distribution of the electric polarization inside the sample film. Fig. 1 shows the working principle of the PPSs method. In this work, the PPSs signals are not calibrated (arbitrary units for the ordinate) so that only information about the polarization distribution along the thickness direction of polymer films is obtained. Comparison of the PPS signals from different samples with different thicknesses is thus not possible, since different sample thicknesses would require appropriate scaling of the overall PPS signal amplitudes. Each P(VDF-TrFE) copolymer film was equipped with aluminum electrodes (diameter ca. 12-15 mm) on both sides, which significantly increases the RC-time constant of the PPS signal [20]. In order to reduce the RC-time constant and to increase the signal bandwidth, an additional (non-electroded) poly(ethylene terephthalate) (PET) film with a thickness of ca. 12 µm was inserted between sample and rubber electrode in the PPS measurement [20]. The observed PPSs signal is a direct image of the polarization distribution in the thickness direction of the film under measurement [17]. For P(VDF-TrFE) copolymer films, a longitudinal sound velocity of 2.4 km/s was assumed [23].

D. Dynamical piezoelectric coefficient (d_{33}) measurements

After cyclical poling (Section B), the copolymer films were subjected to dynamic piezoelectric coefficient (d_{33}) measurements [24]. A static force of ca. 4-10 N was applied in order to ensure stable mechanical contact with the metal-plate electrodes of the dynamical piezoelectricity measuring setup. A measuring frequency of 2 Hz was used, and the average value of 6 consecutive measurements was recorded as the d_{33} coefficient of the respective sample.

E. Fourier-Transformed Infrared (FTIR) Spectroscopy and crystalline phases in the P(VDF-TrFE) copolymers

A Bruker Alpha-P® FTIR spectrometer operated in the ATR (Attenuated Total Reflection) mode at room temperature was used to investigate the chain conformations and the crystalline phases present in the P(VDF-TrFE) copolymer films with different molar compositions not only qualitatively, but also quantitatively.

III. RESULTS AND DISCUSSION

The FTIR spectra of the unpoled P(VDF-TrFE) copolymer samples with the three different compositions are shown in Fig. 2. The characteristic peaks corresponding to the different

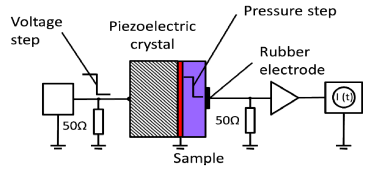

Fig. 1. Measuring principle of the PPSs method (adapted from [20])

crystalline conformations of the copolymer chains are found in the 1500-400 cm^{-1} wavelength section of the FTIR spectra. According to the relevant literature [25-27], the wavenumbers of 1284, 879 and 842 cm^{-1} have been assigned to the polymer chains that are predominantly in the β phase. We can clearly see from the figure that the copolymer shows a strong absorption at these bands – indicating a dominant β phase in all three copolymers, as expected. Subsequently, the wavenumbers at 803, 763 and 613 cm^{-1} [3,28] usually associated with the crystalline fraction in the α phase do not manifest in the form of clear peaks in the spectra. The presence of a certain amount of γ phase is, however, observed via the peak at 505 cm^{-1} [29].

The fraction of the β phase in the individual copolymers with different compositions can be quantified by means of the procedure suggested by Gregorio and Cestari [30]. The values that were observed in our comparative study are found in Table I below. From the table, we can see that the copolymer with 25 mol% TrFE has the highest β-phase content of 87%, while the smallest β-phase fraction is seen in the copolymer with 50 mol% TrFE content. The higher fraction of β phase suggests that the 75/25 mol% should also possess superior electrical properties than the other compositions.

Figs. 3(a), 4(a) and 5(a) depict the polarization hysteresis of the P(VDF-TrFE) copolymer samples with 50/50, 72/28 and 75/25 mol% composition of VDF/TrFE, respectively, after 50 cycles of poling at 100 MV/m. It can be seen that all three compositions show a clear polarization hysteresis, although with different temporal behaviour. Out of the three compositions, the P(VDF-TrFE) copolymer with 75/25 mol% exhibits the highest remnant polarization (P_r) value of ca. 70 mC/m^2 at the end of the cyclical poling procedure – as shown in Table I, which corresponds to the fact that this composition shows the highest fraction of β phase and which also leads to a higher d_{33} coefficient (Table I). The P_r values obtained for the 50/50 and 75/25 mol% compositions are comparable to the

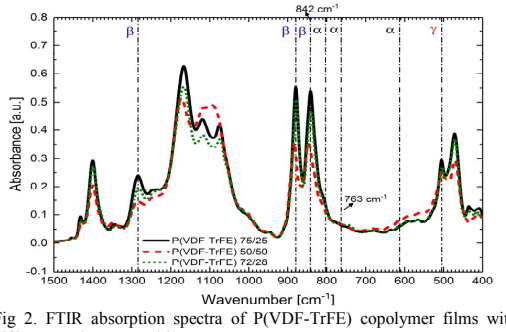

Fig 2. FTIR absorption spectra of P(VDF-TrFE) copolymer films with different molar compositions.

values found in the literature [7,31] for similar compositions.

During cyclical poling at 80 MV/m, the hysteresis curves still continued to grow for all the three compositions at the end of 50 cycles. On increasing the field to 100 MV/m, the hysteresis curves for the 50/50 and 75/25 mol% samples saturated after poling for 10 cycles (Figs. 3 and 5), while the hysteresis curve still continued to grow for the 72/28 mol% composition up to the 50th cycle (Fig. 4). Following this, the 72/28 mol% sample was poled for additional 50 cycles at 100 MV/m, which again led to further growing hysteresis loops. The P_r values increased from 34 mC/m^2 at the end of 50 cycles to 44 mC/m^2 at the end of 100 cycles at 100 MV/m.

Furthermore, looking at the ferroelectric properties of the P(VDF-TrFE) films with 72/28 mol% as listed in Table I, and comparing it with the other two compositions, we observe that its properties are between those of the 50/50 and the 75/25 mol% compositions. It has been shown before that the ferroelectric properties increase with the increase in the TrFE ratio when the molar composition of TrFE is between 50 and 80 mol% [2]. All these findings seem to suggest that the ferroelectric polarization in the 72/28 mol% sample has not yet saturated and that a significantly higher number of cycles might be needed for this particular composition in order for the ferroelectric polarization to saturate and for the sample to arrive at similar d_{33} and P_r values as that of 75/25 mol%. However, one has to take into account also the fatigue behavior in the hysteresis curves when samples are poled for a higher number of cycles in the range of 100-1000 cycles [6,32,33].

Figs. 3(b), 4(b) and 5(b) show the spatial polarization profiles measured with the PPSs method for the 50/50, 72/28 and 75/25 mol% compositions, respectively, at the end of poling the samples at 100 MV/m for 50 cycles. From the figures, we observe that all three compositions show fairly non-uniform polarization distributions throughout their sample thickness. Especially for the 50/50 and 75/25 mol% compositions, even though the P_r saturates at the end of cyclical poling at 100 MV/m, the samples still show an inhomogeneous polarization profile. Again, out of the three compositions, the P(VDF-TrFE) samples with 75/25 mol% composition show a better spatial polarization distribution. Thus, we observe that the TrFE content not only influences the ferroelectric properties, but also the uniformity of the polarization across the sample thickness.

TABLE I. TABLE OF SAMPLE THICKNESSES, β PHASE CONTENTS (BEFORE POLING), REMANENT POLARIZATION (P_r) VALUES AND CALCULATED PIEZOELECTRIC (d_{33}) COEFFICIENTS AT THE END OF THE CYCLICAL POLING FOR THE DIFFERENT COMPOSITIONS OF THE P(VDF-TrFE) COPOLYMER

P(VDF-TrFE)	**50/50 mol %**	**72/28 mol %**	**75/25 mol %**
Sample thickness (µm)	30	27	48
β phase content (%) (from FTIR)	81	85	87
Remanent polarization (P_r) (mC/m^2)	35	34	70
Piezoelectric d_{33} coefficient (pC/N)	- 20	-10	- 27

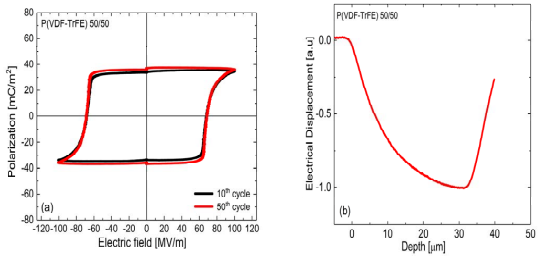

Fig. 3. (a) Polarization-*vs*.-electric-field hysteresis curves for P(VDF-TrFE) copolymer samples with 50/50 mol% composition (tenth and fiftieth poling cycles) and (b) typical spatial polarization profile with the pressure step entering the sample at the electrode that was biased during poling.

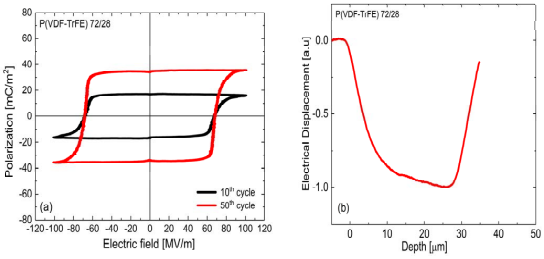

Fig. 4. (a) Polarization-*vs*.-electric-field hysteresis curves for P(VDF-TrFE) copolymer samples with 72/28 mol% composition (tenth and fiftieth poling cycles) and (b) typical spatial polarization profile with the pressure step entering the sample at the electrode that was biased during poling.

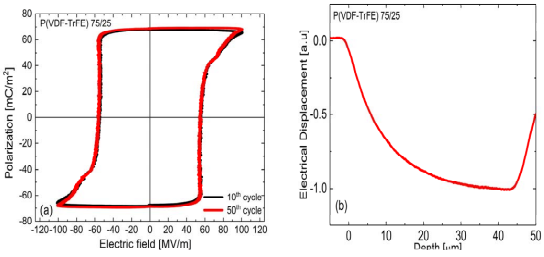

Fig. 5. (a) Polarization-*vs*.-electric-field hysteresis curves for P(VDF-TrFE) copolymer samples with 75/25 mol% composition (tenth and fiftieth poling cycles) and (b) typical spatial polarization profile with the pressure step entering the sample at the electrode that was biased during poling.

IV. CONCLUSIONS

Commercial P(VDF-TrFE) copolymers with VDF/TrFE ratios of 50/50, 72/28 and 75/25 mol% were poled with the Bauer cyclical poling method where the samples have been subjected to 50 hysteresis cycles at an electric field of 80 MV/m, followed by additional 50 cycles at 100 MV/m. The PPSs method was used to investigate the uniformity of the polarization distribution across the sample thickness after poling for all three compositions, and the results were compared with the corresponding hysteresis loops. In addition, the ferroelectric sample properties were studied by calculating the β-phase content from FTIR measurements and by

measuring the dynamic piezoelectric d_{33} coefficients. Among the three compositions, the 75/25 mol% P(VDF-TrFE) films showed the highest remanent polarization values and d_{33} coefficients along with essentially uniform polarization distributions across the sample thickness – corresponding to the fact that the respective copolymer possessed the highest fraction of the polar β phase, which indicates that the TrFE content affects the uniformity of the polarization distribution. Though the hysteresis loops quickly saturate after 10 cycles for the 50/50 and 75/25 mol% compositions, the respective PPSs curves reveal a polarization distribution that as quite non-uniform across the sample thickness even after 50 cycles of poling at 100 MV/m. This suggests that a higher number of poling cycles might still be needed to achieve uniform polarization. The hysteresis behaviour of P(VDF-TrFE) films with 72/28 mol% which does not show a clear hysteresis saturation needs to be analysed further in order to understand the significant differences to the more optimal polymer films with the rather similar composition of 75/25 mol%.

ACKNOWLEDGMENTS

The authors are indebted to Dr.rer.nat.habil. Xunlin Qiu (TU Chemnitz) for stimulating discussions. Quyet D. Nguyen is grateful to Vietnam's International Education Cooperation Department (VIED) for funding his PhD project in Germany.

REFERENCES

[1] H. Kawai, "The Piezoelectricity of Poly (vinylidene Fluoride)," *Jpn. J. Appl. Phys.*, vol. 8, no. 7, p. 975, 1969.

[2] H. S. Nalwa, *Ferroelectric polymers : chemistry, physics, and applications*. New York : M. Dekker, Inc, 1995.

[3] P. Martins, A. C. Lopes, and S. Lanceros-Mendez, "Electroactive phases of poly(vinylidene fluoride): Determination, processing and applications," *Prog. Polym. Sci.*, vol. 39, no. 4, pp. 683–706, 2014.

[4] Prateek, V. K. Thakur, and R. K. Gupta, "Recent Progress on Ferroelectric Polymer-Based Nanocomposites for High Energy Density Capacitors: Synthesis, Dielectric Properties, and Future Aspects," *Chem. Rev.*, vol. 116, no. 7, pp. 4260–4317, 2016.

[5] T. Furukawa, "Ferroelectric properties of vinylidene fluoride copolymers," *Phase Transit.*, vol. 18, no. 3–4, pp. 143–211, 1989.

[6] K. Zaitsu, S. Lee, K. Ishibe, T. Sekitani, and T. Someya, "A field-cycle-induced high-dielectric phase in ferroelectric copolymer," *J. Appl. Phys.*, vol. 107, no. 11, p. 114506, 2010.

[7] T. Furukawa, "Structure and functional properties of ferroelectric polymers," *Adv. Colloid Interface Sci.*, vol. 71-72, no 1, pp. 183–208, 1997.

[8] J. C. Scott and L. D. Bozano, "Nonvolatile Memory Elements Based on Organic Materials," *Adv. Mater.*, vol. 19, no. 11, pp. 1452–1463, 2007.

[9] S. Bauer and F. Bauer, "Piezoelectric Polymers and Their Applications," in *Piezoelectricity: Evolution and Future of a Technology*, Springer, Berlin, Heidelberg, 2008, pp. 157–177.

[10] R. Gerhard(-Multhaupt), G. M. Sessler, J. E. West, K. Holdik, M. Haardt, and W. Eisenmenger, "Investigation of piezoelectricity distributions in poly(vinylidene fluoride) by means of quartz- or laser-generated pressure pulses," *J. Appl. Phys.*, vol. 55, no. 7, pp. 2769–2775, 1984.

[11] G. M. Sessler and A. Berraissoul, "LIPP investigation of piezoelectricity distributions in PVDF poled with various methods," *Ferroelectrics*, vol. 76, no. 1, pp. 489–496, 1987.

[12] B. Fay, P. A. Lewin, G. Ludwig, G. M. Sessler, and G. Yang, "The influence of spatial polarization distribution on spot poled PVDF membrane hydrophone performance," *Ultrasound Med. Biol.*, vol. 18, no. 6, pp. 625–635, 1992.

[13] S. Bauer, G. Eberle, W. Eisenmenger, and H. Schlaich, "Second-harmonic generation with partially poled polymers," *Opt. Lett*, vol. 18, no. 1, pp. 16–18, 1993.

[14] F. Bauer, "Ferroelectric Properties of PVDF Polymer and VF2/C2F3H Copolymers: High Pressure and Shock Response of PVDF Gauges," *Ferroelectrics*, vol. 115, no. 4, pp. 247–266, 1991.

[15] F. Bauer and R. A. Graham, "Very high pressure behavior of precisely-poled PVDF," *Ferroelectrics*, vol. 171, no. 1, pp. 95–102, 1995.

[16] C. Alquie, G. Dreyfus, and J. Lewiner, "Stress-Wave Probing of Electric Field Distributions in Dielectrics," *Phys. Rev. Lett.*, vol. 47, no. 20, pp. 1483–1487, 1981.

[17] W. Eisenmenger and M. Haardt, "Observation of charge compensated polarization zones in polyvinylindenfluoride (PVDF) films by piezoelectric acoustic step-wave response," *Solid State Commun.*, vol. 41, no. 12, pp. 917–920, 1982.

[18] B. Dickens, E. Balizer, A. S. DeReggi, and S. C. Roth, "Hysteresis measurements of remanent polarization and coercive field in polymers," *J. of App. Phys.*, vol. 72, no. 9, p. 4258, 1992.

[19] M. Wegener, "Polarization-electric field hysteresis of ferroelectric PVDF films: Comparison of different measurement regimes," *Rev. Sci. Instrum.*, vol. 79, no. 10, p. 106103, 2008.

[20] R. Gerhard(-Multhaupt), M. Haardt, W. Eisenmenger, G. M. Sessler, "Electric-field profiles in electron-beam-charged polymer electrets," *J. Phys. D: Appl. Phys.*, vol. 16, no. 11, pp. 2247–2256, 1983.

[21] R. Gerhard(-Multhaupt), "Analysis of pressure-wave methods for the nondestructive determination of spatial charge or field distributions in dielectrics," *Phys. Rev. B*, vol. 27, no. 4, pp. 2494–2503, 1983.

[22] G. F. Leal Ferreira, R. Gerhard(-Multhaupt), "Derivation of response equations for the nondestructive probing of charge and polarization profiles," *Phys. Rev. B*, vol. 42, no. 12, pp. 7317–7321, 1990.

[23] H. Ohigashi, K. Koga, M. Suzuki, T. Nakanishi, K. Kimura, and N. Hashimoto, "Piezoelectric and ferroelectric properties of P (VDF-TrFE) copolymers and their application to ultrasonic transducers," *Ferroelectrics*, vol. 60, no. 1, pp. 263–276, 1984.

[24] M. Kappel, M. Abel, R. Gerhard, "Characterization and calibration of piezoelectric polymers: In situ measurements of body vibrations," *Rev. Sci. Instrum.*, vol. 82, no. 7, p. 075110, July 2011.

[25] M. Kobayashi, K. Tashiro, and H. Tadokoro, "Molecular vibrations of three crystal forms of poly (vinylidene fluoride)," *Macromolecules*, vol. 8, no. 2, pp. 158–171, 1975.

[26] H.-M. Bao, J.-F. Song, J. Zhang, Q.-D. Shen, C.-Z. Yang, and Q. M. Zhang, "Phase Transitions and Ferroelectric Relaxor Behavior in P(VDF−TrFE−CFE) Terpolymers," *Macromolecules*, vol. 40, no. 7, pp. 2371–2379, 2007.

[27] K. J. Kim, G. B. Kim, C. L. Vanlencia, and J. F. Rabolt, "Curie transition, ferroelectric crystal structure, and ferroelectricity of a VDF/TrFE (75/25) copolymer 1. The effect of the consecutive annealing in the ferroelectric state on curie transition and ferroelectric crystal structure," *J. Polym. Sci. Pol. Phys.*, vol. 32, no. 15, pp. 2435–2444, 1994.

[28] S. Zhang, B. Chu, B. Neese, K. Ren, X. Zhou, and Q. M. Zhang, "Direct spectroscopic evidence of field-induced solid-state chain conformation transformation in a ferroelectric relaxor polymer," *J. App. Phys.*, vol. 99, no. 4, p. 044107, 2006.

[29] K. Tashiro, M. Kobayashi, and H. Tadokoro, "Vibrational spectra and disorder-order transition of poly (vinylidene fluoride) form III," *Macromolecules*, vol. 14, no. 6, pp. 1757–1764, 1981.

[30] R. Gregorio, Jr. and M. Cestari, "Effect of crystallization temperature on the crystalline phase content and morphology of poly(vinylidene fluoride)," *J. Polym. Sci. Pol. Phys.*, vol. 32, no. 5, pp. 859–870, 1994.

[31] B. Chu, "A Dielectric Polymer with High Electric Energy Density and Fast Discharge Speed," *Science*, vol. 313, no. 5785, pp. 334–336, 2006.

[32] Y. Mabuchi, T. Nakajima, T. Furukawa, and S. Okamura, "Electric-Field-Induced Polarization Enhancement of Vinylidene Fluoride/Trifluoroethylene Copolymer Ultrathin Films," *Appl. Phys. Express*, vol. 4, no. 7, p. 071501, 2011.

[33] S. Z. Yuan *et al.*, "Abnormal polarization enhancement effects of P(VDF-TrFE) films during fatigue process," *Phys. Lett. A*, vol. 375, no. 14, pp. 1612–1614, 2011.